INSTITUTO SUPERIOR TÉCNICO
Universidade Técnica de Lisboa

Capacity Increase in UMTS/HSPA+ Through the Use of MIMO Systems

Telmo André Rodrigues Batista

Dissertation submitted for obtaining the degree of
Master in Electrical and Computer Engineering

Jury

Supervisor: Prof. Luis M. Correia

Co-Supervisor: Mr. Carlos Caseiro

President: Prof. António Topa

Members: Prof. Carlos C. Fernandes

July 2008

To my parents and sisters

"You see, wire telegraph is a kind of a very, very long cat. You pull his tail in New York and his head is meowing in Los Angeles. Do you understand this? And radio operates exactly the same way: you send signals here, they receive them there. The only difference is that there is no cat."

(Albert Einstein)

Acknowledgements

In the first place I would like to thank Professor Luis Correia for giving me the opportunity to write this thesis, and for the constant knowledge and experience sharing. I am thankful for his valuable time during our weekly meetings, where, from the beginning, he helped me with the schedule of my work and gave a lot of valuable hints, which will also be useful in my professional life. His orientation, discipline, availability, constant support, and guidelines, were a key factor to finish this work with the demanded and desired quality.

To Vodafone, especially to Carlos Caseiro, Marco Serrazina, and Pedro Lourenço, for all the constructive critics, technical support, suggestions, advice, and to their precious time to answer all my doubts. Their knowledge and experience were very helpful throughout this journey.

I would like to express my gratitude to all members of GROW. The possibility to participate in the GROW meetings allowed me to contact with several other areas of wireless and mobile communications, as well as to practice my critical thought and presentations. A special thanks to Martijn Kuipers for his knowledge and experience sharing, that were of extreme importance for the development of this work, and for always being able to find time for me.

I also want to thank all the remaining “RF2 lab crew”, for their constructive critics, useful suggestions, different points of view and availability. In a more personal level, I would like to thank to Sara Duarte and Armando Marques, for all of the above, as well as for their friendship, good company and support, which was essential for the completion of this thesis, and to Ricardo Preguiça, for the company at the Vodafone meetings. A special thank to João Lopes for his availability, patience and knowledge sharing, which was of great importance in the development of this thesis.

I owe many thanks to Joana Serralha for her enormous patience and understanding, and to all my friends, especially to Jorge Varandas and Jorge Carvalho, for all the support and encouragement, and for giving me the strength and motivation, without which, the completion of this work would have been a lot difficult task.

At last but not least important, I would like to thank my family, especially my parents and sisters, to whom I am very grateful for their unconditional love, care, understanding, and support, which kept me going in the hardest times.

Abstract

The main purpose of this thesis was to study the implementation of MIMO in UMTS/HSPA+, in terms of gain dependence on scenarios and other MIMO parameters. For this purpose, a model that accounts for different system and MIMO parameters, in a single user scenario, was developed, and implemented in a simulator. The model accounts for several parameters, such as, modulation, layers' overheads, MIMO configuration and receiver, antenna spacing, type of antenna power fed, etc.

The results show that for HSPA+ in DL, the use of MIMO 4×4 jointly with 16QAM and 64QAM enables to achieve throughputs up to 29.5 and 43.8 Mbps, respectively, while in UL the achievable throughputs are up to 23 Mbps. MIMO 2×2 on top of HSPA+ 64QAM offers 19.4 Mbps. These throughputs are achieved within a pico-cell scenario, being lower for the micro-cell one. For UL, within the micro-cell scenario, MIMO 2×4 presents better performance than the 4×4 one, for distances higher than 250 m.

Split power fed in DL does not have a major impact on the throughput; however, for UL, the throughput related to the use of the 4×4 configuration with split power is 22 % lower than the use of dedicated power.

Keywords

UMTS, HSPA+, MIMO, Scenario, Capacity.

Resumo

O principal objectivo desta tese foi estudar a implementação do MIMO no UMTS/HSPA+ em termos da dependência do ganho com os cenários e outros parâmetros do MIMO. Para isso, desenvolveu-se e implementou-se num simulador, um modelo que tem em conta diferentes parâmetros do sistema e do MIMO num cenário de monoutilizador. O modelo considera vários parâmetros, tais como, modulação, cabeçalhos das diferentes camadas, configuração e receptor MIMO, espaçamento das antenas, tipo de alimentação das antenas, etc.

Os resultados mostram que para HSPA+ no DL, o uso de MIMO 4×4 juntamente com 16QAM e 64QAM permite obter débitos binários até 29.5 e 43.8 Mbps, respectivamente, enquanto que no UL o débito binário alcançado pode ir até aos 23 Mbps. HSPA+ 64QAM com MIMO 2×2 oferece 19.4 Mbps. Estes débitos conseguem-se num cenário de pico-célula, sendo menores para um cenário de micro-célula. Para o UL, num cenário de micro-célula, o uso the MIMO 2×4 apresenta melhor performance que o 4×4, para distâncias superiores a 250 m.

A divisão de potência no DL não tem grande impacto no débito binário, no entanto para o UL o débito binário relacionado com o uso da configuração 4×4 com divisão de potência, é 22 % mais baixo que no caso da potência ser dedicada.

Palavras-chave

UMTS, HSPA+, MIMO, Cenário, Capacidade.

Table of Contents

List of Figures

List of Tables

List of Acronyms

2G	Second Generation
3G	Third Generation
3GPP	Third Generation Partnership Project
A-DCH	Associated-DCH
AMC	Adaptive Modulation and Coding
AMR	Adaptative Multirate
AoA	Angle of Arrival
AoD	Angle of Departure
ARQ	Automatic Repeat Request
ASIC	Application-Specific Integrated Circuit
BER	Bit Error Rate
BLAST	Bell Labs Space-Time architecture
BLEP	Block Error Probability
BLER	Block Error Rate
BoD	Bandwidth on Demand
BPSK	Binary Phase Shift Keying
BS	Base Station
CDF	Cumulative Distribution Function
CDMA	Code Division Multiple Access
CIR	Channel Impulse Response
CN	Core Network
CPC	Continuous Packet Connectivity
CQI	Channel Quality Information
CS	Circuit Switch
DCH	Dedicated Channel
DL	Downlink
DOB	DL Optimised Broadcast
DRX	Discontinuous Reception
DS-CDMA	Direct-Sequence-CDMA
DSTTD	Double Space-Time Transmit Diversity
DSTTD-SGRC	DSTTD with Sub Group Rate Control
DTX	Discontinuous Transmission

E-AGCH	E-DCH Absolute Grant Channel
E-DCH	Enhanced Dedicated Channel
E-DPCCH	E-DCH Dedicated Physical Control Channel
E-HICH	E-DCH HARQ indicator channel
E-RGCH	E-DCH Relative Grant Channel
FACH	Forward Access Channel
FDD	Frequency Division Duplex
F-DPCH	Fractional-DPCH
FER	Frame Error Rate
FRC	Fixed Reference Channel
GBSB	Geometrically Based Single Bounce channel model
GPRS	General Radio Packet System
GPS	Global Positioning System
GROW	Group for Research On Wireless
GSCM	Geometry-based Stochastic Channel Models
GSM	Global System for Mobile Communications
HARQ	Hybrid ARQ
HOM	Higher-Order Modulation
HSDPA	High Speed Downlink Packet Access
HS-DPCCH	High-Speed Dedicated Physical Control Channel
HS-DSCH	High-Speed Downlink Shared Channel
HSPA+	High Speed Packet Access Evolution
HS-PDSCH	High-Speed Physical Downlink Shared Channel
HS-SCCH	High-Speed Shared Control Channel
HSUPA	High Speed Uplink Packet Access
IMS	IP Multimedia Sub-system
IP	Internet Protocol
ISDN	Integrated Services Digital Network
ISM	Industry, Scientific and Medical
L1	Layer 1
MAC	Medium Access Control
MAP	Maximum A Posteriori
MBMS	Multimedia Broadcast Multicast Service
ME	Mobile Equipment
MIMO	Multiple Input Multiple Output
MISO	Multiple Input Single Output
ML	Maximum Likelihood
MMS	Multimedia Message Service

MMSE	Minimum Mean Square Error
MOC	Modulation and Coding Schemes
MPC	Multipath Component
MRC	Maximal Ratio Combining
MT	Mobile Terminal
OVSF	Orthogonal Variable Spreading Factor
P-CPICH	Primary-Common Pilot Channel
PDU	Protocol Data Unit
PIFA	Planar Inverted-F Antenna
PLMN	Public Land Mobile Network
PS	Packet Switch
PSTN	Public Switched Telephone Network
QAM	Quadrature Amplitude Modulation
QoS	Quality of Service
QPSK	Quaternary Phase Shift Keying
RLC	Radio Link Control
RMG	Relative MIMO Gain
RNC	Radio Network Controller
RR	Round Robin
RRM	Radio Resource Management
RTT	Round Trip Time
Rx	Receiver
SBSA	Shannon Based Scheduling Algorithms
SF	Spreading Factor
SHO	Soft Handover
SINR	Signal to Interference plus Noise Ratio
SISO	Single Input Single Output
SMS	Short Message Service
SNR	Signal to Noise Ratio
SRB	Signalling Radio Bearer
STC	Space Time Coding
STTD	Space-Time Transmit Diversity
SVD	Singular Value Decomposition
TDD	Time Division Duplex
TMA	Tower Mounted Amplifier
ToA	Time of Arrival
TTI	Transmission Time Interval
Tx	Transmitter

UE	User Equipment
UL	Uplink
UMTS	Universal Mobile Telecommunications System
USIM	UMTS Subscriber Identity Module
UTRA	UMTS Terrestrial Radio Access
UTRAN	UMTS Terrestrial Radio Access Network
V-BLAST	Vertical-BLAST
VoIP	Voice over IP
VRA	Virtual Receive Antenna
WCDMA	Wideband CDMA
WWW	World Wide Web
ZF	Zero Forcing

List of Symbols

α	DL orthogonality factor
α_j	DL channel orthogonality of user *j*
β_{MIMO}	BER function for the MIMO detector
β_{SISO}	BER function for the SISO detector
Γ_s	Reflection coefficient
$\lvert\Gamma_s\rvert$	Magnitude of the reflection coefficient
δ	Sigmoid function
Δf	Signal bandwidth
η_{DL}	DL load factor
η_{UL}	UL load factor
$\overline{\eta_{DL}}$	Average DL load factor value across the cell
λ	Wavelength
μ	Mean value of the distribution
μ_{RMG}	Average RMG
$\bar{\xi}$	Mean correlation between links in a MIMO system
ρ	Signal to Noise Ratio
ρ_I	Signal-to-Interference-plus-Noise Ratio
ρ_{pilot}	P-CPICH E_c/N_0 when HSDPA is active
σ^2	Variance
σ^2_{RMG}	RMG distribution variance depending on the cell-type, N_T and N_R
σ	Standard deviation
$\mathbf{\Sigma}$	singular values of matrix $\boldsymbol{H}$
φ	Road orientation with respect to the direct radio path
Φ_s	Phase of the reflection coefficient
C_{MIMO}	Capacity gain of a MIMO system
C_{SISO}	Capacity gain of a SISO system
d	Distance between BS and MT
E_b	Signal energy per bit
E_c	Energy of the data chip stream
$\bar{e}$	Relative mean error
F	Receiver's noise figure

g	Inverse of the RMG distribution
G_{div}	Diversity gain
$G_{M/S}$	Relative MIMO Gain
G_P	Processing gain
G_{Pj}	Processing gain of user j
G_r	Receiving antenna gain
G_{SHO}	Soft handover gain
G_t	Transmitting antenna gain
$\mathbf{H}$	Matrix containing CIRs
H_B	Buildings height
h_b	BS height
h_{ij}	CIR between signal from the j^{th} Tx antenna to the i^{th} Rx antenna
h_m	MT height
i	Ratio of inter- to intra-cell interferences
i_j	Ratio of inter- to intra-cell interferences for user j
$\boldsymbol{I_{NR}}$	N_R dimensional identity matrix
k_a	Increase of path loss for BS antennas below roof tops of adjacent buildings
k_d	Dependence of multi-screen diffraction loss vs. distance
k_f	Dependence of multi-screen diffraction loss vs. frequency
$\overline{L}$	Path loss between Node B and user j
L_0	Free space loss
L_{bsh}	Losses due to the fact that BS antennas are above/below the roof-tops
L_c	Cable losses between transceiver and antenna
L_{ind}	Indoor penetration losses
L_{ori}	Street orientation loss
L_p	Path loss
L_{p_j}	Path loss between BS and user j;
$L_{p\ total}$	Total path loss
L_{rm}	Roof-top-to-street diffraction and scatter loss
L_{rt}	Multiple screen diffraction loss
L_u	Body losses
M_{FF}	Fast fading margin
$M_I^{UL/DL}$	Interference margin
M_{SF}	Slow fading margin
$\mathbf{n}$	Vector containing power of noise received by each antenna
N	Total noise power
N_{ds}	Number of detected signals
N_{ts}	Number of total signals

N_s	Number of samples.
N_0	Noise spectral density
N_R	Number of Rx antennas
N_T	Number of Tx antennas
N_u	Number of users per cell
O_{App}	Application overhead
$O_{MAC\&RLC}$	MAC and RLC overheads
P_d	Detection percentage
P_{HSDPA}	HSDPA transmit power
$P_{\text{HS-DSCH}}$	Received power of HS-DSCH
P_{inter}	Received inter-cell interference
P_{intra}	Received intra-cell interference
P_{pilot}	P-CPICH transmit power
P_r	Available receiving power at antenna port
P_{Rx}	Received power at receiver input
P_{Sig}	Signalling power
P_t	Transmitting power at antenna port
P_{Tx}	Total BS transmit power
R_b	Bit rate
R_{bj}	Bit rate of user *j*
R_c	WCDMA chip rate
s	Slope of the Sigmoid function
S_R	Symbol rate
S_b	Symbols per bit
SF_{16}	SF of 16
T_F	Final throughput
$\overline{T_s}$	Average simulated throughput
$\mathbf{T}$	Matrix containing the channel transfer gains for each par of antennas
T_P	Physical layer throughput
$T_{P/C}$	Physical layer throughput per code
T_{SISO}	SISO throughput
$\mathbf{U}$	Unitary matrix containing the singular vectors of matrix $\boldsymbol{H}$ after SVD
u	Random value with a Uniform distribution
$\mathbf{V}$	Unitary matrix containing the singular vectors of matrix $\boldsymbol{H}$ after SVD
v_j	Activity factor of user *j*
w_B	Distance between middle points of adjacent buildings
w_s	Street width

$\overline{x^2}$	Rayleigh distribution mean square error
$\overline{x}$	Gaussian distribution mean
$\mathbf{x}$	Vector of transmitted symbols from input antennas
$\mathbf{X}$	Fourier transform of $\mathbf{x}$
$\mathbf{y}$	Vector of symbols on the receiving site
$\mathbf{Y}$	Fourier transform of $\mathbf{y}$
z_i	sample i
z_r	Reference value
$\overline{z}$	Average
Det	Determinant of a matrix
E	Statistical expectation
erf	Error function

List of Software

Microsoft Word	Text editor tool
Microsoft Excel	Calculation tool
Microsoft Visio	Design tool (e.g. flowcharts, diagrams, etc)
Matlab	Computational math tool
Borland C++ Builder	ANSI C++ Integrated Development Environment

Chapter 1

Introduction

This chapter gives a brief overview of the work. It provides the scope and motivations of the thesis. At the end of the chapter, the layout of the work is presented.

1.1 Overview and Motivation

Mobility and communication are two fundamental features inherent to the human nature, being even more relevant in nowadays fast paced life. With the wired communications unable to fully meet these demands, wireless communications emerged and became a rapidly growing segment of the communications industry, with the potential to provide high-speed and high-quality information exchange between portable devices located anywhere in the world. In fact, the architecture of wireless systems consists of both core network (i.e., high speed fibre cables) and radio interface, which is many times a bottleneck of the system. Radio frequency spectrum is a renewable but finite resource, thus, the bandwidth allocated for a wireless system must be limited, which is why many systems are able to coexist in one medium and not interfere with each other.

Second-generation telecommunication systems, such as the Global System for Mobile Communications (GSM), enabled voice traffic to go wireless, with the number of mobile phones exceeding the number of landline ones, and the mobile phone penetration going beyond 100% in several markets. However, the data-handling capabilities of second-generation systems are limited, and third-generation systems are needed to provide the high bit-rate services that enable high-quality images and video to be transmitted and received, and to provide access to the Web with higher data rates. One of these third-generation mobile communication systems is the Universal Mobile Telecommunication System (UMTS) [Hoto07].

In January 1998, the European Telecommunications Standard Institute (ETSI) decided upon Wideband Code Division Multiple Access (WCDMA) as the third-generation air interface; deployment has been started in Europe and Asia, including Japan and Korea, in the same frequency band, around 2 GHz [DPSB07]. The first full set of specifications was completed at the end of 1999, called Release 99. In Japan, during 2001, the first commercial network was opened for use in key areas; in Europe, it was at the beginning of 2002 for the pre-commercial testing phase, and for commercial use during 2003. UTMS is designed for coexistence with GSM, including seamless handovers and dual-mode handsets, most of the UMTS networks being deployed on top of the existing GSM ones [HoTo07]. GSM and UMTS together account for 85% of the global mobile subscriptions, and their share keeps increasing, with global subscriptions to all mobile network technologies exceeding 3.3 billion [UMFO08].

Release 99, in theory, enables 2 Mbps, but in practice gives 384 kbps [HoTo07], therefore, the exponential growth of data communications over mobile phones forced a further development of systems that would be capable of offering higher capacity, throughput and enhanced multimedia services, available to consumers ‘anywhere, anytime’, [LaWN06].

3rd Generation Partnership Project (3GPP) specified important evolution steps on top of Release 99, for Downlink and Uplink (DL and UL), these enhancements being commonly known as High Speed Packet Access (HSPA). High Speed Downlink Packet Access (HSDPA) was set as a standard in

Release 5 with the first specifications made available in March 2002. HSDPA was commercially deployed in 2005, with initial peak data rate of 1.8 Mbps, increased to 3.6 Mbps during 2006, and by the end of 2007, 7.2 Mbps were available [HoTo06]. Nowadays, the maximum peak data rate of 14.4 Mbps is already provided by some operators. In December 2004, the UL counterpart was launched by 3GPP in Release 6 with the Enhanced Dedicated Channel (E-DCH), also known as High Speed Uplink Packet Access (HSUPA). Following the success accomplished by HSDPA, by the end of 2007 HSUPA started to be deployed, pushing at first the UL bit rates up to 1.45 Mbps, and up to 5.7 Mbps in later releases [DPSB07]. Further HSPA evolution is specified in 3GPP Release 7, and its commercial deployment is expected by 2009. HSPA evolution is also known as HSPA+.

3GPP is also working to specify a new radio system called Long-Term Evolution (LTE). Release 7 and 8, solutions for HSPA evolution, will be worked in parallel with LTE development, and some aspects of LTE work are also expected to reflect on HSPA evolution.

HSPA evolution in Release 7 brings a maximum throughput of 28 Mbps in DL and 11 Mbps in UL, [HoTo07]. LTE will then further push the peak rates beyond 100 Mbps in DL and 50 Mbps in UL by using a 20 MHz bandwidth, instead of a 5 MHz one as in HSPA, Figure 1.1.

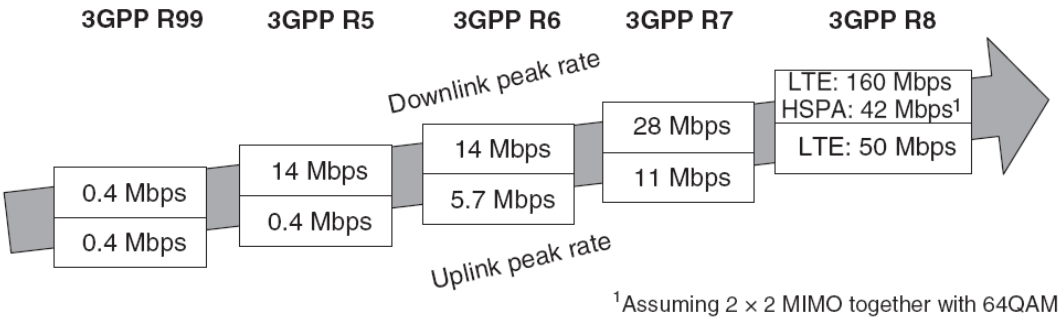

Figure 1.1 Peak data rate evolution for WCDMA (extracted from [HoTo07]).

Latest figures confirm that global subscriptions to UMTS networks have passed the 200 million milestone, almost 20 million being already subscribers to HSPA mobile broadband networks. Meanwhile, more than 165 UMTS networks have been upgraded to HSPA, and according to Wireless Intelligence, the current HSPA subscriber numbers will double this year, exceeding 40 million by the end of 2008 [UMFO08].

Multiple-Input Multiple-Output (MIMO) systems can enhance the previously mentioned radio systems, which are based on Single Input Single Output (SISO) ones. A MIMO system consists of a few input and output antennas, though MIMO can not be treated as an antenna array where all antenna elements are treated as a single stream. In the MIMO case, each antenna is a single element that must be considered separately. All pairs of input and output antennas establish parallel links between the receive and transmit sides. If the links are independent, a gain on the radio channel can be observed, and the Shannon border for the capacity in the Gaussian radio channel can be crossed, [FoGa98]. The independence of the links between input and output is related with the propagation environment, which has a major influence on the correlation between Channel Impulse Responses

(CIRs). A decorrelation of the radio channels, (i.e., links independence) can only exist in an environment, where a multipath phenomenon takes place, with the potential gain of a MIMO system depending on how strong this phenomenon is. The gain of a MIMO system is related with some parameters, as the number of input and output antennas, spacing between them, and also time resolution of the Receiver (Rx). An increase of the number of input and/or output antennas leads to an increase of the number of parallel channels, hence, to a higher MIMO gain, if under favourable conditions. A higher antenna separation gives a greater decorrelation among links, because the influence of each obstruction in the environment is more significant, while an increase of the time resolution allows to distinguish more Multi Path Components (MPCs).

The main purpose of this thesis is to study the impact on capacity of UMTS/HSPA+ systems through the use of MIMO systems, and to inspect MIMO implementation aspects. These objectives were accomplished through the development of a model that accounts for various MIMO parameters, and through collecting and analysing information that provides solutions to MIMO implementation. The main results of the model are the SISO and MIMO application throughputs at a certain distance. Underlying the model development was the use of some previously developed ones, namely the Relative MIMO Gain (RMG) model [KuCo07], which makes use of the Geometrically Based Single Bounce (GBSB) channel model [MaCo04] and [Koko05]. However, the RMG model does not contemplate SNR and antenna spacing variation, therefore, simulations were performed in order to obtain correction values and/or functions that account for these parameters variation as accurately as possible. Thus, in the developed model, these variations are already taken into account. The model was afterwards implemented in a simulator, allowing several analyses regarding MIMO parameters variation. For a comparison purpose, the MIMO impact on earlier 3GPP releases is studied as well. The gain of a MIMO system should be checked in different conditions of propagation with dissimilar distributions of the scatterers. So, in this work, the application of MIMO in different scenarios is analysed, with three scenarios being considered: pico-, micro- and macro-cells. Moreover, the impact of varying some parameters, such as MIMO configurations, antenna spacing, type of MIMO detector, and the use of different strategies of antenna power fed, are also analysed. A comparison between DL and UL is addressed, regarding each parameter variation.

This thesis was made in collaboration with the mobile operator Vodafone. Several technical details were discussed with the company, and the suggested values for several parameters have been used throughout this thesis. The type and content of the results analysis had also been discussed, with the presented analysis being the ones that fit better the aim of this work, therefore, providing the most relevant results.

The main contribution of this thesis is the analysis of the MIMO impact on UMTS/HSPA+ systems capacity, and its scenario dependency. A model to calculate the MIMO application throughput as a function of distance was implemented. The model allows analysing several MIMO parameter variations, as antenna configuration, type of detector, as well as the impact on earlier 3GPP releases. The simulator permits to evaluate the influence of the different parameters on system performance.

1.2 Structure of the Dissertation

This work is composed by 6 Chapters, followed by a set of annexes.

In Chapter 2, an introduction to UMTS, HSDPA, HSUPA and HSPA+ is performed. UMTS basic aspects are explained, and afterwards HSDPA and HSUPA new features are presented. Following this, is the presentation of HSPA+ and its new improvements. This work being related to MIMO, in this chapter some basic information about this technique is presented. Moreover, the main advantages of this system are addressed, and considerations related to MIMO systems capacity can be found. In the last two sections a brief state of the art is also presented, and some MIMO implementations aspects are described.

Chapter 3 starts by presenting the GBSB channel model, as well as the description of three types of scenarios over which it can be applied. The RMG model is presented next, describing at first the default model, followed by the analysis performed to stress out the impact on the RMG value of the Signal to Noise Ratio (SNR) and antenna spacing variation. The last section of the chapter provides the description of the link model, which has been developed to evaluate the MIMO capacity improvements on UMTS.

All issues related to the implementation of the models in the simulator can be found in Chapter 4. At the beginning a simulator overview is given, concerning architecture, functionality and data flow among the different modules. Afterwards, a detailed description of the different simulator modules is performed, as well as of the used algorithms, highlighting the input and output parameters. This chapter finishes with the assessment of the simulator.

Chapter 5 begins with the description of the scenarios that were taken for simulations. In the following parts of the chapter, results for DL and UL simulations are presented, concerning average simulated and final application throughputs, with the latter accounting for the average detection percentages. First, the study of DL is examined, starting by presenting the default scenario over which several parameters are varied one at each time. The study is performed for different UMTS releases, MIMO configurations, antenna spacing, detector and type of antenna power fed. Afterwards, the same analyses are presented for UL, being also performed a DL vs. UL comparison. For UL a further analysis of the throughput impact of using a TMA and additional reception diversity is presented.

This thesis concludes with Chapter 6, where the main conclusions of the work are drawn and suggestions for future work are pointed out.

A set of annexes with auxiliary information and results is also included. In Annex A, the UMTS networks services and applications are presented. Annex B contains information regarding capacity and interference aspects for UMTS/HSPA. In Annex C, additional information regarding the RMG model is shown. In Annex D and E, the detailed link budget used throughout this thesis is presented, as well as the throughput interpolations for the different considered systems. The propagation model

considered in this thesis is described in Annex F. Detectors information, as well as the respective interpolation functions, is presented in Annex G. In Annex H, one presents the simulator user's manual, and in Annex I the implemented power control algorithm is shown. Finally, in Annexes J and K, auxiliary results regarding the results analysis are presented for DL and UL, respectively.

Chapter 2

Basic Concepts

This chapter provides a brief overview of the main technologies that are related to the scope of this thesis, namely UMTS, HSPA and MIMO, giving particular emphasis to the radio aspects.

2.1 UMTS

In this section, UMTS (Release 99) basic concepts are presented, based on [HoTo04], regarding the network architecture and radio interface. Concerning the network architecture, more emphasis is given to the radio related modules, due to the scope of the thesis.

UMTS uses the same well-known architecture that has been used by all second generation systems (2G), and even by some first generation ones. Network elements can be grouped based on similar functionalities, as shown in Figure 2.1; there are three high level modules, namely the User Equipment (UE), the UMTS Terrestrial Radio Access Network (UTRAN), and the Core Network (CN).

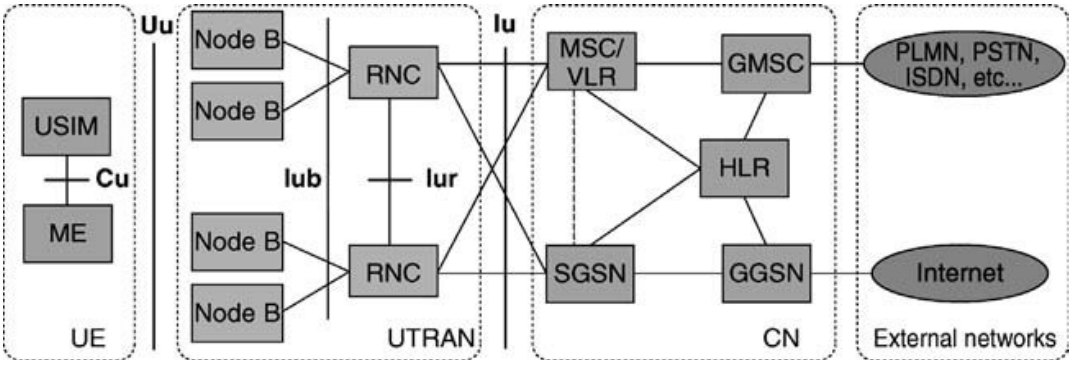

Figure 2.1 UMTS system architecture (extracted from [HoTo04]).

The UE consists of two parts:

- The Mobile Equipment (ME) is the Mobile Terminal (MT), used for radio communication over the Uu interface, i.e., the WCDMA radio interface.
- The UMTS Subscriber Identity Module (USIM) is a smartcard that holds the subscriber identity, performs authentication algorithms, stores authentication and encryption keys, and some subscription information that is needed at the MT.

UTRAN consists of two distinct elements:

- The Node B (i.e., the Base Station (BS)) converts the data flow between the Iub and Uu interfaces. It also participates in Radio Resource Management (RRM).
- The Radio Network Controller (RNC) owns and controls the radio resources in its domain (the Node Bs connected to it). RNC is the service access point for all services UTRAN provides to the CN, e.g., management of connections to the UE.

The CN is out of the scope of this thesis, though, it plays a very important role in UMTS architecture, by being responsible for switching and routing calls and data connections to external networks. These external networks may belong to the Circuit Switch (CS) domain, such as PLMN, PSTN and ISDN, or to the Packet Switch (PS) one, the Internet being a good example.

As specified by the 3GPP, in UMTS, the air interface is based on WCDMA, a wideband

Direct-Sequence Code Division Multiple Access (DS-CDMA) system, which leads to a very high bandwidth, theoretically enabling the use of unlimited channels per carrier, and having been designed to be deployed in conjunction with GSM/General Radio Packet System (GPRS), with supported handovers between systems. WCDMA main parameters are summarised in Table 2.1.

Indoor and micro-cell BSs deployment is easy, due to the asynchronous BS operation (no need for receiving GPS signal). It supports highly variable user data rates, i.e., Bandwidth on Demand (BoD) and allows Quality of Service (QoS) differentiation, with the different services and applications of UMTS networks being presented in Annex A. The user data rate is kept constant during each 10 ms frame, however, the data capacity among users can change from frame to frame. Information regarding capacity and interference aspects can be found in Annex B.

There are two basic modes supported, i.e., Frequency Division Duplex (FDD) and Time Division Duplex (TDD); in this thesis, only the FDD mode is analysed, where separate 5MHz carrier frequencies are used for UL and DL. The UMTS band for Europe, Asia and some Latin American countries, like Brazil, is [1920, 1980] MHz for UL and [2110, 2170] MHz for DL.

Table 2.1 Main WCDMA parameters (adapted from [HoTo04]).

Multiple access method	DS-CDMA
Duplexing method	Frequency division duplex/time division duplex
Base station	Asynchronous operation
Chip rate [Mcps]	3.84
Carrier bandwidth [MHz]	4.4
Frame length [ms]	10
Service multiplexing	Multiple services with different QoS requirements multiplexed on one connection
Multirate concept	Variable spreading factor and multicode
Detection	Coherent using pilot symbols or common pilot
Multiuser detection, smart antennas	Supported by the standard, optional in the implementation
Modulation	UL: Binary Phase Shift Keying (BPSK) DL: Quaternary Phase Shift Keying (QPSK),

The spreading operation in WCDMA, also known as channelisation, results in spread data with the same random appearance as the spreading code. The channelisation code increases the transmission bandwidth and uses the Orthogonal Variable Spreading Factor (OVSF) technique, which allows the Spreading Factor (SF) to be changed, while maintaining orthogonality among codes with different lengths. Scrambling codes, used at the channelisation ones, do not change the transmission bandwidth, and may use the Gold family for long codes and Extended S(2) code family for short ones.

UTRA radio interface channels can be classified as logical, transport and physical. Logical channels

are mapped onto transport channels, which are again mapped onto physical ones. Logical to Transport channel conversion happens in the Medium Access Control (MAC) layer, which is a lower sublayer in Data Link Layer (Layer 2).

A very important key feature of WCDMA is power control, without which an MT could block a whole cell, giving rise to the so-called near-far problem of CDMA. Other key features, such as handover, also exist, although they are not covered in this work.

2.2 HSPA

In this section, HSDPA and HSUPA concepts are presented based on [HoTo06], giving a brief overview of the main differences between Release 99 and HSDPA/HSUPA, such as new technologies and channels.

HSDPA was designed to be deployed together with Release 99 and it works as an enhancement of UMTS, increasing DL packet data throughput by means of fast physical layer (L1) retransmission, fast scheduling, as well as fast link adaptation controlled by the BS. In order to allow higher data rates, this new technology supports the 16 Quadrature Amplitude Modulation (16QAM) with 4 bits per symbol, which can only be used under good radio signal quality, due to additional decision boundaries.

While, in Release 99, the operation of transmitting a new packet or retransmitting one, had the same impact on the network, since the retransmitting was done by the RNC, in HSDPA, the BS has a buffer that first receives the packet and keeps it after sending it to the user, allowing the BS to retransmit the packet, if needed, without RNC intervention, this way minimising latency. RNC-based retransmission can still be applied on top in case of physical layer failure, using a Radio Link Control (RLC)-acknowledged mode of operation. Concerning scheduling and link adaptation, these operations take place after the BS estimates the channel quality of each active user, based on the physical layer feedback in UL.

The fact that all the elements of the network can be shared, make the upgrade cost, from Release 99 to HSDPA, very attractive, since it only requires new software package and, perhaps, some new pieces of hardware in the BS and RNC, to support the higher data rates and capacity; however, on the user side, a new terminal is required.

HSDPA does not support Dedicated Channel (DCH) features, as power control and soft handover, although, as in Release 99, HSDPA is always operated with the DCH running in parallel, since at least the Signalling Radio Bearer (SRB) is carried if the service is only for packet data. For HSDPA to operate, there was a need to had new channels, such as the High-Speed Downlink Shared Channel (HS-DSCH), for data, which is mapped onto the High-Speed Physical Downlink Shared Channel (HS-PDSCH), and for signalling, the High-Speed Shared Control Channel (HS-SCCH) and the

High-Speed Dedicated Physical Control Channel (HS-DPCCH), for DL and UL, respectively. When only packet services are active in DL, other than the SRB, it was felt, especially with lower rates, that the DL DCH introduces too much overhead, and can also consume too much code space, if looking for a large number of users using a low data rate service, like Voice over IP (VoIP). In this case the system uses the Fractional-DPCH (F-DPCH), that handles power control.

The HS-DSCH is the transport channel used to carry the user data in HSDPA. This channel supports 16QAM, besides QPSK, which is used to maximise coverage and robustness, and it has a dynamic resource sharing based on the BS scheduling with a Transmission Time Interval (TTI) of 2ms. During the TTI there is no Discontinuous Transmission (DTX). It uses a fixed Spreading Factor (SF) of 16 for multicode operation, with a maximum of 15 codes per MT, and only turbo-coding is used, since it outperforms the convolutional one for higher data rates.

HSDPA has enhanced DL capabilities, therefore, there was a need to enhance UL in order to match these capabilities. As a response to this need, in Release 6, HSUPA is introduced. HSUPA is not a stand alone feature, rather more an add-on one, since it uses most of the basic features of Release 99, the only changes being the new way of delivering data from the MT to the BS and the introduction of QPSK, maintaining all the other specifications untouched, e.g., power control is just as essential as in Release 99.

HSUPA brought to UL some of the same features as the HSDPA with its new transport channel (E-DCH), namely fast Node B based scheduling, fast physical layer Hybrid Automatic Repeat Request (HARQ) and, optionally, a shorter TTI of 2ms. In HSUPA, the HARQ is fully synchronous, has incremental redundancy, and it also operates in soft handover. Scheduling, contrary to HSDPA, has a many-to-one structure, thus, leading to the use of the dedicated channel. Despite the fact that in [HoTo06] the only assumed modulation for HSUPA is BPSK, regarding [PWST07], QPSK modulation was also introduced in Release 6. A comparison between the main features of the transport channels of Release 99, HSDPA and HSUPA is shown in Table 2.2.

Table 2.2 DCH, HSDPA and HSUPA comparison table (adapted from [HoTo06]).

Feature	DCH	HSDPA (HS-DSCH)	HSUPA (E-DCH)
Variable SF	Yes	No	Yes
Fast power control	Yes	No	Yes
Adaptative modulation	No	Yes	Yes
BS based scheduling	No	Yes	Yes
Fast L1 HARQ	No	Yes	Yes
Soft handover	Yes	No	Yes
TTI length [ms]	80, 40, 20, 10	2	10, 2

Similar to HSDPA, for HSUPA operation new channels were introduced. For DL, the E-DCH Absolute Grant Channel (E-AGCH) and the E-DCH Relative Grant Channel (E-RGCH), have been introduced

for scheduling control, and the E-DCH HARQ indicator channel (E-HICH), for retransmission support. In UL, the E-DCH Dedicated Physical Control Channel (E-DPCCH) for new control information, and for carrying data the E-DCH Dedicated Physical Data Channel (E-DPDCH). The DCH channels from Release 99 were left unchanged. In HSUPA, the E-DCH is a dedicated channel, similar to Release 99, but with fast retransmission and scheduling, while for HSDPA, the HS-DSCH is a shared one.

Jointly with Release 99, additional information regarding HSPA capacity and interference is presented in Annex B.

2.3 HSPA+

In this section, HSPA+ main concepts are presented, based on [PWST07] and [BEGG08], which is currently being standardised by 3GPP in Releases 7 and 8.

The aim of HSPA evolution is to further improve the performance of UMTS, through higher peak rates, lower latency, greater capacity, increased battery times, better support for VoIP, and improved multi/broadcast capabilities. In order to support these improvements, HSPA+ introduces:

- Higher-Order Modulation (HOM);
- MIMO;
- Continuous Packet Connectivity (CPC);
- Layer-2 enhancements.

Furthermore, for future releases, 3GPP is considering multi-carrier operation, Downlink-Optimised Broadcast (DOB), Enhanced Cell-Forward Access Channel (Cell-FACH), and more advanced receivers, which will yield higher data rates. For instance, in Release 8, the peak data rates will theoretically reach up to 42 Mbps in DL and 11 Mbps in UL (per 5 MHz carrier).

HOM enables users to experience significantly higher data rates, under favourable radio-propagation conditions. In Release 6, 16QAM and QPSK modulations are supported for DL and UL respectively, providing reasonable data rates for macro-cells, however, for pico- and micro-cells, higher SNRs are normally achieved, thus, HOMs can be used. Release 7 introduces 64QAM in DL, increasing the peak data bit rate by 50%, from about 14 Mbps to 21 Mbps, Figure 2.2. Note that the enhancements inherent to HSPA+ are reflected in the 16QAM modulation for DL, with the need of a smaller SNR value, to achieve the peak data rate, compared to HSDPA of Release 5 depicted in Figure B.1.

In UL, the introduction of 16QAM, allows peak data rates to reach about 11.5 Mbps, featuring an increase of 100% compared with the 5.74 Mbps of the enhanced UL in Release 6, with QPSK, as shown in Figure 2.3.

Moreover, in order to support the signalling of the new modulation schemes, larger transport block sizes and larger range for the Channel Quality Information (CQI), the physical control channels (HS-SCCH, HS-DPCCH, E-AGCH and E-DPCCH), have been modified. The best combination of

modulation and coding rate for a given SNR is determined by Modulation and Coding Scheme (MSC) tables, leading to a limited peak data rate, due to the use of the higher modulation and least amount of coding possible, for each value of SNR.

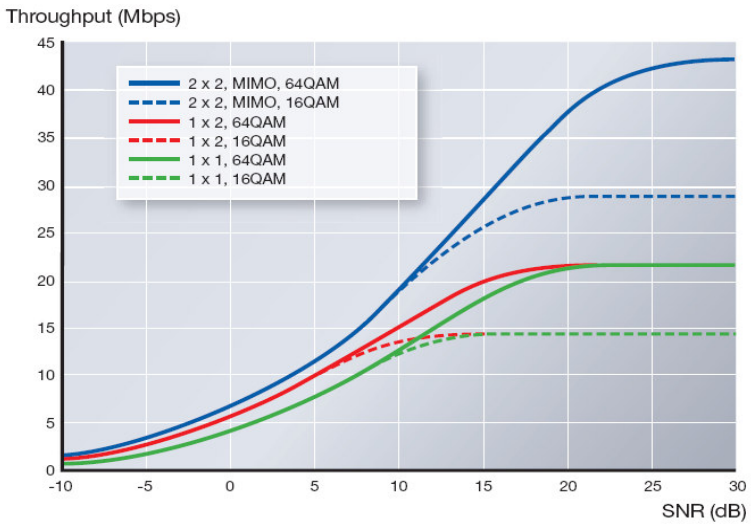

Figure 2.2 The 90th percentile throughput in Pedestrian A channel for HOM and MIMO (extracted from [BEGG08]).

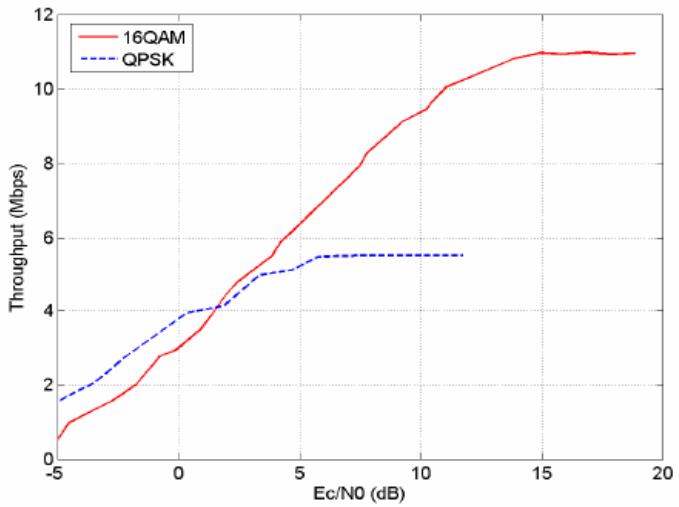

Figure 2.3 Throughput as a function of E_c/N_0 in Pedestrian A channel for uplink HOM (extracted from [PWST07]).

Concerning MIMO, the standardisation of the multilayer transmission scheme is a prerequisite, since with the knowledge of channel properties and coding scheme, the receiver is able to separate the multiple data streams. The MIMO scheme chosen for HSPA+ is based on precoded and rank adaptative multi-codeword transmission, thus, each layer (substream) carries separate transport blocks, and the number of parallel streams can be adapted to the current channel conditions (rank adaptation). The multi-codeword principle allows transmitting two separately encoded streams to an MT, facilitating the use of successive interference cancellation receivers, which are expected to boost

the performance compared to linear receivers, such as Minimum Mean Square Error (MMSE) based ones. Before transmitting data, the modulated and spread signal is spatially weighted (precoded), meaning that, the data streams are transmitted over separate transmit antennas, using different transmission weights. Precoding has, as main benefit, the fact that even when a single transport block is transmitted, both power amplifiers are loaded, thus, when two streams are transmitted, each stream contains the same channelisation codes. In Release 7, MIMO is defined for transmitting up to two streams (2×2 MIMO scheme), which for DL, using 16QAM for each stream, leads to peak data rates of approximately 28 Mbps. The peak data rate is theoretically extended to 42 Mbps, with the combination of MIMO and 64QAM modulation, as depicted in Figure 2.2, being considered for Release 8. Moreover, undetected blocks can be retransmitted independently between the two streams, since HARQ acknowledges each stream separately and independently.

With the activity level of packet data users, varying considerably over time, there is a need to efficiently support continuously connected applications. The solution presented by 3GPP in Release 7 is CPC, which consists of two main features called UE Discontinuous Transmission and Reception (UE DTX/DRX), and HS-SCCH-less operation. The introduction of UE DTX/DRX in active state leads to benefits, such as, reduced battery consumption and increased capacity. Simulations show that the CPC concept, in Release 7, boosts capacity for VoIP by 40% in UL and 10% in DL.

In order to support MIMO and 64QAM modulation, a larger RLC Protocol Data Unit (PDU) is needed, therefore, in Release 7, flexible RLC PDU sizes are adopted, as well as MAC segmentation, and improved MAC multiplexing for DL transmission; hence, reducing the limitation of the DL peak data rate, due to RLC PDU size. Level-2 protocol overhead is reduced, by reducing RLC header overhead, which is a consequence of the ability of the transmitter to flexibly select the size of RLC PDUs. Additionally, in Release 8, the enhancements made to the DL protocol will be applied to the UL protocol, improving UL coverage, and reducing processing and level-2 overhead.

2.4 Multiple Input Multiple Output

In this section, the general aspects of MIMO are briefly presented as well as the capacity aspects of these systems.

The idea of using multiple receive and multiple transmit antennas has emerged as one of the most significant technical breakthroughs in modern wireless communications. In a multipath propagation environment, the Rx antenna is reached by many copies of the transmitted signal. The difference in each component propagation path results in diversity of Time of Arrival (ToA), Angle of Arrival (AoA), signal amplitude and phase. In order to achieve a better performance, Multiple Input Multiple Output (MIMO) systems take advantage of all arriving arrays [Dziu04]. Hence, MIMO, or spatial multiplexing, should mainly be seen as a tool to improve the end-user throughput by acting as a ‘data-rate booster’,

which will also, to some extent, result in an increased system throughput [DPSB07].

Diversity reception, well known in various radio applications, improves only the BER statistics and reduces the probability of total outage. However, the MIMO scheme, which is the result of parallel deployment of several space-separated antennas at input and output, does not only improve BER performance, but also causes an increase of channel capacity [Dziu04]. In order to achieve higher throughputs, a correspondingly higher carrier-to-interference ratio is required at the receiver; therefore, spatial multiplexing is mainly applicable in smaller cells or close to the BS, where high carrier-to-interference ratios are common [DPSB07]. Nevertheless, the capacity in such a system strongly depends on the propagation conditions in the radio channel and can vary significantly [Dziu04].

In Figure 2.4, a MIMO scheme is depicted, composed of N_T Transmit (Tx) antennas and N_R Rx ones. A relation between transmitted and received signal is [FoGa98]:

$$\mathbf{y} = \mathbf{H} * \mathbf{x} + \mathbf{n} \tag{2.1}$$

where:

- **y**=[y_i]: vector of symbols on the receiving site;
- **x**=[x_j]: vector of transmitted symbols;
- **n**: vector containing power of noise received by each antenna;
- **H**=[h_{ij}]: a matrix containing the CIRs between signals from the j^{th} Tx antenna to the i^{th} Rx antenna;
- *: Convolution operator.

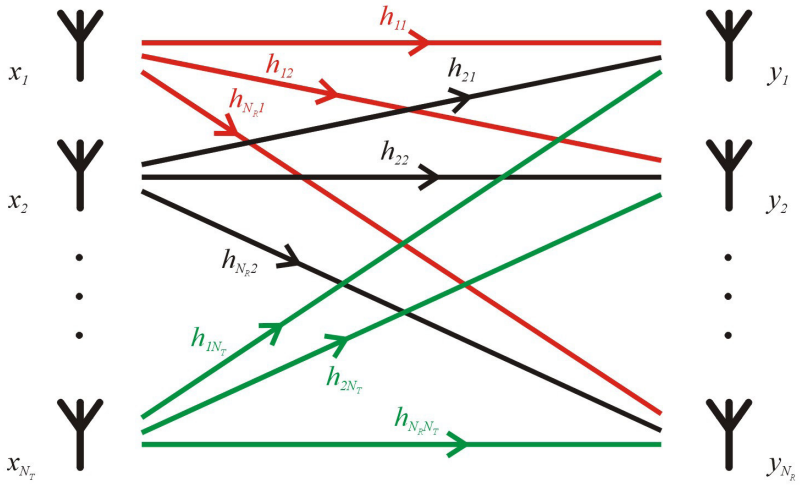

Figure 2.4 MIMO scheme (extracted from [Maćk07])

The mean correlation between links in a MIMO system, $\bar{\xi}$, can be defined as [Maćk07]:

$$\bar{\xi} = \frac{1}{(N_T N_R)^2} \sum_{k=1}^{N_T} \sum_{l=1}^{N_R} \sum_{m=1}^{N_T} \sum_{n=1}^{N_R} \xi(h_{kl}, h_{mn}) \tag{2.2}$$

After using the Fourier Transform and Singular Value Decomposition (SVD), which is a way of checking if the system is solvable, the system equation takes the form of (2.3), which is helpful in the

detection process [Dziu04], since it can be interpreted as parallel independent subchannels between Tx and Rx.

$$\mathbf{Y'} = \sum \mathbf{X'} + \mathbf{N'} \tag{2.3}$$

where:

- $\mathbf{Y'} = \mathbf{U^{-1}Y}$;
- **Y:** Fourier transform of **y;**
- $\mathbf{X'} = \mathbf{V^{H}X}$;
- **X:** Fourier transform of **x;**
- $\mathbf{\Sigma} = \text{diag}[\sigma_1, \sigma_2, \ldots, \sigma_{\min(NT, NR)}]$: singular values of **H**;
- **U,V**: unitary matrices containing the singular vectors of **H** after SVD;
- ^{H}: Hermitian operation.

The number of parallels subchannels depends on the rank of **H**, which is determined by a number of non-zero singular values. The existence of a high number of parallel subchannels is only possible in an environment rich in scatterers, since they generate many MPCs.

The main feature of MIMO is the ability to operate with a throughput greater than the capacity determined by Shannon's rule [Proa01], which represents the capacity of a SISO system, normally taken as reference:

$$C_{SISO[\text{bps/Hz}]} = \log_2(1+\rho) \tag{2.4}$$

where:

- ρ: SNR.

This means that, in MIMO systems, it is possible to establish multiple parallel subchannels, which operate simultaneously on the same frequency band and at the same time. With some assumptions, the theoretical capacity of such a system has been presented in [FoGa98]:

$$C_{MIMO\ [\text{bps/Hz}]} = \log_2 \left\{ \det \left[\mathbf{I}_{N_R} + \frac{\rho}{N_T} \mathbf{H_n H_n^H} \right] \right\} \tag{2.5}$$

where:

- $\mathbf{I}_{N_R}$: N_R dimensional identity matrix;
- ρ: defined at each Rx antenna as:

$$\rho = \frac{P_{Tx}}{N^2} b \tag{2.6}$$

- P_{Tx}: total BS transmit power;
- N: total noise power;
- $\mathbf{H_n}$: normalised channel transfer matrix related to **T** as:

$$\mathbf{H_n} = \frac{\mathbf{T}}{b} \tag{2.7}$$

- **T**: matrix containing the channel transfer gains for each par of antennas;

- *b*: defined as:

$$b^2 = E\left[|\mathbf{T}|\right]^2 = \frac{1}{N_T N_R}\sum_{m=1}^{N_R}\sum_{n=1}^{N_T}|\mathbf{T}_{mn}|^2 \tag{2.8}$$

Since the correlation of a channel is between 0 and 1, it is possible to derive the upper and lower bounds for capacity from (2.5). If there is no correlation between parallel paths, i.e., ξ=0, and additionally assuming that the signal is propagating without path loss, the maximum capacity is achieved (2.9), matrix **H** being the identity one:

$$C_{MIMO_{\xi=0}\ [\text{bps/Hz}]} = N_{\min}\log_2\left(1+\frac{\rho}{N_T}\right) \tag{2.9}$$

where:

- $N_{\min}=\min\{N_T, N_R\}$

On the contrary, the minimum capacity of a MIMO channel occurs when all subchannels are totally correlated, ξ=1:

$$C_{MIMO_{\xi=1}\ [\text{bps/Hz}]} = \log_2\left(1+N_{\min}\frac{\rho}{N_T}\right) \tag{2.10}$$

Having knowledge on the correlation between the subchannels at the Tx, power can be allocated in the most profitable way, making use of a distribution known as waterfilling [ATEM02], allowing to achieve maximum capacity in specified conditions.

A good way to quantify how much MIMO can increase capacity is to use the RMG (2.11), since it is defined as the relation between the capacity of a MIMO system relative to the SISO one:

$$G_{M/S} = \frac{C_{MIMO}}{C_{SISO}} \tag{2.11}$$

2.5 State of the art

A brief overview of the state of the art is presented in this section, in order to show what has been done in this field up to now, thus, emphasising the importance of this work.

The performance of several proposal extensions to the Alamouti space-time block code supporting very high transmit and receiver diversity have been evaluated by [MeRu04] for MIMO over HSDPA. The results of this paper show that the receiver complexity is kept approximately proportional to the transmitted data rate when, considering the combination of conventional Bell Labs Space-Time (BLAST) and those new extended Alamouti schemes, while offering a trade-off between diversity gain (thus, QoS) and supported data rate, allowing very high flexibility.

In order to compare MIMO techniques in HSDPA, such as Space Time Coding (STC) and BLAST,

[AsZe04] takes the effect of fast fading into account, as well as mobility and cell area coverage. It is shown that STC seems to perform better than BLAST, by means of improving the use of higher order modulations, leading to an improvement in cell capacity. Other conclusions are that adaptative MIMO achieves higher cell capacity than non adaptative one, leading to 300 kbps for STC and 200 kbps for BLAST, and that for a decrease of 9% of the cell area coverage, the cell capacity increases about 9% for STC and 13% for BLAST.

In [ViQR05], HSDPA capacity enhancement using MIMO in a pico-cell environment was studied. The MIMO channel model is the COST 259 Directional Channel Model, and the simulations were done considering 95% satisfied user ratio with 720 users distributed over the cell. Two types of MIMO sets were considered, using 2 and 4 isotropic antennas at each end of the link, half wavelength spaced, besides SISO. With Shannon Based Scheduling Algorithms (SBSAs), the BS shows average throughputs around 12 Mbps. An average capacity increase of 27 and 130 % is noticed for MIMO 2×2 and 4×4, respectively, when using the Round Robin (RR) scheduler, along with 4 and 28 % decrease average Frame Error Rate (FER) percentages comparing with SISO. With Fair Capacity SBSA, an average throughput increase of around 200 and 300 % was achieved for MIMO 2×2 and 4×4, respectively, which is quite impressive. A similar study was previously done in [ViRo04], the three possible scenarios being considered, i.e., pico-, micro- and macro-cells. In [ViRo04], the results for the RR scheduler are of 50 and 160 % average capacity increase for MIMO 2×2 and 4×4, respectively, along with 10 and 20 % decrease FER percentages compared to SISO, while for Maximum Capacity SBSA, a capacity increase of 30 and 60 % is achieved. The bigger capacity increase is achieved by using Fair Capacity SBSA, where results show that a 100 and 180 % average throughput increase for MIMO 2×2 and 4×4, respectively.

The measurements done by [MeML05] reveal that when using a BLER of 10 % as a target for the CQI, as specified by 3GPP, for comparison among different schemes, such as SISO, Space-Time Transmit Diversity (STTD) and Double Space-Time Transmit Diversity (DSTTD) for HSDPA, SISO is outperformed by about 6 dB by STTD. STTD also needs about 2 dB less SNR than the DSTTD to achieve 10 % BLER. Concerning throughput with DSTTD, a significant gain of 4 dB between the three and the two receive antenna scheme was measured; on the other hand, a fourth receive antenna does not change significantly the throughput. Furthermore, it is shown that the DSTTD scheme works very well in indoor scenarios with an antenna spacing of $\lambda/2$.

It has been proved by [SoSS07] that the expected capacity gains that MIMO schemes, for HSDPA, can provide with more complex receivers lead to a reduced point-to-multipoint Multimedia Broadcast Multicast Service (MBMS) transmission power, and guarantee an optimal distribution of QoS independently of the MBMS mode.

A novel spectral equaliser is introduced in [MaGH05] for single carrier systems, with applications to CDMA: UMTS FDD – HSDPA and HSUPA systems, SISO and MIMO. The performance of HSUPA is measured assuming 1 and 8 antennas at the BS, with a SF of 32 and a set of MTs with 8 or 24

antennas with 1, 3, 24 or 31 employed codes, which can be re-used or not by distinct MTs. When passing from 3 to 31 employed codes per MT, an approximately 3 dB loss is observed, however the throughput increases about 10 times

With the purpose of improving capacity and handle the near-far problem, a low complexity multi-user MIMO detector of QAM signals based on long scrambling codes is proposed by [NSZL06]. Simulations have shown that this proposal provides satisfactory performance enhancement, ensuring a promising technique for HSUPA, although the research in this field is still ongoing.

Although some work has been done in this area, due to the small life time of HSDPA, a lot of work is still needed, in order to confirm if MIMO is a mandatory technology to increase capacity on UMTS/HSDPA. In HSUPA, there has not been done much work concerning MIMO techniques as a way to increase capacity, mainly due to the fact that HSUPA is a very recent technology, even compared with HSDPA. However, as in HSDPA, the research in this matter is still ongoing. The use of MIMO jointly with HSPA+ has been standardised in Release 7, though there are no real implementations yet available, due to its recent standardisation.

2.6 Implementation Aspects

MIMO has been proposed as extensions to HSDPA and HSUPA in order to achieve high data throughput with significantly increased spectral efficiency. From the theoretical view point, it is a very attractive technology with several studies made and ongoing in this area proving so, and continuing to offer more and more solutions and improvements in terms of signal processing and algorithms, concerning MIMO transmission and detection, as well as type and size of antennas. However, from the practical point of view, there are a lot of constrains turning those idealistic theoretical results impossible to accomplish, mainly due to the size of the MT and the increase of power consumption inherent to multiple antennas, which might lead us to ask if MIMO is viable.

Regarding the recent standardisation of MIMO on UMTS/HSPA+ there are no real products yet available, and information about how these products (prototypes) could/should be is hard to find, possibly due to business confidentiality. Nevertheless, and despite the short amount of information, there are some interesting solutions, which give an optimistic answer to the previous question in terms of real MIMO implementations, solving mainly problems, such as MIMO transmission and reception, coding, detection and decoding of the signals, as well as the issue of fitting multiple antennas into a small MT without increasing much of its complexity and power consumption.

UMTS is based on CDMA, thus, a RAKE receiver should be used, which offers the ability to exploit the advantages of multipath propagation at a reasonable implementation cost. Considering the Vertical-BLAST (V-BLAST) architecture proposed in [WFGV98], this type of receiver can make use of various detection techniques, namely Zero Forcing (ZF), MMSE and Maximum Likelihood (ML). The

MIMO detector must separate the transmit streams using the spatial signatures that are created by a rich multipath fading environment, with the optimal detection strategy being the ML, which perform a search over all the possible transmitted symbol vectors and find the best candidate. However, the use of combined detector strategies might be attractive, since the ML detection strategy complexity increases with the number of antennas, leading to high complex systems, which are not desirable. On the other hand, if a ZF or MMSE detection strategy is used, despite its low complexity, the MIMO gains are easily lost, due to the fact of these strategies being much less accurate. Thus, a combined strategy would offer a better tradeoff between accuracy and complexity than a single strategy detector, although none is yet commercially available. Some of these proposed combined detectors can be found in literature, namely in [WBKK04] and [TrLF05]. Other interesting solutions worth mentioning are approximate ML detectors, which make use of several complexity reduction techniques e.g., spherical decoding and lattice reduction; some examples of these detectors can be found in [RuGW04], [GDBH04], [LePB06], [BWLY07], and [KiLB07]. However, despite the large amount of information concerning this matter, the lack of coherence among different authors is quite significant.

In [DGWB03], a physical layer receiver system architecture is presented for baseband processing, aiming essentially at the practical implementation to meet the demanding computational requirements of MIMO, which are MIMO detection and high throughput turbo decoding. For each of these functions, Application-Specific Integrated Circuits (ASICs) prototypes have been presented. A receiver architecture is proposed with the future possibility to ultimately integrate all of its components into a single ship solution, in order to reduce size and power.

The detector, in [DGWB03], has three main functions required to transform the incoming baseband samples into soft-hit estimates: channel estimation, dispreading, and symbol level MIMO detection. These three functions, including a full ML search on the received symbols, can be integrated in a practical silicon implementation for the MIMO data rates currently under consideration for HSDPA. The core area of the implementation is 7.3 mm^2 in a 0.18 μm technology and the device operates at 122.88 MHz with power consumption ranges from 101 mW for 4.8 Mbps up to 192 mW for the 19.2 Mbps rate at the 1.5 V supply voltage. Furthermore, the ASIC can handle configurations up to 4×4 QPSK, 2×2 8PSK (optional proposed modulation scheme leading to a richer set of schemes for consideration in MIMO scenarios) or 2×2 16QAM.

For the decoder, [DGWB03] proposes a turbo ASIC that supports a maximum throughput of 24 Mbps, based upon a radix-4 Maximum A Posteriori (MAP) processor operating in the log-domain. Although it is possible to precisely implement the radix-4 logsum calculation, it is extremely large and slow, instead an approximate logsum unit design is used, which makes use of a power reduction technique that has been observed to reduce the power consumption of the decoder by up to 81 % as a function of channel quality.

Two of the key components for MIMO implementation exist as fabricated silicon devices, and since the overall system complexity is manageable, all of the components could ultimately be integrated into a single chip solution for a MIMO HSDPA receiver capable of delivering DL packet data speeds up to

14.4 Mbps to an MT (e.g., a PDA or a laptop computer).

The size of the antennas is also an important factor, if not the most important one, since in what regards to size the MT can be very restrictive allowing in some cases a maximum of two antennas (e.g., a mobile phone). A Planar Inverted-F Antenna (PIFA) with fractal shaped edges configuration, a two PIFA configuration suitable for MIMO, and a quad inverted-F antenna, are three solutions for this problem, presented in [GuMP04], [Peix06] and [MCRS05] respectively.

In [GuMP04] the antenna has been implemented in microstrip planar technology, and a finite ground plane of 100×45 mm^2 was chosen to represent a common handset size. Due to the use of fractal shaped edges in a PIFA configuration, the patch element length has been reduced by 62 % in comparison with the simple rectangular patch, on which it was first based on, for design purposes. Regarding the very small size of the patch element, it turns out that it can be successfully used in compact multi-element antenna arrangements. In Figure 2.5, a photo of the case studied in [GuMP04] is shown for a N_T×2 configuration, since a significant throughput increase is also achievable with only two antennas at the receiver compared to SISO.

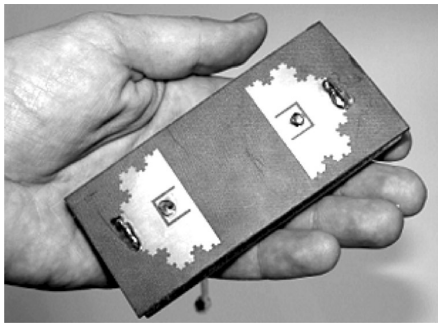

Figure 2.5 Photo of the two-element fractal MIMO antenna prototype (extracted from [GuMP04]).

The two identical fractal PIFA elements have been disposed to ensure physical symmetry of the antenna structure, and the two element arrangement was based on the same structure of the one element, that is a 1.57 mm thick Duroid 5880 substrate is used on top of a 10 mm thick air gap and a ground plane of 100×45 mm^2 is again taken into account. Furthermore, because three different bands (GSM1800, UMTS and Hiperlan2) were studied, it is important to notice that the use of fractal shapes in antenna field allows reducing the mutual coupling in multi-element antenna arrangements, which could be a major problem in multiple multiband antennas in small terminals. In spite of the small structure size, the mutual coupling between elements is acceptable for MIMO.

This type of antennas seems to be a viable option for mobile MIMO terminals, since they meet the requirements of size, present acceptable mutual coupling levels and do not have radiation patterns with strong directivity properties [GuMP04].

The configuration presented in [Peix06], consists of two PIFAs on top of each other, each one having an L-shaped slot, and using three shorting pins to minimise antenna length. The distance between them is only 10 mm, this configuration being suitable for MIMO applications, in what regards small handsets. The consideration for cellular communications (GSM 1800 and UMTS) and WLAN

(IEEE 802.11b) multi-standard terminals is viable, since the antenna system presents wideband characteristics. Besides the fact of the two elements being closely spaced, the correlation is low, hence, anticipating a significant increase in MIMO capacity. The design procedure has been validated, regarding the good agreement obtained between numerical simulation and experimental results.

A quad inverted-F antenna has been proposed by [MCRS05], which is a realistic antenna array that could be built into a mobile phone. The size of this array incorporating four individual antennas is only 34×34 mm^2, Figure 2.6, although high spatial correlation between the antennas might be expected due to the small size. In this study, throughput measurements of Double Space Time Transmit Diversity with Sub Group Rate Control (DSTTD-SGRC), a candidate for the MIMO extension of UMTS, are presented, with emphasise on the quad inverted-F antenna, and comparisons between it and some linear arrays.

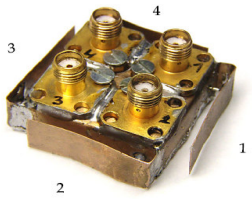

Figure 2.6 Picture of the whole quad inverted-F antenna (extracted from [MCRS05]).

The frequency used in measurements was the 2.45 GHz ISM (Industry, Scientific and Medical), because it is very close to the UMTS frequencies with similar wave propagation, thus, resulting in representative measures for UMTS. In order to reduce hardware complexity, the number of antennas at the MT should be kept at the minimum, therefore, this work, [MCRS05], focus on the throughput comparison between arrays composed by two antennas, and in the quad inverted-F case, which combination of its four elements should be used. The conclusions drawn show that it makes no difference which two of the four elements of the quad inverted-F antenna are used for reception, since the multiple combinations yield nearly the same throughput. Additionally, when using three elements of the quad inverted-F antenna, an optimum tradeoff between handset complexity and performance is achieved. Moreover, the measurements have shown that the quad inverted-F antenna is perfectly suited as an internal MIMO antenna of an MT, and it performs approximately like a linear antenna array with 0.5 λ spacing.

Other studies have been made with interesting results, yet there are no practical implementations of those products. One of them, worth mentioning, is based on the concept of Virtual Receive Antenna (VRA), which simulations results show that it outperforms the Multiple Input Single Output (MISO) ML detector and supports less Rx than TX antennas, which, in DL, is the most important case. More detailed information about this can be found in [So07].

Concerning the BS, the amount of information is even fewer, since it only refers to the number of antennas not regarding size and power issues, which, similar to MTs, are the main constraints, though on a different scale. However, in [GaKg07], some solutions for MIMO BSs were discussed and

proposed as attractive ones, presented in the context of a workshop talk, leading to a reduced amount of technical information. Although some details are worthwhile mentioning, such as, the preferable use of X-Polarised dipoles in the arrays arrangement in a two column configuration antenna, with high isolation between columns (> 25 dB) and a distance between columns of λ/2.

Furthermore, despite the lack of information regarding power issues, two approaches can be foreseen. The first one assumes the same feeding power for all the antennas as for SISO, i.e., assuming, e.g., 44 dBm, all antennas would be fed with this power. In this approach, there is a need to add a power amplifier for each new added antenna, which leads to significant additional upgrade costs, since the power amplifier represents a non-negligible share in the BS budget. Contrary, the second approach considers that the overall power available for the SISO system is split among the antennas, i.e., the additionally introduced antennas for the use of MIMO are fed with a portion of the power used for SISO, proportional to the number of antennas. Hence, there is no need for additional power amplifiers, lowering the upgrade costs, substantially. Nevertheless, in the second approach, lower throughputs are expected, thus, despite the higher costs inherent to the first approach, the higher coverage and throughputs, must be considered, in order to attain conclusions on which is the most suitable approach, for a specific scenario. In other words, a tradeoff between, higher performance and cost is inevitable. These two approaches are both applicable for MTs as well.

Regarding the correlation between signals, inherent to the use of multiple transmitting antennas, visual impact and space restrictions, the space between the BS antennas might be relevant. Two approaches are shown, in Figure 2.7, for X-Polarised antennas. The first approach consists of using previously separated columns of 2 or 3 m, used to combine receive spatial diversity with polarisation diversity; this way, for MIMO, the probability of uncorrelated signals is higher, than if the antennas are closely spaced. This is the case of the second approach, where the two antennas are placed closely (e.g. λ or λ/2), which might lead to the use of a single enclosure antenna box. Higher levels of correlation are expected, however, when less visual impact is required or there are space restrictions, it is a viable option.

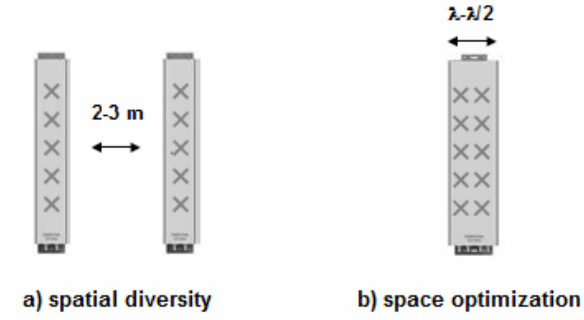

Figure 2.7 BS antenna configuration (adapted from HoTo04).

In conclusion, a lot has to be done in this area in order to obtain the best configuration of MIMO parameters for UMTS. With the measurements and simulation results of the various studies seeming attractive, there is still the need to put them into practice in a viable way, meaning the less changes possible in MT and BS, and extracting the maximum of its benefits.

Chapter 3

Model Development

This chapter provides an overview of the models that are related to the scope of this thesis. First the channel model is described, followed by the description of the various scenarios to which it can be applied. Furthermore, the description of the model used to measure the capacity improvements of MIMO, is presented, finalising with the model used to calculate SISO and MIMO throughputs for the various systems considered in this thesis.

3.1 Channel Model

The performance of MIMO is highly dependent on the environment, which implies the need for an appropriate channel model, allowing for the evaluation of which situations are the most adequate for its use, as well as for assessing the performance improvements to be expected from MIMO from different adaptative algorithms [MaCo04].

There are three crucial radio channel parameters: path loss, fading and delay. The first two were already considerate in first generation mobile systems, while the later has only started to be considerate in second generation ones. A new variable must be taken into account, i.e., angle, since Angle of Arrival (AoA) and Angle of Departure (AoD) are now the additional contributing factors in adaptative algorithms.

In general, channel models can be divided into three categories: statistical, geometrical and mixed. Statistical models assume that signals arrive at the receiver according to a specific statistical distribution, whereas in geometrical models the received signal only depends on the geometrical properties of the propagation environment, with its accuracy being entirely dependent on the environment reproduction. Geometrical models can reach a higher accuracy, but demand a very deep knowledge of the environment, while statistical models are more flexible, but their accuracy is not very high. Mixed models are a combined solution of the two mentioned above, since they are able to meet the accuracy-complexity compromise.

In this thesis, a mixed channel model is used: the GBSB channel model, which was developed by the Group for Research On Wireless (GROW) of Instituto Superior Técnico (IST) and is presented in detail in this section [MaCo04]. The idea beyond the GBSB model is that the multipath characteristic of a radio channel is the result of signal bounce over numerous scatterers. Measurements results have shown that in most cases signals arrive in clusters from a particular direction; the model considers each contributor as a cluster of individual scatterers, where each scatterer originates a single-specular reflection, being characterised by its own reflection coefficient (3.1); thus, each signal bounce over a scatterer generates one MPC, as shown in Figure 3.1. The cluster's shape is provided by a Gaussian distribution of scatterers, while a Poisson distribution provides the number of scatterers.

$$\Gamma_s = |\Gamma_s| e^{j\Phi_s} \tag{3.1}$$

where:

- $|\Gamma|$: the magnitude of the reflection coefficient, which has a uniform distribution in [0,1];
- Φ_s: the phase of the reflection coefficient, which has a uniform distribution in [0,2π];

In conclusion, the GBSB, can be considered as a combination of deterministic (parameters like AoA, AoD and Time of Arrival (ToA), which are computed based on environment geometry) and statistical features (coordinates of scatterers are generated randomly, and each scatterer is described by a random reflection complex coefficient).

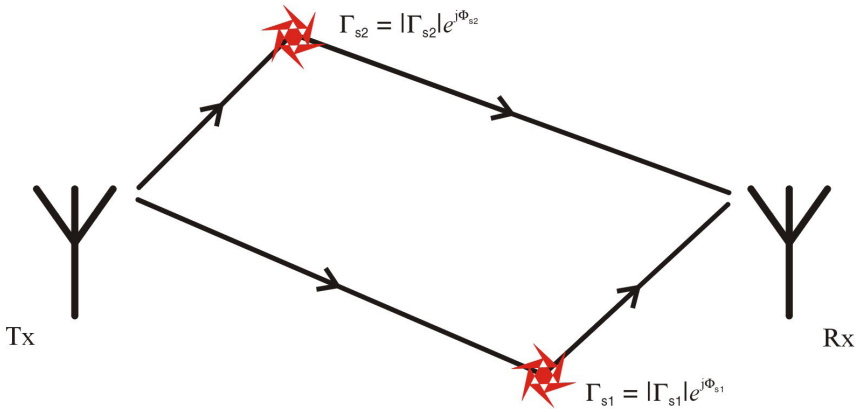

Figure 3.1 Scatterers in GBSB model (extracted from [Maćk07]).

The output parameters (amplitude, phase, AoA, AoD and ToA) for each MPC are calculated according to the positions of Tx and Rx antennas, and the distribution of scatterers. To simplify calculations in this model, scattering by rough surfaces, diffraction, Multi Bounce and other aspects of propagation are not included [LiRa99].

Regarding the application of this channel model to MIMO, the Geometry-based Stochastic Channel Models (GSCM) is briefly described, which characterises the impulse response by the wave propagation between Tx, Rx, and scatterers; in order to reflect reality better, scatterers are placed in a stochastic random manner.

An example of a GSCM is the Geometrically Based Single Bounce MIMO Channel Model [Koko05]. The main assumption of this model is that the MIMO system can be treated like *n* independent SISO ones, meaning that each pair of input and output antennas can be treated separately, therefore, the GBSB radio channel model can be used without significant modifications. It is worth while to notice that clusters of scatterers are common for the pairs of antennas, and because each pair has it own set of multipath components, the delays, signal phase and amplitude are different. The total number of MPCs is equal to the number of scatterers multiplied by the number of antenna pairs; despite the small spacing between antennas, the CIR for each multipath link is different if the number of scatterers is significant.

3.2 Scenarios

Usually, three main typical scenarios are taken into account: pico-, micro- and macro-cells. The main feature that distinguishes these scenarios is the location of the BS and the MT with reference to the deployment of scatterers [MaCo04]. Another important factor that is helpful to sort the mentioned scenarios is the radius of the cell. According to the definition of Prasad [Pras98], the pico-cell has radius smaller than 200 m, the micro-cell has radius within [200, 1000] m, and the macro-cell is larger than 1 km; however, these are not standardised sizes.

The area of the pico-cell is bounded by a circle, with the BS at its centre. The location of the MT is not defined, and depends on the actual position of the user. The LoS component exists in this scenario. A density of scatterers, Figure 3.2, is specific to each individual environment. The pico-cell is usually located inside buildings, e.g., hall of shopping centres. The dimensions of the place, where the pico-cell is established, mainly influences the radius of the circle.

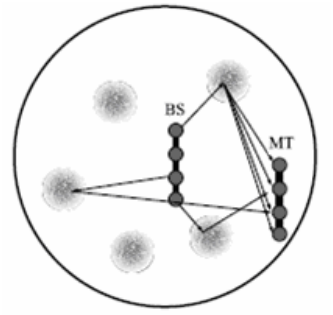

Figure 3.2 Pico-cell scaterring model (extracted from [KuCo07]).

In micro-cells, the scattering takes place in the surroundings of both the BS and the MT, and also in the region in between. The micro-cell scenario usually occurs when both the BS and the MT are located bellow rooftops, e.g., a street in the urban area with LoS. Scatterers are deployed, with the same density, around the BS, the MT, and in the zone in between. The street width should bound the considered region when modelling a street-type environment. The area of multipath propagation has the shape of an ellipse, Figure 3.3, whose foci are the BS and the MT, and the minor axis are determined by the width of the street.

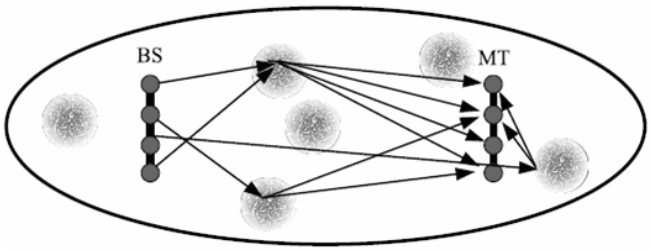

Figure 3.3 Micro-cell scattering model (extracted from [KuCo07]).

In the macro-cell scenario, the scattering contributions are located in the area around the MT, which is a consequence of the height of the BS antenna being larger than the MT one. In the macro-cell case, the region of influence has the shape of a circle, Figure 3.4. The scaterring contributions in the vicinity of the BS will be disregarded and there is no LoS component.

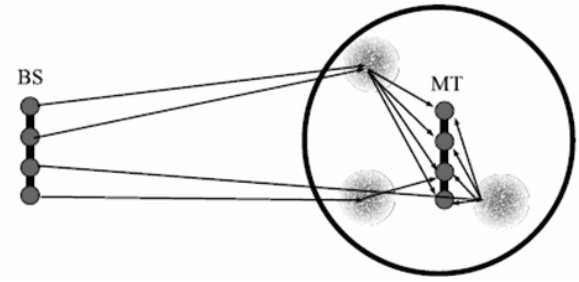

Figure 3.4 Macro-cell scattering model (extracted from [KuCo07]).

3.3 Relative MIMO Gain Model

3.3.1 Original RMG Model

In order to predict the improvements in capacity of using MIMO over SISO based on simulation results, the RMG Model, [KuCo07], was chosen, since it seems to be the one that fits better the demands and scope of this thesis. The description of such model is presented next, based on [KuCo07]. The model of the capacity gains of MIMO described in [KuCo07] is based on simulation results from a MIMO radio channel simulator that takes into account the GBSB channel model described in Section 3.1. Moreover, the RMG model assumes that the antennas are isotropic.

The RMG is defined as the ratio between the MIMO and SISO capacities of a radio link (2.11), with the RMG model being a statistical model developed to approximate the distribution of the RMG, based on simulation results, making it easier to be incorporated into system-level simulators. The simulation parameters are shown in Table C.1. In order to maintain a low-complexity for the model, the distribution of the RMG is modelled by an inverse Sigmoid function (also known as logistic function or *S*-shape function), which is completely modelled by its mean and variance. The general sigmoid function is given by [Segg03]:

$$\delta(x,\mu,s) = \frac{1}{1+e^{-\frac{x-\mu}{s}}} \tag{3.2}$$

where:

- μ: mean value of the distribution;
- s: determines the slope, which is related to σ^2 by:

$$\sigma^2 = \frac{\pi^2}{3}s^2 \tag{3.3}$$

- σ^2: variance;

Both the mean value and the variance depend on the number of Tx and Rx antennas, while the mean value also depends on the distance between Tx and Rx, whereas the variance has a dependency on the cell type.

Since, for a certain number of Tx and Rx antennas, the variance is very low for pico-, micro- and macro-cells, this means that the slope of the sigmoid function does not change much within the same cell range, therefore, it has been assumed that the slope is constant within a cell type.

Focusing on obtaining a model that gives a realistic statistical RMG as a result, the inverse of the distribution is required, and it is given by:

$$g(u,\mu_{RMG},\sigma_{RMG}) = \mu_{RMG}(d,N_T,N_R) - \frac{\sqrt{3\sigma^2_{RMG}(d,N_T,N_R)}}{\pi}\ln\frac{1-u}{u} \tag{3.4}$$

where:

- u: random value with a Uniform distribution, i.e., $u = U[0,1]$;

- d: distance between BS and MT;
- $\sigma^2_{RMG}(d,N_T,N_R)$: variance depending on the cell type, N_T and N_R;
- $\mu_{RMG}(d,N_T,N_R)$: average RMG depending on the cell type, N_T and N_R;

Parameter $\sigma^2_{RMG}(d,N_T,N_R)$ is shown in Table C.2, for all antennas configurations studied and different cell-types, while in Table C.3 and Table C.4 $\mu_{RMG}(d,N_T,N_R)$ is shown, which has been approximated by 0^{th} and 1^{st} order functions. In what concerns Table C.3, it shows the results for the scenarios with either 2 Tx and/or 2 Rx antennas, these configurations being approximated by a 0^{th} order function. For these configurations, the cell-type is not very relevant, thus, they can be defined for all distances considered. The higher antenna configuration results are shown in Table C.4, and since for these cases the cell type is relevant, the differences for the different distances are depicted.

The largest relative mean error and relative mean square error for the RMG are obtained for the 16×16 MIMO system, with values of 5.9 and 7.5 % respectively.

The results from the RMG model are plotted in Figure C.1 for a 4×4 MIMO system and distances of 100, 200 and 300 m. The model is a little bit more optimistic than the simulation results in the high region, yet it remains within the capacity limits that can be obtained by MIMO [KuCo07].

In the RMG model, accuracy had to be traded off with complexity, since the more antennas the system has the less accurate the model becomes. A relative root mean error below 6% and a relative mean square error below 7.5% show that the use of simple 0^{th} or 1^{st} order equations gives already a good fit of the mean value of the RMG for different distances. Besides the exception of the antenna configurations with 2 or 16 Tx antennas, the distribution of the *RMG* shows a good fit with a root mean square error of around 5%, though the relative mean square error is below 7% for all antenna configurations. In Figure 3.5, one can see the modelled values of the RMG plotted for various antenna configurations and it variation with distance.

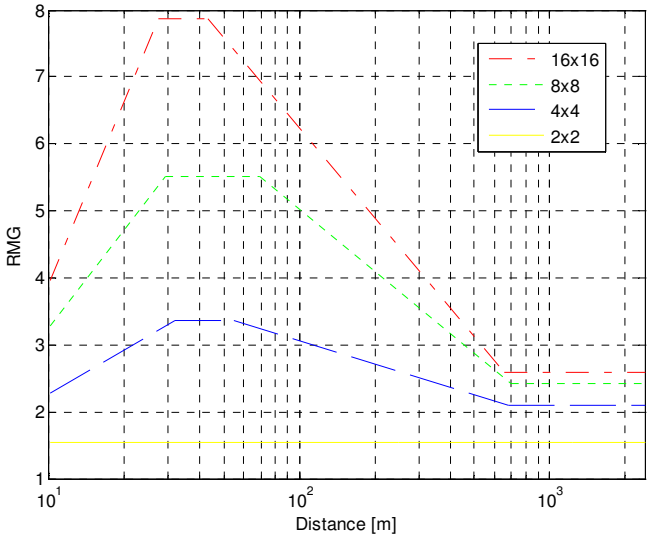

Figure 3.5 Modelled distribution of the RMG for multiple antenna configurations (adapted from [KuCo07]).

The RMG increases in the pico-cell region, distances up to 30 m, with the highest antenna configuration having the steepest slope. After 30 m, the RMG remains more or less constant until it enters the micro-cell region where it starts to decline. This decline stops at the macro-cell region, where the RMG has shown to be constant. Independently of the cell-type, the highest gains are achieved by the 16×16 (reaching almost 8) system, whereas the lowest gains are obtained for the 2×2 system, which present an approximately constant gain for all the distances (cell-types) considered. Thus, as expected, a tradeoff between capacity gain and complexity is inherent.

3.3.2 SNR Variation Effect

Regarding the scope of this thesis, it is inherent the need to assess the influence on the RMG of the SNR variation. With the objective of doing so, 50 simulations were carried out, since it seemed to be a good compromise between time and results validity.

For the simulations, four different distances were taken into account, despite the fact that there are three different scenarios, though for the pico-cell scenario it is relevant to simulate two different distances regarding the different slopes of the RMG mean function, within this cell type, Figure 3.5. The distances considered were 20 and 50 m for the pico-cell, 400 m for the micro-cell, and 1000 m for the macro-cell. Note that these values are about the middle distances for the four different RMG mean slopes, with the exception of the 2×2 MIMO system that presents an approximately constant behaviour, Figure 3.5. The antenna configurations considered for simulation, were the 2×2, 2×4 (4×2) and the 4×4, since these are the configurations that fit better the demands of this work, besides being the ones that are more suitable to be implemented, due to problems that range from technical details (e.g., size constraints, limited power and detection complexity), to urban details like, the visual impact that, e.g., 8 antennas would have on the top of a building, not to mention 16.

Concerning the SNR variation, the range of values considered is from 5 to 30 dB, with an interval of 5 dB, hence, six different values were taken into account. The 10 dB value is considered, since it is the reference value, Table C.1, and the maximum SNR simulated value is 30 dB, since it is a value high enough to give a good perspective of the RMG behaviour with different SNR values. The results obtained are depicted in Figure C.2, Figure C.3, and Figure 3.6, for the 2×2, 2×4 (4×2) and 4×4 antenna configurations, respectively, where pico20 and pico50 stand for the distances simulated within the pico-cell scenario, i.e., 20 and 50 m, respectively.

It is possible to observe that the differences between the RMG value for the default SNR value, and for the other ones considered, is of small relative magnitude, hence, the possibility to consider no difference at all seems a valid option. However, this option can not be taken for granted without stressing out the relative mean error to the 10 dB of SNR value, for each of the considered antenna configurations. These values are presented in Table 3.1, and it turns out that for the 4×4 system, the relative mean error is significant, whereas for the other three antenna configurations, the option is assumed to be valid, hence, no difference in the RMG value is considered independently of the SNR

value, with the relative mean error of doing so being below 5.5 %.

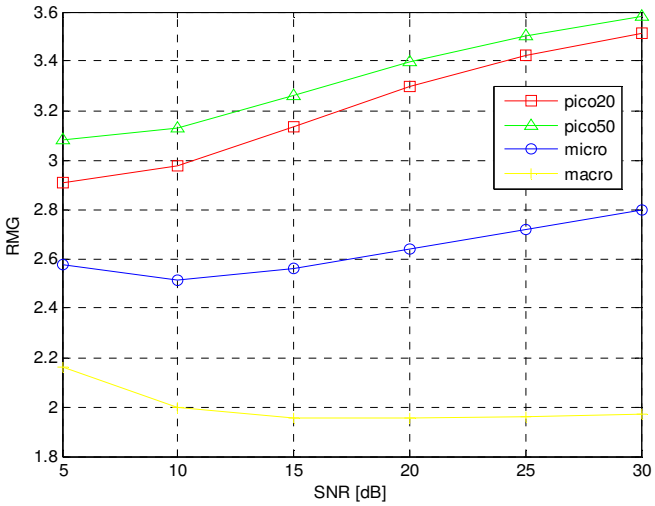

Figure 3.6 RMG variation with the SNR for a 4x4 MIMO system.

Table 3.1 Relative mean error to the default SNR value.

	Relative mean error to the SNR of 10 dB [%]			
MIMO	**Pico20**	**Pico50**	**Micro**	**Macro**
2×2	5.4	4.7	4.8	5.3
2×4 and 4×2	4.0	3.4	3.8	4.3
4×4	9.2	7.4	5.3	2.9

For the 4×4 system, the effect of the SNR in the RMG value has to be taken into account; however, despite the option considered, the RMG must remain a continuous function, thus, a different corrective value for each simulated distance is not a valid option, because this would lead to an RMG non-continuous function. Hence, the option of taking the mean of the 4×4 system curves, Figure 3.6, is analysed, and the relative mean error, of each simulated distance, to these new mean values is stressed out. After this analyse, the resulting relative mean errors for the curves of each simulated distance related to the mean of the curves are 3.8, 2.2, 0.7 and 6.9 % for Pico20, Pico50, Micro and Macro, respectively. With the error being below 7%, the mean of the curves is the considered option.

Regarding the previous results, the function that accounts for the effect of the SNR variation on the RMG is given by (3.5), were for SNR values higher than 30 dB it is assumed that the RMG takes the same value as for SNR equal to 30 dB, due to the lack of results for higher SNR values. It should be pointed out that the mean of the curves has been normalised, with the objective of giving a correction value to the default RMG, for each SNR value.

$$G_{M/S\ SNR} = \begin{cases} 1.0 \times G_{M/S} & , \quad 5 \le \rho_{[dB]} \le 10 \\ (0.00533 \times \rho_{[dB]} + 0.9465) \times G_{M/S} & , \quad 10 < \rho_{[dB]} \le 30 \\ 1.1064 \times G_{M/S} & , \quad \rho_{[dB]} > 30 \end{cases} \tag{3.5}$$

3.3.3 Antenna Spacing Variation Effect

In order to account for the antenna spacing effect, which is the same of accounting for the correlation of the signals due to the more or less space between the BS or MT antennas, two different cases of antenna spacing have been considered, namely λ and λ/2; thus, four different cases are possible, when combining the different spacing in the Tx and Rx, where the λ-λ (BS-MT) case is the default one, Table C.1.

Similar to the evaluation of the SNR variation effect, 50 simulations were performed, with the simulation results for the different antenna spacing also presenting differences to the default value of low relative magnitude. However, despite the option of considering no difference due to antenna spacing, the relative mean error to the default antenna spacing has been calculated and is presented in Table 3.2, where 2×2, 2×4 and 4×4 stand for the MIMO systems, with the results for 2×4 being also valid for the 4×2 MIMO configuration.

Table 3.2 Relative mean error to the default antenna spacing.

Ant. Spacing		**Relative mean error to the default antenna spacing [%]**											
BS	**MT**	**Pico20**			**Pico50**			**Micro**			**Macro**		
		2×2	**2×4**	**4×4**	**2×2**	**2×4**	**4×4**	**2×2**	**2×4**	**4×4**	**2×2**	**2×4**	**4×4**
λ	λ/2	1.2	2.0	3.9	0.9	3.4	4.2	1.3	5.7	2.6	0.4	4.5	0.2
λ/2	λ	2.6	1.2	3.2	3.7	0.7	1.8	0.4	0.7	7.5	<0.1	<0.1	<0.1
λ/2	λ/2	2.0	4.3	0.2	1.1	2.4	2.6	1.5	5.7	9.0	0.4	4.5	0.1

The error for not considering the antenna spacing in the cases of 2×2 and 2×4 (4×2), is below 6 %, which is assumed to be negligible, hence, no difference is considered related to the default RMG. For the 4×4 antenna configuration, the errors presented for the λ-λ/2 case are also negligible, while for the λ/2-λ and λ/2-λ/2 situations, in a micro-cell scenario the errors due to not considering any difference are significant, having values of 7.5 and 9 %, respectively. Therefore, the effect has to be considered.

The first approach to the problem is to consider the same correction value for all the other scenarios as for the micro-cell one, this way guaranteeing the continuity of the RMG function. However, the errors obtained for this option are even higher than the previous situation, with the exception of the micro-cell scenario, as expected. The second approach consists of normalising the values of the RMG as a function of the antenna spacing for each distance considered, to the default value for each distances, and then to consider the mean value as the correction value to be applied to the default values, thus, guaranteeing the continuity of the RMG function. However, when considering the values presented in Table 3.3 the errors are still above 6 %, hence, they should not be neglected, and a third approach has to considered. The third approach consists of varying the correction value obtained in the second approach, in order to obtain a relative mean error below 6 %. After some attempts, the values were reached, Table 3.3, jointly with the associated relative mean errors for the three approaches, where the worst values are highlighted in red and the considered ones highlighted in

green. The function that describes the effect of the different antenna spacing for the 4×4 systems is given by (3.6), while for the other three configurations the default value of the RMG is considered.

Table 3.3 Correction values and relative mean errors for the 4×4 system.

Approach	Ant.		Relative mean error to the default antenna [%]				Correction value
	BS	MT	Pico20	Pico50	Micro	Macro	
First	λ/2	λ	10.3	9.1	0	7.5	0.925
	λ/2	λ/2	9.2	6.6	0	9.1	0.910
Second	λ/2	λ	3.7	2.4	7.4	0.6	0.994
	λ/2	λ/2	3.0	0.2	6.8	3.0	0.972
Third	λ/2	λ	5.5	4.2	5.4	2.5	0.975
	λ/2	λ/2	4.6	1.9	5.0	4.6	0.955

$$G_{M/S\ Corr} = \begin{cases} 1.0 \times G_{M/S}, & \mathrm{BS}_{spacing} = \lambda,\ \mathrm{MT}_{spacing} = \lambda \\ 1.0 \times G_{M/S}, & \mathrm{BS}_{spacing} = \lambda,\ \mathrm{MT}_{spacing} = \lambda/2 \\ 0.975 \times G_{M/S}, & \mathrm{BS}_{spacing} = \lambda/2,\ \mathrm{MT}_{spacing} = \lambda \\ 0.955 \times G_{M/S}, & \mathrm{BS}_{spacing} = \lambda/2,\ \mathrm{MT}_{spacing} = \lambda/2 \end{cases} \tag{3.6}$$

3.4 Link Model

Regarding the scope of this thesis, a model to calculate the throughput as a function of distance has been developed. The link model can be divided into two major throughput calculations:

- SISO;
- MIMO.

The throughput is calculated considering that there is only one user in the cell (single user situation), and four different systems are taken into account, namely Release 99, HSDPA, HSUPA and HSPA+. Moreover, besides DL and UL being defined for Release 99 and HSPA+, the model contemplates the different number of HS-PDSCH codes for HSDPA, and two optional modulations for HSUPA the BPSK or QPSK, and 16QAM or 64QAM for HSPA+ DL.

For Release 99, the throughput presents a stepwise behaviour as a function of the E_b/N_0, Table E.2, meaning that it can take values of 384, 128 or 64 kbps regarding the value of E_b/N_0. It is considered that these values are at the application level, thus, no RLC, MAC or application overheads are subtracted. In what regards BER, it is not considered for the Release 99, SISO throughput calculation, since these throughput values are at the application level; however, for the MIMO throughput calculation, BER is subtracted to the throughput, due to the fact that the use of MIMO brings additional complexity to the signals detection. The procedure for Release 99 is almost the same for DL and UL, with the only differences residing in the path loss calculation and the BER value, since, different

parameters are inherent for each link direction, namely: frequency, signalling and control power percentage and modulation.

For HSDPA, from (3.7) and (3.8), the maximum throughput at the physical layer, for 16QAM (4 symbols per bit), is 0.96 Mbps per HS-PDSCH code, thus, resulting in 4.8, 9.6 and 14.4 Mbps for 5, 10 and 15 codes, respectively. However, in real networks, only 14 HS-PDSCH codes are actually used for data, since usually 2 HS-PDSCH codes must be reserved for signalling and control (HS-SCCH and Associated DCH (A-DCH)). From now on, it is referred 15 HS-PDSCH codes, although the analysis performed considers that only 14 HS-PDSCH codes are available for data. Therefore, the maximum throughput at the physical level is 13.44 Mbps.

$$S_{R[\text{MHz}]} = \frac{T_{P/C[\text{Mbps}]}}{S_b} \tag{3.7}$$

where:

- S_R: Symbol rate;
- $T_{P/C}$: physical layer throughput per code;
- S_b: Symbols per bit.

$$SF_{16} = \frac{R_{c[\text{Mcps}]}}{S_{R[\text{MHz}]}} \Leftrightarrow T_{P/C[\text{Mbps}]} = \frac{R_{c[\text{Mcps}]}}{SF_{16}/S_b} \tag{3.8}$$

Considering a 75 % coding rate, the maximum throughput at the physical layer is 3.6, 7.2 and 10.08 Mbps, for 5, 10 and 15 HS-PDSCH codes, respectively. At the RLC layer, considering a reduction of 11 %, due to the overheads of the MAC and RLC layers, the maximum achievable throughput is 3.2, 6.41 and 8.97 Mbps, for 5, 10 and 15 HS-PDSCH codes, respectively. In order to calculate the throughput at the application level, for both SISO and MIMO, despite the consideration of an application overhead of 5 %, which leads to a more realistic throughput of 3.04, 6.09 and 8.52 Mbps, it is necessary to know the SINR to take BER into account, since for each SINR a different BER is considered, see Annex G.

Concerning HSUPA, the main differences from HSDPA are related to the fact that in the former the number of HS-PDSCH are not differentiated and the modulations taken into account are BPSK and QPSK, as previously mentioned. Additional parameters, such as the antenna diversity, due to polarisation diversity, are now considered.

With BSPK modulation, regarding MT limitations, the maximum physical layer throughput is 1.45 Mbps, already considering a coding rate of 75 %, thus, leading to a RLC layer throughput of 1.42 Mbps, due to a MAC and RLC overhead of 2 %. Similar to HSDPA, in order to calculate the throughput application for both the SISO and MIMO, the value of the E_b/N_0 has to be known, since for each E_b/N_0 a different BER is considered, despite the consideration of a 5 % application overhead which leads to a maximum throughput of 1.35 Mbps, without BER.

The use of QPSK in HSUPA enhances the maximum physical throughput to 5.74 Mbps [PWST07], although the value considered is 5.5 Mbps, since this is the maximum value achieved in the

simulations performed in [PWST07], Figure 2.3. After considering a coding rate of 75 %, similar to HSUPA for BSPK, the maximum physical throughput value is 4.125 Mbps. Due to MAC and RLC overheads, the maximum throughput at the RLC layer is 4.04 Mbps. For the application throughput, the procedure is the same as for HSDPA and HSUPA with BPSK, leading to a maximum throughput, without taking BER into account, of 3.84 Mbps.

With one of the main upgrades introduced by HSPA+ being the use of HOM, in both links, the algorithm to calculate the application throughput differs from HSDPA and HSUPA for DL and UL, respectively, mainly due to the consideration of the enhancements introduced by the new modulations, 64QAM for DL and 16QAM for UL.

From (3.8), for 64QAM (6 symbols per bit), the maximum throughput at the physical layer is 1.44 Mbps per HS-PDSCH code, thus, resulting in 21.6 for 15 codes. Similar to HSDPA, only 14 HS-PDSCH codes are considered, thus, resulting in a maximum physical layer throughput of 20.16 Mbps. For HSPA+ DL, due to the lack of information, the coding rate considered is of 75 % as well as the MAC and RLC overheads of 11 %, which will lead to a maximum throughput at the physical layer of 15.12 Mbps, and 13.46 Mbps at the RLC one. The calculation of the application throughput is limited by the same problem of the previously described systems, with the application overhead considered being the same and equal to 5 %, which without the BER consideration leads to a maximum throughput of 12.79 Mbps. In HSPA+, the throughput for the 16QAM modulation is the same as for HSDPA with 15 codes, for all layers, with the only difference residing in the fact that a lower SNR value is required in order to achieve the maximum throughput value.

For HSPA+ UL, the considered modulation is 16QAM. Similar to HSUPA with QPSK, the maximum considered value for this throughput is 11 Mbps, since it is the maximum value achieved by the simulation in [PWST07], despite the maximum theoretical possible value of 11.5 Mbps. With an enhancement in the physical layer maximum throughput of about 7.2 Mbps, when considering a coding rate of 75 %, regarding a maximum physical layer throughput of 8.25 Mbps. After taking the MAC and RLC overheads of 2 % and the application overhead of 5 %, the maximum RLC layer throughput is 8.09 Mbps, and the application throughput without considering BER is 7.68 Mbps.

It is important to point out the fact that, even though it is considered that HSDPA uses two modulations, QPSK and 16QAM, the former being used for lower values of SINR and the latter for higher ones, for the BER calculation it is used a 16QAM MIMO detector. The reason for this is that in Figure B.1, as well as in its origin [HoTo06], there is no solid information regarding the value of SINR on which the transition between QPSK and 16QAM is done, thus, the worst scenario is used, since a higher order modulation leads to higher BERs.

The maximum throughput values for the considered systems are summarised in Table E.2, jointly with the corresponding SNR and/or E_c/N_0 minimum value for which these throughputs can be achieved, where the values for Release 99 are based on [Corr08].

The objective of this model is to calculate the throughput of the previously described systems for a certain scenario when using MIMO. Inherent to the definition of each scenario, Section 3.2, a set of distances are considered, and for each distance the correspondent SINR or E_c/N_0, is mapped onto throughput, using Figure E.1, Figure E.2 and Figure E.5 for HSDPA, HSUPA with BPSK and HSUPA with QPSK respectively, and using Figure E.4 and Figure E.5 for HSPA+ DL and UL, respectively.

SNR, as well as all the parameters that are associated to it (e.g., EIRP and path loss), are calculated based on the link budget presented in Annex D. The interference margin is not considered, due to a single user situation. Furthermore, besides the model being based on a snapshot of the link at a certain distance, the slow and fast fading margins were taken into account, with the former being described by a Gaussian distribution and the latter by a Rayleigh one.

Underlying the objective of the link model is the need to compare SISO and MIMO systems in terms of throughput as a function of distance. With this in mind, the model gives both as result. The SISO throughput, T_{SISO}, as a function of distance is given by (3.9), while (3.10) gives the MIMO throughput, T_{MIMO}. In (3.9), an ML SISO detector is used, with the limitation of being BPSK for all systems, an approximation that has to be made due to the lack of coherent information; however, doing this can only increase the SISO throughput, since for lower order modulations the BER is lower,

$$T_{SISO[\text{Mbps}]} = T_{P[\text{Mbps}]} \times \left[(1 - O_{MAC\&RLC}) \times (1 - O_{App}) \times \left[1 - \beta_{SISO}(\rho) \right] \right] \tag{3.9}$$

where:

- $O_{MAC\&RLC}$: MAC and RLC overheads;
- O_{App}: Application overhead;
- T_P: physical layer throughput (Annex D);
- β_{SISO} : BER function for the SISO detector (Annex G);

$$T_{MIMO\ [\text{Mbps}]} = \left[T_{P\ [\text{Mbps}]} \times \left[(1 - O_{MAC\&RLC}) \times (1 - O_{App}) \times \left[1 - \beta_{MIMO}(\rho) \right] \right] \right] \times G_{M/S}(N_T, N_R, d_{[\text{m}]}) \tag{3.10}$$

where:

- β_{MIMO} : BER function for the MIMO detector (Annex G).

The main differences presented in (3.10) related to (3.9), are that in the former a different MIMO detector is used for each system, with the possibility of being an ML one, or a ZF or MMSE for some modulations, and the RMG model is used to calculate the effects of MIMO in the final throughput. For a 4×4 MIMO system, the RMG model is affected by some constants, regarding the effect of SNR variation and antenna spacing presented in Subsections 3.3.2 and 3.3.3, respectively. As a consequence, for this configuration the relative MIMO gain takes the form of:

$$G_{M/S\ 4\times4} = G_{M/S}(4,4,d_{[\text{m}]}) \times G_{M/S\ SNR}(\rho) \times G_{M/S\ Corr}(\text{BS}_{spacing}, \text{MT}_{spacing}) \tag{3.11}$$

The relative mean error of not considering the SNR variation from the default value of 10 dB, for the other antenna configurations, is below 5 %, while for the fact of not considering the correlation effect, due to variation of the antenna spacing from the default value λ, for the other antenna configurations, the relative mean error is below 6 %, as described in Subsections 3.3.2 and 3.3.3, respectively.

It should be pointed out that (3.9) and (3.10) do not account for the detection percentage, i.e., in some situations the signal might not be detected/received, hence, it has to be retransmitted, making use of resources that were supposed to transmit new data instead of retransmitting the former one, consequently lowering the final application throughput. Therefore, the implementation of the link model in a simulator platform leads to a certain throughput per unit distance, that in fact does not account for this retransmission, though the throughput might be 0 Mbps, meaning that the signal has not been detected, which enables the detection percentage calculation and to further account for it. The procedure to calculate the final throughput regarding the detection percentages and the average simulated throughput is given by:

$$T_{F[\text{Mbps}]} = \overline{T}_{s[\text{Mbps}]} \times P_d \tag{3.12}$$

where:

- T_F: final throughput;
- $\overline{T_s}$: average simulated throughput;
- P_d: detection percentage, defined as:

$$P_d = \frac{N_{ds}}{N_{ts}} \tag{3.13}$$

where:

- N_{ds}: number of detected signals;
- N_{ts}: number of total signals.

Though, one must bear in mind that this analysis is a best case approach to reality, since it is assumed that the data that was not transmitted at first attempt will be certainly transmitted at the second one, which might not happen in reality. In other words, it is assumed that one retransmission is enough to transmit the data.

Chapter 4

Model Implementation

The present chapter provides a functional description of the simulator platform on which the models used and developed within the scope of this thesis were implemented. After giving an overview of the simulator, the description of the simulator functional modules is presented. The last section shows the simulator assessment.

4.1 Simulator Overview

For the purpose of evaluating the impact on the capacity of UMTS/HSPA regarding the use of MIMO, from a single user view point, a complete simulator tool was implemented: SiMIMO3G+. The main goals underlying the development of the simulator was to build a platform enabling the analysis of the following four main tasks and to do so, the closest to reality as possible:

- capacity increase due to the use of MIMO on several systems, namely, Release 99 (DL and UL), HSDPA, HSUPA and HSPA+ (DL and UL);
- throughput variation with different antenna configuration (e.g., 2×2 or 4×4), for the same distance;
- scenarios influence on throughput;
- MIMO detectors influence.

The tool is able to simulate the experienced user throughput at given distances, taking several previously set parameters into account (e.g. physical conditions, antenna configurations and type of system). Moreover, the program can be run in various modes, related to the MIMO configuration, antenna power fed (dedicated or divided among the various Tx antennas), MIMO detector and system. The possibility of combining each of these modes in several ways, gives the simulator a wide range of outputs, which lead to interesting analysis, regarding the relative influence of specific parameters on the overall output. In order to average results and calculate statistics for outputs, the simulator can be run automatically a number of times set by the user. The structure of the simulator can be decomposed into three modules: Link, Antennas/Receiver and System, Figure 4.1.

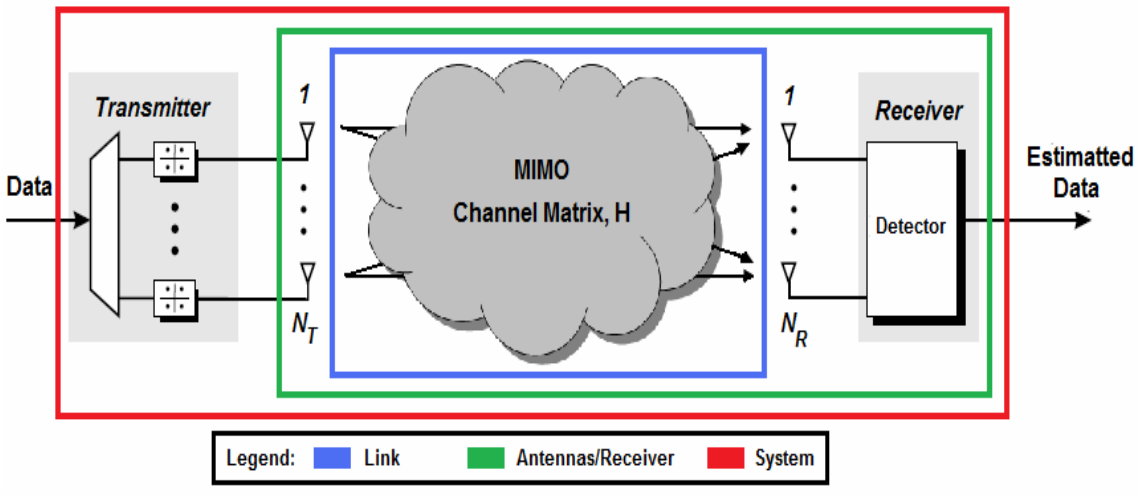

Figure 4.1 Simulator module structure.

The Link module is associated to the input parameters needed to calculate the SNR, the simulation interval and number of simulations being also set in this module. The Antennas/Receiver block is associated to the input parameters regarding antennas and receiver characteristics, and it deals with the option of the type of antenna power fed. The heart of the program is the System block, where the simulation scenario is simulated. The throughput is calculated based on the Link model, described in

Section 3.4, the SISO and MIMO throughputs being calculated by (3.9) and (3.10), respectively, with the RMG taking the form of (3.11) for the 4×4 configuration. The Link model makes use of the parameters and results of the previous blocks, the link budget presented in Annex D, the systems throughput functions presented in Annex E, the RMG model and of the detectors presented in Annex G. In other words, all the systems and models described in this thesis were implemented in the simulator (directly or by results dependency, e.g., GBSB model).

The simulator has been programmed in object oriented C++ (Borland C++ Builder), allowing to keep each module in a different class, which enables a flexible and easily upgradeable simulator structure. In Annex H, the simulator user's manual is presented.

4.2 Simulator Description

4.2.1 Link and Antennas/Receiver Modules

The first two modules of the simulator are presented together, since they have an analogous function, which is to read the input parameters, set by the user, and store them in memory, to be used later on by other modules. These input parameters are related to the link and simulation characteristics, antennas and type of receiver. In Figure 4.2, the flow of information between the modules is depicted.

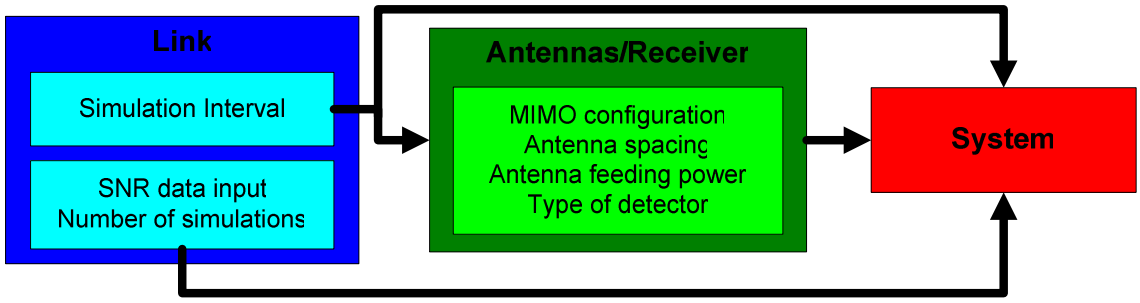

Figure 4.2 Flow of information between the simulator modules.

Regarding the main objectives of the simulator, the need to calculate the SNR is inherent and mandatory. The link module has as essential function to collect the information needed for the calculation. First a set of parameters related to the Equivalent Isotropic Radiated Power (EIRP) are requested, which constitute a simple but of extreme importance step, since the transmission power is one of the most limiting factors in telecommunications. The EIRP requested parameters are:

- BS and MT transmission power;
- BS and MT antenna gain (isotropic);
- user losses;
- cable losses;
- use of UL receive diversity? If yes, which gain;
- system signalling and control power.

After the EIRP, input data for the calculation of the path loss is requested, another parameter of great influence in the transmission. Since the propagation model used in this thesis is the COST-231 Walfisch-Ikegami [DaCo99], the parameters requested to the user are the ones needed as input to the propagation model, see Annex F. Besides the considered path loss, as presented in Annex D, the total pathloss depends on some additional margins, which input data is also requested at this time. There is a need to emphasise the relative importance of two of these parameters, which are related to the slow and fast fading margins, being described by Gaussian and Rayleigh distributions, respectively, and which impact on the overall results is quite significant. With the objective to emulate different channel conditions the standard deviation of the fading distributions can be changed, as well as all the remaining requested parameters. Input data, for the noise power calculation follows the path loss, with the option of considering a Tower Mounted Amplifier (TMA) being presented, having influence on the UL noise figure and cable losses compensation. The load factor for the calculus of the interference margin is also requested, which in a single user scenario is pointless, however in future possible extensions for multi user, it is of great importance. In conclusion the requested parameters for the path loss and noise power calculation are:

- path loss:
  - DL and UL frequency;
  - BS and MT height;
  - buildings height;
  - street width;
  - width between buildings centres;
  - Rayleigh and Gaussian distributions standard deviation;
  - type of environment.
- Noise power:
  - DL and UL Noise figure;
  - use of TMA?.

The last input parameters of this module establish the simulation interval, as well as the number of simulations desired, therefore, the requested parameters are:

- minimum simulation distance;
- maximum simulation distance;
- step (simulation distance increment);
- number of simulations.

It should be pointed out that each of the simulated distances are also input parameters for the path loss calculation.

With MIMO being on the basis of the main scope of this thesis, a whole module has been reserved to collect its data input, thus, the requested parameters and related simulation options are:

- MIMO configuration;
- antenna spacing;
- antenna feeding power;

- type of detector.

First the MIMO configuration is requested, followed by the possibility of visualisation of the expected RMG impact on the system SISO throughput. This result is based on the RMG model presented in Subsection 3.3.1, though the effects of the SNR variation and the antenna spacing (different correlation) presented in Subsection 3.3.2 and 3.3.3, respectively, are not yet considered, being the last parameter to be requested. For the antenna spacing, two options are available (λ or $\lambda/2$) for each of the antennas (BS and MT), allowing for four different cases to be taken into account. Another requested parameter is the type of antenna feeding power option, which can be split or dedicated. This option is expected to have a major impact on throughput and coverage, by means of greater detection percentage. Since for a signal to be received there is an inherent need for it to be detected, with this in mind, the next option available is a set of MIMO detectors, namely ML, ZF and MMSE, in order to obtain the value of BER for a specific SNR. The purpose of this option is to study the impact of each detector on the overall throughput, though due to the lack of (coherent) information, only the ML is defined for all configurations and systems. More information about this can be found in Annex G.

4.2.2 System Module

The system/results module main responsibility is to do the overall calculations that will lead to the final output, i.e., the throughput as a function of distance, for a given system. This is done regarding the previously collected and stored data, which is the output of the former two modules. However, these data are not enough to meet the demands of this thesis, therefore, in this module more input parameters and simulation options are requested to the user:

- System;
- link direction (when applicable);
- number of HS-PDSCH codes (for HSDPA);
- type of modulation (when applicable);
- BER system target;
- SNR system target;
- type of power control.

In order to analyse the effect of MIMO on all systems and to compare relative performances, there is a need to choose the type of system based on which the simulations are going to be executed. Nevertheless, this information is not of much use if the system by itself does not have inherent the link (e.g., Release 99 and HSPA+), therefore the user has to select DL or UL. Moreover in HSDPA, HSUPA and HSPA+ DL, there are some other options that have to be done, since for HSDPA the simulations can be performed for 5, 10 and 15 HS-PDSCH codes, and for HSUPA and HSPA+ DL, the user can choose between two available modulations, BPSK and QPSK or 16QAM and 64QAM, respectively. Following this procedure, the system targets are requested, namely BER and SNR, since the simulator has the option of detecting only signals that are bellow a specific BER target. Despite the fact that the simulator only detects signals with SNR higher than 5 dB, all of the data rates for Release 99 (DL and UL) and HSUPA (only BPSK) could be achieved with a SNR equal or below 5 dB,

though it might be interesting to study other SNR targets. However it is essential to increase the value of the SNR target in order to have the maximum data rate for the other considered systems, and for the majority of the systems this value is significantly higher than 5 dB. The value assumed as default for the BER target is 10 %, though it can be modified.

The last option, which will have a major impact on the overall results, is the type of power control. The simulator can run in two different modes, with “perfect” power control or with “imperfect” power control. The algorithm for these two modes is described in Figure I.1. The difference between these two modes is that in the former the fading margins are taken into account when calculating the Tx power that is needed to achieve a certain SNR value, while in the latter the fading margins are not considered in the pathloss, thus, the calculated power, may or may not be enough to meet the demands of a specific SNR value. In other words, when considering perfect power control, the BS has perfect information about all the channel characteristics, contrary to imperfect power control.

With all the necessary data collected, the system module is now able to calculate the throughput for each of the simulated distances. The procedure is depicted in Figure 4.3. First the simulator verifies in which type of scenario the distance fits in, in order to choose the street angle to use in the path loss calculation (0º to the pico- and micro-cell scenarios and 90º for the macro-cell one). At this time, the fading margins are also calculated, according to the respective distribution, and the type of system is verified. After this data inspection, the path loss is calculated based on the COST 231 Walfisch-Ikegami model presented in Annex F, and the noise power is calculated based on the link budget presented in Annex D. If the system set by the user for simulation is for DL or Release 99, the simulator uses the SNR target to calculate the needed transmission power and proceeds to the SNR calculation, making use of the power control algorithm; if the system is for UL and different from R99, the simulator has to calculate the E_c/N_0 target, based on the SNR target using (D.18). For each distance, the SNR value calculated is verified, and if it is below 5 dB, the signal is not detected, however the SNR being equal or above 5 dB does not guarantee signal detection, since if the BER that corresponds to that SNR for the specific simulated system at that distance is above the BER target, the signal is not detected.

Contrary to the situation where the signals are not detected, is the situation where both conditions are verified, i.e., SNR equal or above 5 dB and BER lower than the BER target. When this happens, the signal is considered to be detected; hence, the SISO and MIMO throughputs are calculated based on the respective system, SNR, BER and MIMO configuration, making use of the link model described in Section 3.4, using (3.9), (3.10) and (3.11), which make use of the link budget presented in Annex D, the systems throughput interpolation functions presented in Annex E, the RMG model presented in Section 3.3 and of the detectors functions presented in Annex G. In what concerns the throughput interpolation functions, the simulator choose from (E.1) to (E.10) the appropriate one, regarding the type of system and modulation set for simulation. The same principle is applied for the detectors functions, though for this situation the decision is made regarding the MIMO configuration and modulation, set by the user, with the possibility of the applied function ranging from (G.1) to (G.20).

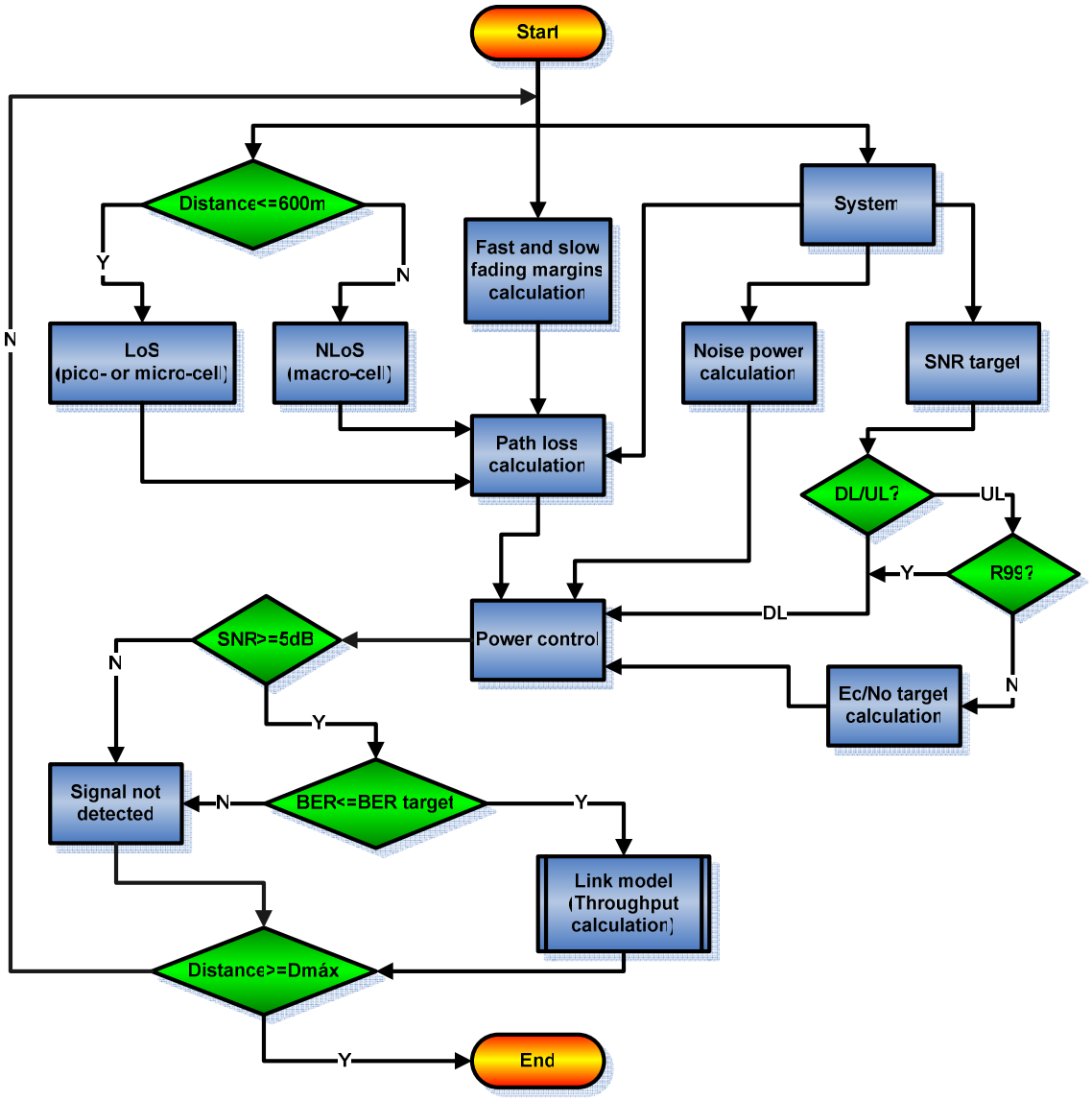

Figure 4.3 Throughput vs. distance calculation algorithm.

After the conclusion of the simulation(s), the results are displayed in several plots, namely:

- throughput vs. distance;
- Tx power vs. Distance;
- SNR vs. Distance;
- BER vs. SNR;
- fading vs. distance;
- fading Cumulative Distribution Functions (CDFs).

In the Throughput vs. Distance plot, both SISO and MIMO throughputs are presented, hence, the user has an immediate perception of the MIMO effect over the SISO system. However, this plot is merely for instant visualisation of the output parameters, Figure H.2. The purpose of the other plots is essentially for instant assessment of the results, since the SNR, Tx power and Fading behaviour with

distance, must fit within an expected range of values, as well as the BER variation with SNR. For this matter, it should be pointed out that, in this thesis, power control is used for HSDPA and HSPA+ DL, in order to obtain more realistic (meaningful) SNR values, despite the fact that these systems do not support power control, except in some exceptional conditions as referred in Section 2.2. Regarding the Fading CDFs plot, it is only to make sure that each type of fading is obtained by the corresponding distribution.

Despite the mentioned plots, the simulator generates a file, results.xls, with the results of the simulation(s), which contain the calculated values of the SISO and MIMO throughput, for each distance and simulation. With the purpose of making the results analysis easier and faster, the generated file has a .xls extension which can be opened directly with Microsoft Excel sheet.

4.3 Assessment

Before performing simulations and its results analysis, the simulator must be assessed, concerning the validity of the output and number of simulations that ensure statistical relevance. All steps responsible for carrying out calculations were validated, making use of several tools and approaches, namely averages, relative mean errors and standard deviations were inspected using (4.1), (4.2) and (4.3), respectively.

$$\bar{z} = \frac{\sum_{i=1}^{n} z_i}{N_s} \tag{4.1}$$

where:

- z_i: sample i;
- N_s: number of samples;

$$\bar{e} = \left| \frac{z_r - z_i}{z_r} \right| \tag{4.2}$$

where:

- z_r: reference value;

$$\sigma = \sqrt{\frac{1}{N_s} \sum_{i=1}^{N_s} (z_i - \bar{z})^2} \tag{4.3}$$

The values that are used as input of the propagation model and link budget were confirmed one by one, as well as their expressions, with several calculations performed, using Matlab and Excel, to ensure that results were correct and according to the theoretical models.

Regarding the statistical distribution considered for describing the fading margins, simulations were performed for each one, in order to evaluate if the simulated results are coherent with the theoretical ones. The obtained results are very similar, with the average mean error being below 0.8 and 1.1 % for the Rayleigh and Gauss distributions, respectively. The error for the Rayleigh distribution is mainly due to computational approximations, while for the Gaussian distribution it also has to do with the numerical approximation that has to be performed for the inverse of the error function. Note that what is really implemented in the simulator is the inverse of the distributions, since what is needed is the value of the distribution and not the probability of it occurring. Random generated values, described by a uniform distribution which take values between 0 and 1, are used as inputs for these inverse distributions.

Since SNR is not an output parameter of the simulator, its assessment has been performed for several distances and simulations, by analysing the variables and expressions that are used for its calculation. SNR being the main parameter that influences throughput, in order to observe the impact of its variation over distance, 100 simulations have been performed for HSDPA system, with 15 codes, since this system is one of the most demanding in terms of requested SNR to attain the maximum throughput, hence, the SNR variation with distance is more perceptible. In other words, the magnitude of the SNR variation with distance is expected to be high, thus, enabling an easier validation of the results. Furthermore, the simulations have been performed for the 2×2, 2×4, 4×2 and 4×4 configurations, with the objective of ensuring that the MIMO effects on the SISO throughput were coherent with the ones presented in the RMG model. The results of these simulations are depicted in Figure 4.4 and it can be noticed that the SISO throughput is decreasing with distance, as expected, hence, the SNR is also decreasing. Moreover, the throughput significantly decreases after 600 m, which is the distance that delimits the micro-cell, and beyond which the expressions used to calculate the path loss differs, due to the street angle variation from 0º to 90º.

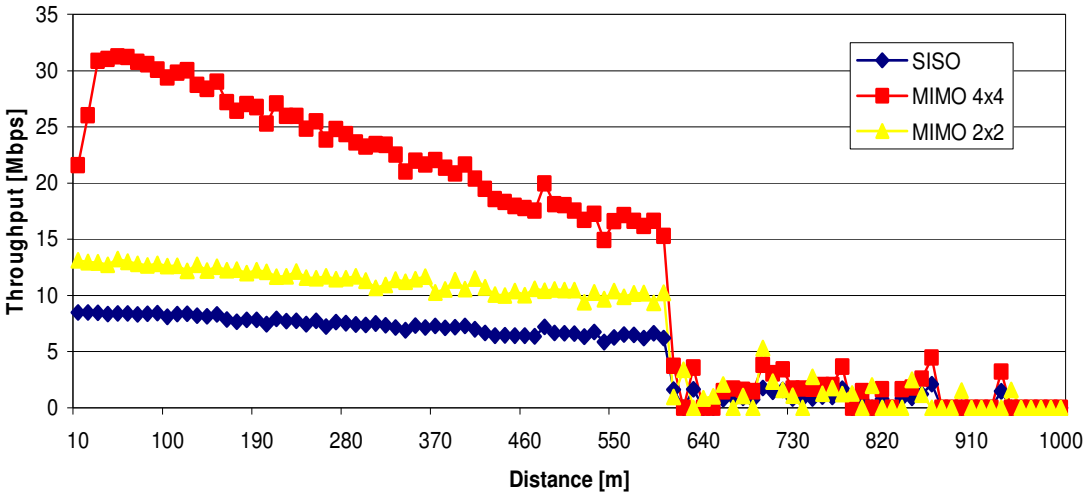

Figure 4.4 Throughput vs. Distance for HSDPA with 15 HS-PDSCH codes.

One can further observe that the MIMO gain over the SISO throughput is coherent with the one described by the RMG model, however, some slight variations can be observed that are related to the

randomness inherent to the RMG model. Note that the results presented are only for 2×2 and 4×4, though simulations were performed for all the other available MIMO configurations, which also confirmed the coherence.

Despite the fact that for the macro-cell region there are average throughput results higher than 0 Mbps displayed in Figure 4.4, this type of cell is not considered for the analysis to determine the number of simulations that one should consider as statistically relevant. The reason for doing so is that even though the average for a certain macro-cell distance is higher than 0 Mbps, the average percentage of detected signals for 100 simulations in the macro-cell scenario is below 1%, while for the pico-cell and micro-cell scenarios it is above 97%.

Regarding the type of power fed (split or dedicated), detector (ML, MMSE or ZF), and power control (perfect or imperfect), every variable, expression and calculation step has been carefully monitored, through several simulations, making use of the debug and observation point in the simulator code, concluding that everything is working according to the respective algorithms.

With all the randomness associated to the throughputs calculation, in order to ensure the results validation several simulations must be performed, as done to obtain the results depicted in Figure 4.5. For those results 100 simulations were carried out; however, taking the average simulation duration of 100 simulations of about 1 hour into account (for the most demanding system), this seemed inappropriate, since there is no significant variation of the standard deviation when the number of simulations increase. Hence, an analysis was performed in order to obtain the most suitable number of simulations concerning simulation time and statistical validity of the results. Note that the simulation time is not equal for all systems, since each system is associated to a different number of decisions, which are related to the number of function branches of each specific system, detector and MIMO configuration.

For this analysis, 2×2 HSPA+ for DL using 16QAM was chosen, since it seemed appropriate regarding the main scope of this thesis, and the fact that MIMO is already standardised in Release 7 for HSPA+ DL with 16QAM. Note that despite the differences in terms of throughput calculation of the other systems and links, the simulator principle is basically the same. Moreover, instead of considering several distances, only three have been considered. The criteria for choosing them was the same used in Subsections 3.3.2 and 3.3.3, that is the middle distances of the different chunks of the RMG model functions (20, 50 and 400 m), with the exception of the macro-cell scenario, as explained earlier.

The throughput evolution is depicted in Figure 4.5, for the three considered distances for 100 simulations, and as one can observe the mean value and standard deviation have no relevant variations for simulations equal or greater than 50. However, these relative values must be evaluated by analysing the ratio of the standard deviations over average values. The results of this ratio are presented in Figure 4.6, confirming the small variation of results for a number of simulations greater than 50.

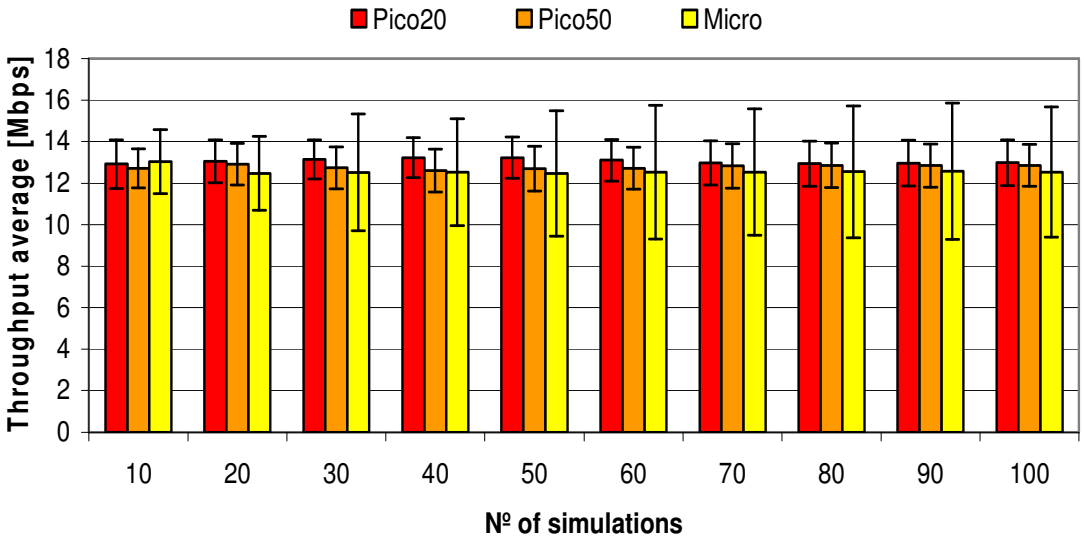

Figure 4.5 Evolution of the throughput average and standard deviation of three considered scenarios for 100 simulations.

Moreover, if one is considering performing a smaller number of simulations, first the relative mean error to the assumed reference number of 100 simulations must be stressed. This relative mean error is shown in Figure 4.7, and it is possible to observe that the relative mean error variation is below 4 % for all the considered number of simulations, though its behaviour stabilises for a number of simulations higher than 50, with the error being below 2 % for 50 simulations. Thus, increasing the number of simulations would have minimal impact on the results.

Considering all the results of performed analysis to stress out the proper number of simulations, it can be concluded that 50 simulations seem to be the most suitable number of simulations, reducing the simulation time to about half an hour (for the most demanding system), and still having statistical relevant results.

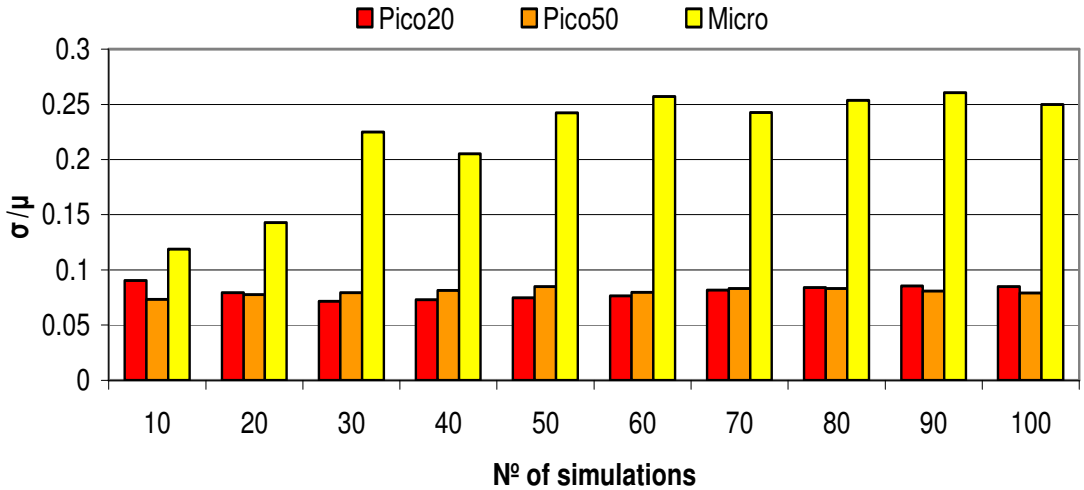

Figure 4.6 Standard deviation over average ratio for 100 simulations.

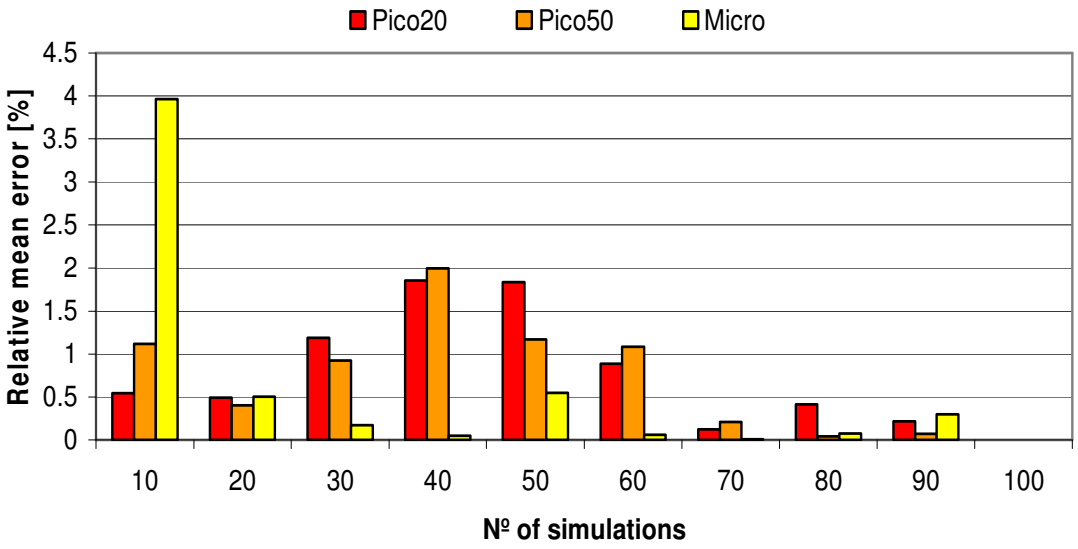

Figure 4.7 Relative mean error evolution for 100 simulations as reference.

It should be pointed out that this analysis has been performed for the other considered systems, and the output results have been confirmed by means of averages, relative mean errors and standard deviations, using (4.1), (4.2) and (4.3). However, these analyses are not presented here, since it seemed unnecessary, though they confirm the presented results, namely in what regards the most suitable number of simulations. Furthermore, the simulations performed for the simulator assessment, considered the default values of the simulator, namely 10 and 7 dB for the Rayleigh and Gaussian distributions standard deviation, as well as ML detector, dedicated feeding power and perfect power control.

Chapter 5

Results Analysis

This chapter contains the descriptions of the used scenarios and the analysis of results. First the simulation scenarios are presented, followed by the presentation of simulation results considering several parameter variations, such as system, MIMO configuration, antenna spacing, detector, and type of antenna power fed. While analysing the UL, the use of TMA and reception diversity is also considered, and a comparison between DL and UL is performed regarding each parameter variation.

5.1 Simulation Scenarios

As the main objective of this thesis is to assess the MIMO impact on UMTS/HSPA+ capacity, a set of simulation scenarios was conceived, in order to measure and compare this impact, regarding several MIMO parameters variation, as well as the type of system. Bearing this in mind, a default scenario was chosen, over which one performs the parameters variation and comparisons. The system and MIMO parameters considered for the default scenario are presented in Table 5.1.

Table 5.1 Default scenario system and MIMO parameters.

MIMO configuration (Tx-Rx)	4×4
Antenna spacing (BS-MT)	λ-λ
Antenna feeding power	Dedicated
Detector	ML
System	HSPA+ with 16QAM (DL/UL)
BER target [%]	10
SNR target [dB]	15
Power control	Perfect

HSPA+ was considered as the default system, with the use of 16QAM for DL and UL, since it is the modulation for which one has more available information, thus, resulting in a more viable analysis. Despite the fact that only the MIMO 2×2 has been standardised in Release 7, for the default scenario the considered configuration is the 4×4 one, since SNR and antenna spacing variation effects are only considered for this configuration, as described in Subsections 3.3.2 and 3.3.3, respectively, and due to the fact that ZF and MMSE detectors are only defined for this configuration when considering 16QAM, thus allowing proper comparisons. Note that the SNR target used for these simulations is 15 dB, guaranteeing that a considerable percentage of the signals for all MIMO configurations are detected. In other words, regarding the 4×2 configuration, and the corresponding detector presented in Figure G.3, one can observe that if a smaller SNR target was considered, e.g., 12.2 dB, MIMO signals would never be detected when this target was achieved, since they would have a BER greater than 10 %; thus, an SNR of 15 dB gives a proper margin for avoiding that situation, and makes the analysis and comparisons for all available MIMO configurations possible. Underlying the values and options of the remaining default parameters, is the idea of a best case scenario, i.e., a system operating with uncorrelated signals, making use of the best available detector, with a perfect channel knowledge, and with the same power dedicated to each antenna as for a SISO system.

For the default scenario, the parameters used to calculate the link budget are the ones set by default in the simulator, Table 5.2.

In order to highlight the impact of different MIMO parameters, the first set of simulations has the objective to present the ideal systems, the default scenarios for DL and UL, which are expected to be

upper bounds in terms of throughput. Note that for HSPA+ DL with 64QAM, one should experience higher throughputs, though it is not considered as the default scenario, since only the 2×2 detector is defined for this specific system.

Table 5.2 Default values in the link budget calculation.

Parameter	**Default value**			
	BS		**MT**	
Transmission power [dBm]	44.7		24	
Antenna gain [dBi]	17		0	
Height [m]	26		1.8	
Buildings height [m]	24			
Street width [m]	15			
Width between buildings centres [m]	30			
User losses [dB]	1			
Cable losses [dB]	3			
Rayleigh standard deviation [dB]	10			
Gaussian standard deviation [dB]	7			
	DL		**UL**	
Signalling and control power [%]	**R99**	**HSDPA/HSPA+**	**R99**	**HSUPA/HSPA+**
	25	6	0	13
Frequency [MHz]	2117.8		1927.8	
Noise figure [dB]	8		6	
Simulation interval [m]	**Pico-cell**		**Micro-cell**	
	10 - 60		60 - 600	

After the default scenario presentation, a second set of simulations was performed, by varying the systems, within the different cell types, thus, providing the trends of throughput variation with distance, and enabling a comparison among the various systems, with the analysis performed separately for DL and UL. The macro-cell analysis is not performed, since, as described in Section 4.3, the percentage of detection is very low, thus, leading to inexact and inadequate conclusions.

The main objective of the previous analysis is to show how much MIMO could have improved the previous releases, and to pick the systems with better performance for DL and UL, which are the ones from the later releases. For these systems, simulations were performed, for DL and UL, varying the available MIMO configurations, with the objective to evaluate the relative impact, in terms of throughput and coverage, of using different antenna configurations.

A further evaluation of the impact of using different spacing between antennas, different detector, and different antenna power feeding options, is then carried out for these systems, i.e., HSPA+ DL and UL.

In order to do so, a set of simulations were performed by varying the referred parameters, for the different cell-types. Note that for the different spacing between antennas and different detector, the analysis is only possible for the 4×4 configuration, due to the lack of results for the other configurations; hence for DL HSPA+ with 64QAM the analysis is not performed. Moreover, a comparison for DL and UL performances is carried through, regarding the previous analysis, i.e., comparing the influence of each parameter in DL with its influence in UL.

The last set of simulations is intended to evaluate alternative scenarios for UL, considering, the use of TMA and/or reception diversity.

5.2 DL MIMO Impact Evaluation

In this section, DL simulation results are analysed. First, the results of the default scenario introduced in Section 5.1 are examined. Afterwards, simulation results considering system and MIMO parameters variation, as well as cell type, are studied.

5.2.1 Default Scenario

All the results presented in this subsection were obtained with the objective of giving a more specific insight into the MIMO impact on throughput for each scenario.

The throughput variation with distance in a pico-cell scenario for HSPA+ DL using 16QAM is presented in Figure 5.1, with throughput increasing from about 20.5 to 29.5 Mbps in the 10 to 40 m region of the cell, after which it decreases. This increment in throughput is coherent with the RMG model and can be explained by the increase on the number of MPCs and by the decorrelation among them, since the distance travelled by the signals is higher, as well as the probability of having more scatterers within this range, thus, resulting in higher RMG values.

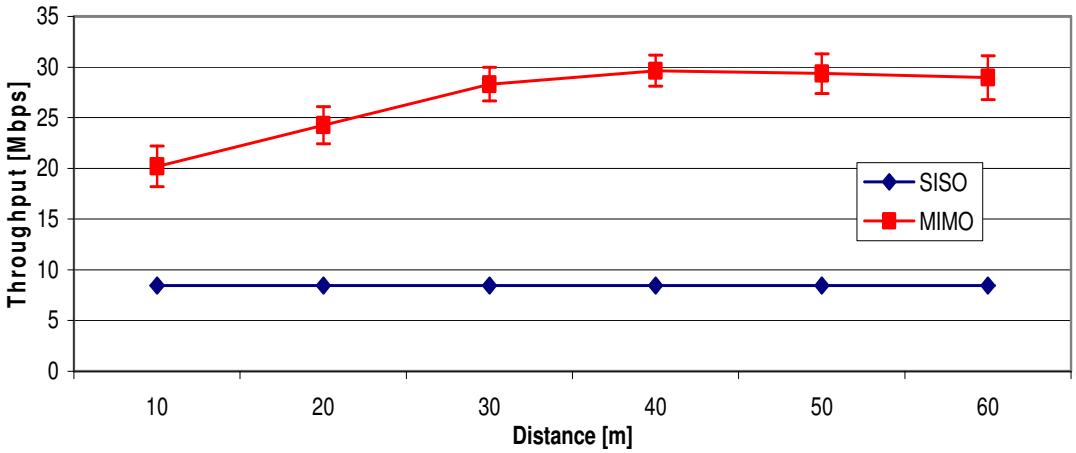

Figure 5.1 Default scenario throughput vs. distance for DL in a pico-cell scenario.

Since the improvements in DL brought by HSPA+ for 16QAM require lower SNR to transmit at the maximum bit rate than the SNR required for HSDPA, the SNR target value used for these simulations was of 15 dB instead of the 35.8 dB used for HSDPA with 15 codes, Table E.2, thus, explaining the reason why the SISO throughput presents an approximately constant behaviour even in the micro-cell scenario, with its value being about 8.4 Mbps. In Figure 5.2, one can observe that the throughput within the micro-cell scenario decreases from about 29.5 to about 20 Mbps. This decrease is explained by the decrease of the MPC signal strength (power), since each time a signal is reflected it loses part of his power, hence, decreasing the RMG value due to less number of MPCs that reach the receiving antennas with sufficient SNR to provide high bit rates, or even to be detected.

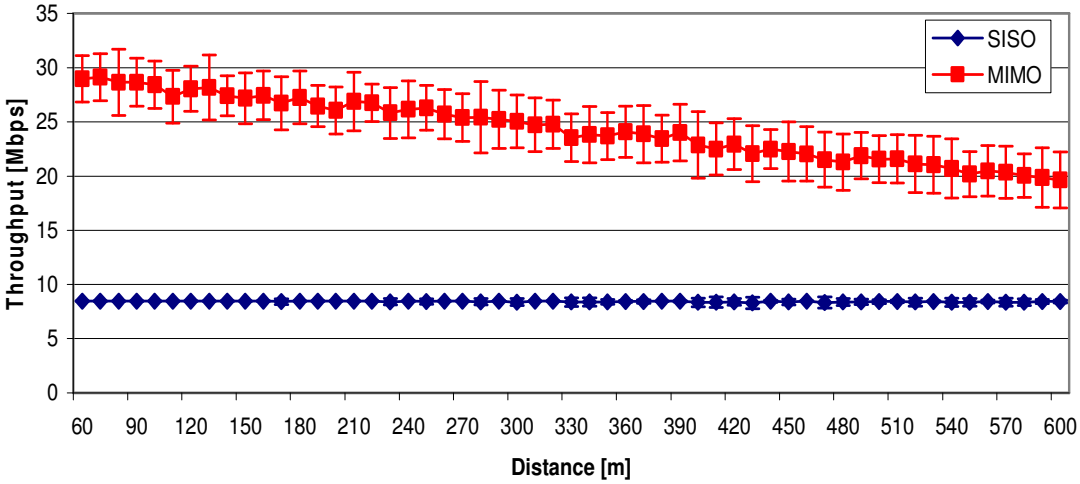

Figure 5.2 Default scenario throughput vs. distance for DL in a micro-cell scenario.

Furthermore, from Figure 5.1 and Figure 5.2, it can be noticed that the standard deviation presents a constant behaviour, thus, validating the results for all distances presented. Despite the fact that a lower SNR is necessary to achieve the highest throughput compared with HSDPA, it must be emphasised that the results are for a single user situation, where all the resources are allocated to him/her and no service differentiation is performed, hence, allowing the transmission of the same throughput until the edge of the micro-cell scenario (600 m), which is not an accurate picture of reality at all.

Moreover, note that the presented throughputs are an average of the detected signals throughput, thus, it is assumed that there are no retransmissions due to excessive BER. However, when analysing the average detection percentage of the simulation results, using (3.13), one can observe that this throughput is not a fair representation of the results, since higher distances are associated to lower detection percentages, Figure 5.3.

In order to present more reliable throughput results, the 'final' application throughput is calculated regarding both results, the average simulated throughputs, and the detection percentages. After applying (3.12) the obtained throughput is the one presented in Figure 5.4. Note that the changes in throughput are only verified for the micro-cell scenario, since, as one can observe from Figure 5.3,

within the pico-cell scenario, signals are always detected. It can be observed that the new throughput results, which account for retransmissions, present at the edge of the micro-cell a throughput of less 2.5 Mbps for the MIMO situation, and of less 1 Mbps for the SISO situation. With these new results, representing reality more accurately, since if a signal is not transmitted (detected), it has to be retransmitted, hence, using resources and consequently lowering the final throughput.

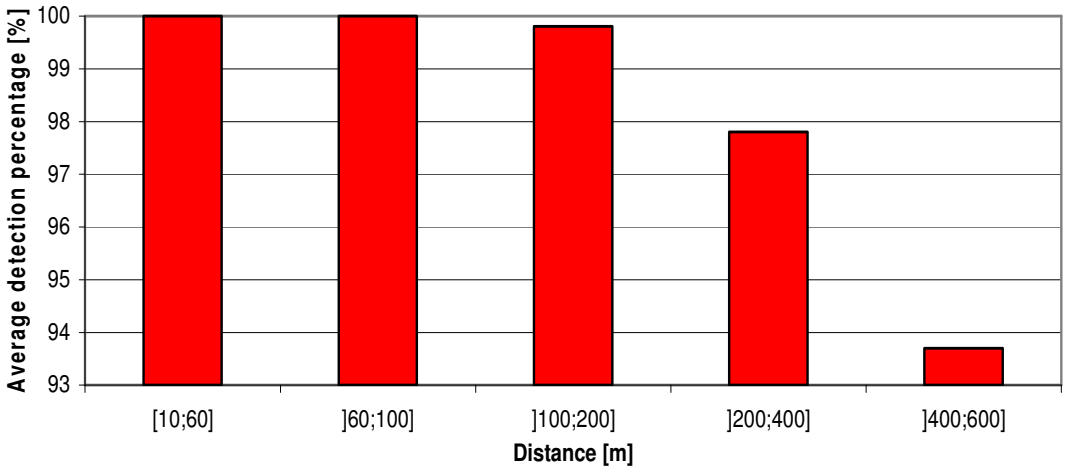

Figure 5.3 Average detection percentage for the default DL scenario.

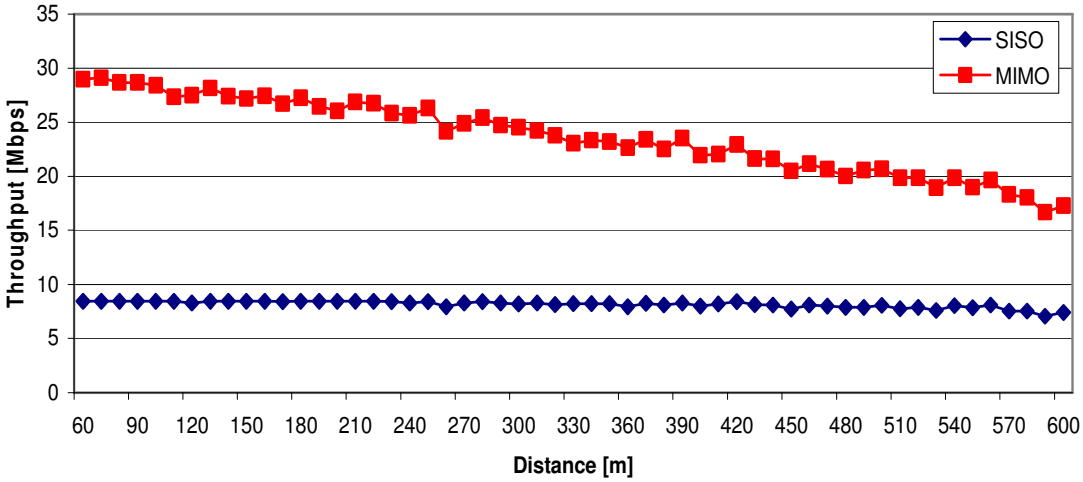

Figure 5.4 Final DL default scenario throughput in a micro-cell scenario.

5.2.2 System Variation

In this subsection, the results for the MIMO impact on the various considered systems are presented, i.e., from Release 99 to Release 8. For each system, the throughput increase due to MIMO is analysed for the pico- and micro-cell scenarios regarding a 4×4 MIMO configuration, for a matter of coherence with the default scenario, thus, enabling performance comparisons.

In what concerns HSDPA, the study of MIMO was performed for each number of HS-PDSCH codes, namely 5, 10 and 15. HSPA+ using 64QAM is also presented here, however, one is considering a 4×4

MIMO system despite the fact that the use of MIMO jointly with 64QAM is only predicted to be standardised in Release 8 for a 2×2 configuration. It should be pointed out that for, this system, there is only one detector defined, that is the 2×2 one; hence, the obtained results are slightly lower than if a proper detector was used instead, since, in general, lower BERs are associated to higher antenna configurations. Moreover, for the same reason as for the default scenario, for Release 99 the SNR target used was of 10 dB, which is higher than the one needed to accomplish the maximum throughput. For the other considered systems, there was no need to do so, hence the SNR targets considered were the ones presented in Table E.2.

The simulation results regarding throughput variation with distance for the various considered systems, for pico- and micro-cell scenarios are presented in Figure 5.5 and Figure J.1, respectively.

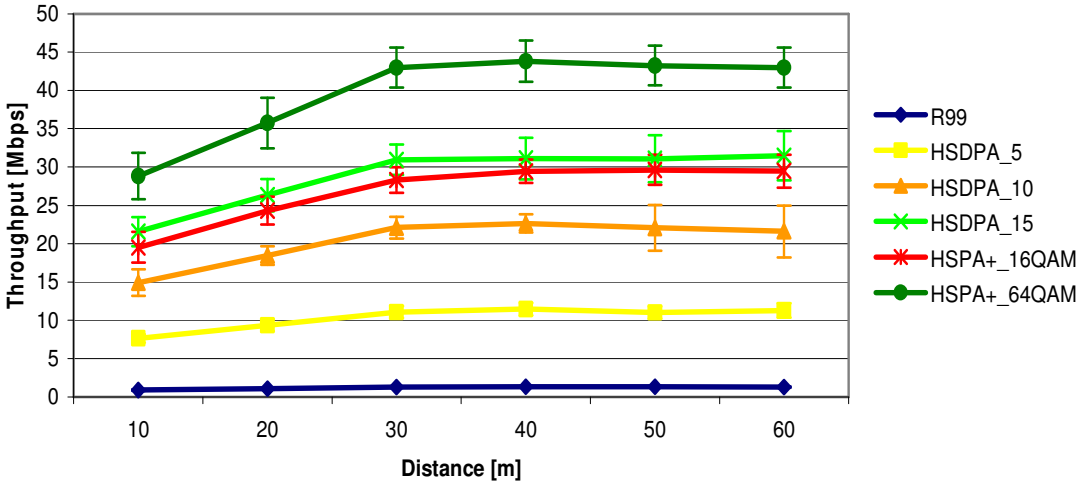

Figure 5.5 DL Throughput vs. distance for various systems and 4×4 MIMO in a pico-cell scenario.

As expected, the system with better performance is HSPA+ with 64QAM, while the system with the worst performance is Release 99, with the remaining curves fitting in between these two. However, these results do not contemplate the detection percentages, presented in Figure 5.6, associated to each system for each distance. Therefore, similar to what has been previously done, the final throughput that accounts for possible retransmissions is presented in Figure 5.7, which presents slightly lower throughputs than the ones presented in Figure J.1, due to the lower detection percentages inherent to each system. Note that the final throughput results are only different for the micro-cell scenario, since as one can observe from Figure 5.6, the average detection percentage for distances up to 100 m is of 100 %, thus, including the pico-cell scenario. It can be further noticed that the percentage detections for HSDPA, and for HSPA+ 16QAM are very similar, since these systems use the same modulation, hence, the same detector. The sligh variations are inherent to the simulator randomness. As previously mentioned, the modulation used for DL in Release 99 is QPSK, which, by the fact of being more robust than 16QAM, has associated a detector that presents lower BERs for the same SNR, and, as a consequence, higher detection percentages. Regarding HSPA+ with 64QAM, the situation is the opposite of Release 99, since 64QAM is a more demanding modulation, therefore, having the detector that presents the higher BERs for the same SNR value, and consequently the

worst detection percentages (see Annex G).

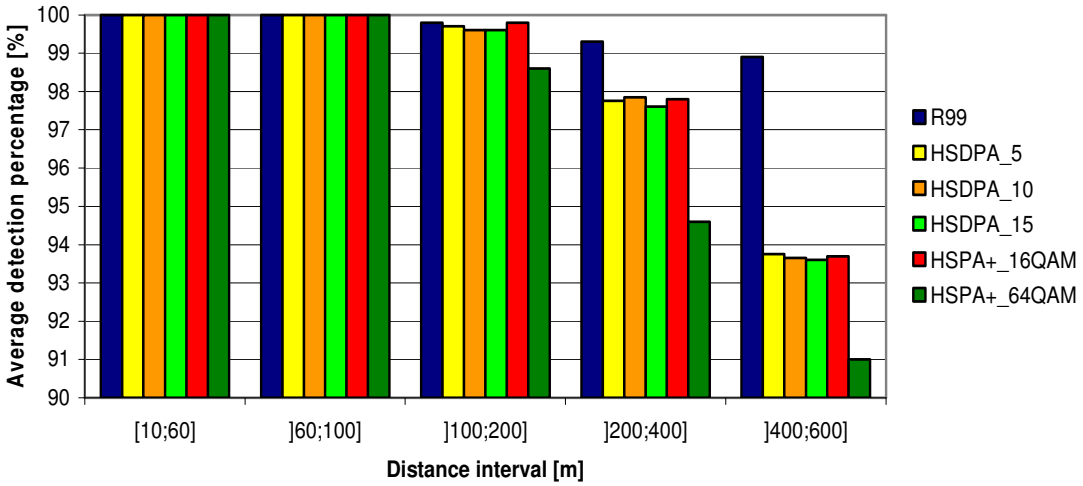

Figure 5.6 Average detection percentage for different DL systems with 4×4 MIMO.

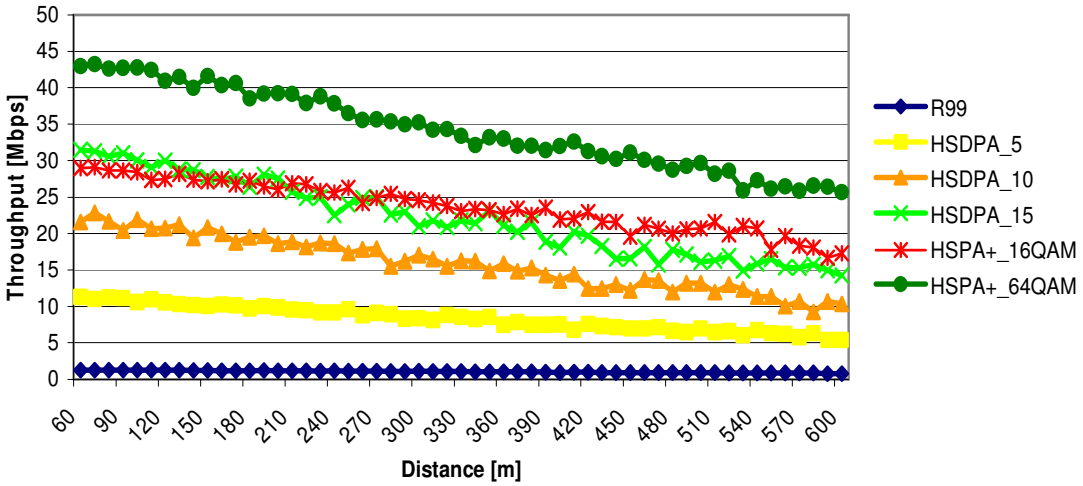

Figure 5.7 Final DL throughput in a micro-cell scenario for different systems.

Analysing the values achieved by the use of the 4×4 configuration on top of Release 99, Figure 5.5, it is possible to observe that, in the pico-cell scenario, there is a throughput increase from 10 to 40 m of about 0.9 to 1.3 Mbps, while in the micro-cell one, Figure 5.7, the throughput decreases within all cell from 1.3 to around 0.8 Mbps. One can notice that even the maximum achieved bit rate for Release 99 by using 4×4 is below the throughput that can be achieved by HSDPA SISO with only 5 codes, Figure B.1, thus, the use of MIMO jointly with Release 99 would not bring considerable performance improvements.

With the RMG being exactly what the name suggests, a relative MIMO gain, when applying MIMO to HSDPA the gain of MIMO is the same as for Release 99, though at a completely different scale; for instance, if one has a RMG value of 2, in Release 99 this would result in a throughput increase of 384 kbps (in reality is less, due to the BER), on the other hand, if one considers the same RMG value

for HSDPA, even with 5 codes, the throughput increase is of about 3 Mbps, consequently having much more impact on the network, and increasing range and QoS of the services that a user can request.

Concerning HSDPA with 5 and 10 codes, the final throughput behaviour with distance is very similar, with the main difference being in terms of bit rate magnitude, which is substantially lower in the former, Figure 5.5 and Figure 5.7. In the pico-cell scenario, the throughput increases from about 7.5 to 11.3 Mbps for HSDPA with 5 codes, while for 10 HS-PDSCH codes the increase is from around 15 to 21.6 Mbps. Note that these increments are from 10 to around 40 m, becoming approximately constant to the end of the pico-cell for the 5 codes system and presenting a slightly decrease of about 1 Mbps for the 10 codes situation. Contrary to the pico-cell, in the micro-cell there is a final throughput decrease throughout all the cell range from about 11.3 to 5.5 Mbps and from 21.6 to 10.3 Mbps for HSDPA with 5 and 10 codes, respectively. It can be further noticed that within the micro-cell scenario the final throughput decrease does not present the same behaviour for HSDPA with 5 and 10 codes, with one of the reasons of so to happen being the fact that for the 10 codes system the SNR target needed to transmit at higher throughputs is higher than for the 5 codes system; thus, the throughput starts decreasing with a steepest slope than for the 5 codes system, since for higher distances it is more difficult to meet the SNR demands of the high throughputs. Moreover, one has to bear in mind that for each number of codes for HSDPA there is a throughput vs. SINR curve associated, and the higher the number of codes the higher the slope of the curves, hence, with the SINR decrease, the throughput decrease is expected to be also higher, Figure E.1.

For the three number of HS-PDSCH codes used in HSDPA, 15 is the one that enables better performance. Despite the fact that MIMO has not been standardised to be used with HSDPA, the use of MIMO on top of this technology, specifically when using 15 codes, leads to high bit rates compared with the ‘elderly’ Release 99. For instance, by using MIMO 4×4 one can get about 32 Mbps, at the application level, in a pico-cell scenario, Figure 5.5. However, it should be pointed out that in order to reach these throughputs, the requested SNR is very high, with its minimum value being 35.8 dB. Due to this, one can observe a slightly difference in the maximum throughput achieved in the simulations by HSDPA with 15 codes and HSPA+ DL 16QAM, since the SNR target used for the latter was of 15 dB; as one knows, the BER for a higher SNR is lower, thus, resulting in a higher application throughput. In a pico-cell scenario, making use of all the available power, the BS manages to reach the requested value of SNR, however, when focusing on the micro-cell scenario, Figure 5.7, the situation is quite different, with the final throughput rapidly decreasing for HSDPA, while for HSPA+ the decrease is smoother. Note that the previous differences, due to the SNR target, were favouring HSDPA, though with the increase in distance the situation is inverted, since HSPA+ requires a smaller SNR to achieve the maximum throughput. Within the pico-cell scenario for 15 codes, HSDPA presents an increase on the throughput from 10 to 40 m of around 21.5 to 31.6 Mbps, while for HSPA+ 16QAM this increase is from 19.5 to 29.5 Mbps, hence, the throughput difference can be here noticed, being about 2 Mbps lower in HSPA+. When looking at the micro-cell scenario, the situation starts inverting at around 200 m, with the HSPA+ throughput now presenting higher values, Figure 5.7. The bit rate

within the micro-cell scenario decreases for both systems, though the amplitude of this decrease is significantly higher for HSDPA, which varies from 31.5 to 14.3 Mbps, while for HSPA+ it varies from about 29.5 to 17.6 Mbps. Note that these results are coherent with the previous explanation of the throughput variation for these two systems.

Regarding HSPA+ with 64QAM, the final throughput within the pico-cell scenario, Figure 5.5, similar to the previous systems, increases from 10 to about 40 m from 28.8 to 43.8 Mbps, with a slightly decrease of 0.8 Mbps being observed from 40 m to the end of the cell. In the micro-cell scenario, the throughput decreases from the beginning to the end of the cell, with values ranging from 43 to 26.6 Mbps. Note that the peak bit rate using 4×4 MIMO (in the best MIMO BER scenario) is only about 1 Mbps above the theoretical expected bit rates (42 Mbps) for the use of 2×2 MIMO on top of 64QAM [BEGG08], hence, the 2×2 MIMO is more likely to have maximum throughputs in the order of 20 Mbps, (the results for the 2×2 antenna configuration are presented later on, when analysing the variation of the MIMO configuration).

It should be pointed out that the MIMO throughputs present smooth variations for all systems, which can be observed especially within the micro-cell scenario, being related to the implicit randomness of the RMG model. Moreover, the variations for HSDPA with 15 codes are more intense after about 180 m, due to the fact that the system in some situations is able to meet higher SNRs, thus, reaching consequently higher throughputs. For this system, a slightly variation in SNR might lead to considerable variations in throughput, as previously mentioned, Figure E.1.

5.2.3 Different MIMO Configuration Impact

Underlying MIMO systems is the use of multiple antennas at the transmitter and receiver, with the possibility of having symmetric or asymmetric configurations, i.e., different number of antennas transmitting and receiving. As mentioned before in Section 3.3, in this thesis only four configurations are considered, since they seem to be the ones that are most likely to be implemented, thus, worthwhile studying. In this section, one varies the MIMO configurations for the default system, with the SISO results being also presented for a comparison purpose.

The throughput variation with distance in a pico-cell scenario for HSPA+ DL using 16QAM is presented in Figure 5.8, regarding all the available MIMO configurations. Since in Subsection 5.2.2 one already showed the 4×4 MIMO impact on HSPA+ with 64QAM, for a matter of comparison, it seemed appropriate to perform simulations for HSPA+ with 64QAM regarding other antenna configurations. However, with the objective of avoiding more errors, due to the lack of results, the simulations were only performed for the 2×2 configuration, since it is the one for which one has a proper detector. The results of these simulations for the pico-cell scenario are plotted in Figure 5.8 jointly with the ones of HSPA+ 16QAM, thus, allowing a better visual comparison.

Within the pico-cell scenario, the throughput accomplished for HSPA+ 16QAM by the 2×2, 2×4 and 4×2 MIMO is about 13, 14.5 and 13.8 Mbps, presenting an approximately constant behaviour, due to

the value for the SISO system being also constant, Figure 5.8. However, for the 4×4 MIMO configuration, the situation is different, with throughput increasing from about 20.5 to 29.5 Mbps in the 10 to 40 m region. This increase is explained in Subsection 5.2.1, being coherent with the RMG model. Note that this behaviour is only observed for the 4×4 configuration, because the other configurations have less transmitted signals, less antennas to detect them, or both, hence, making impossible this throughput increase.

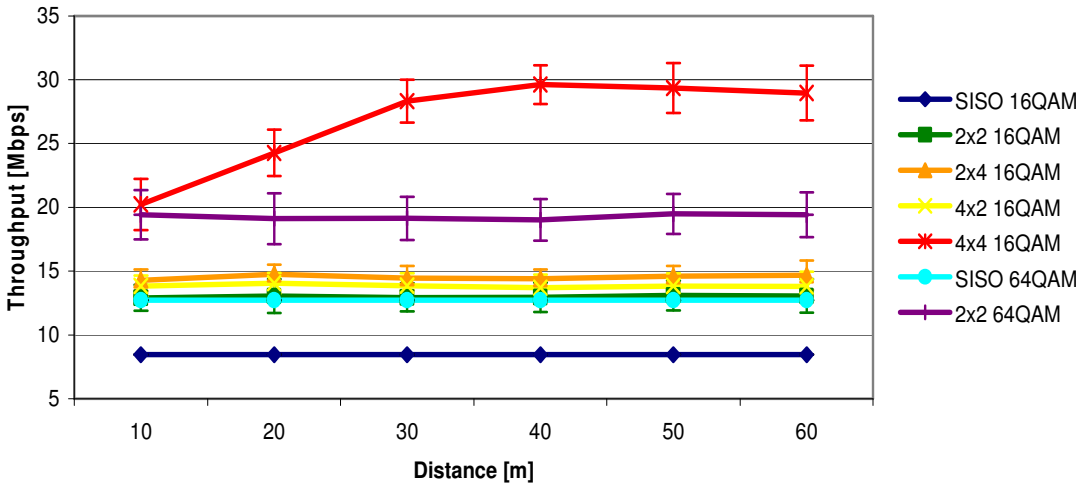

Figure 5.8 DL Throughput vs. distance for different MIMO configurations applied to the default system in a pico-cell scenario.

It should be pointed out that the reason why the throughput for the 4×2 configuration is slightly below the one for the 2×4 configuration is that, for the former, the detector presents higher BER for the same SNR, therefore, resulting in lower throughputs, or even in undetected signals, since BER demands are more difficult to accomplish. As a consequence, despite the throughputs being approximately of the same order, the 2×2 and 2×4 configurations are more reliable than the 4×2 one; however, 2×4 requires 4 antennas at the MT, which is quite a challenge for a small device.

For the reasons explained in Subsection 5.2.1, the average simulated SISO throughput for HSPA+ with 16QAM presents an approximately constant behaviour even within the micro-cell scenario, as shown in Figure J.2, thus, the 4×4 MIMO throughput for the default system, is the exact reflection of the RMG model. As a consequence, regarding the 2×2, 2×4 and 4×2 configurations, the throughput variation with distance can also be considered constant within the micro-cell scenario, Figure J.2, with the values being the same as for the pico-cell.

In what regards HSPA+ 64QAM, the throughput within the pico-cell scenario for the 2×2 configuration presents an approximately constant value of 19.4 Mbps, due to the fact that the SISO throughput is also constant (about 12.7 Mbps). Within the micro-cell scenario, Figure J.2, a slightly SISO throughput decrease of about 0.3 Mbps is verified, leading to a MIMO throughput decrease of approximately 1 Mbps, i.e., from 19.4 to 18.4 Mbps. Bearing this in mind, the use of a 2×2 MIMO configuration on top of HSPA+ with 64QAM allows to achieve throughputs higher than the use of MIMO on HSPA+

16QAM, with the exception being the 4×4 MIMO configuration, which can deliver up to 10 Mbps more than HSPA+ with 64QAM and 2×2 MIMO. Moreover, the use of a 2×2 configuration on HSPA+ 16QAM lead to throughputs that can almost be achieved by the use of the HSPA+ 64QAM SISO system. However, it should be pointed out that, due to the fact that a single user is considered, and all the resources are allocated to him/her, with the simulations having results for distances up to 600 m, though the transmission for these distances, with 64QAM modulation, is unlikely to happen, since it is a very demanding modulation in terms of SNR, regarding the symbol decision boundaries.

Regarding the previous analysis, one should notice that similar to the system variation analysis, associated to each antenna configuration is a different detector performance, as presented in Annex G; as a consequence, there are also different detection percentages that will have some influence in the final throughput. Moreover, in this analysis, not only the antenna configuration is varied, but also the 64QAM modulation is analysed for the HSPA+ 2×2 MIMO system, though the detection percentages presented for this configuration are the same as for the 4×4 one, presented in Subsection 5.2.2, since only one detector is defined for this modulation. With the objective of stressing out the throughput associated to each antenna configuration accounting for the dropped connections, one presents in Figure 5.9 the detection percentages that were used to calculate the final throughput by using (3.12).

Since for the SISO situation, only the ML BPSK detector is defined, the SISO detection is assumed to be limited by the MIMO detector, thus, it is not presented in Figure 5.9, since it is equal to the default one for 16QAM, and for 64QAM it is equal to the 2×2 64QAM case.

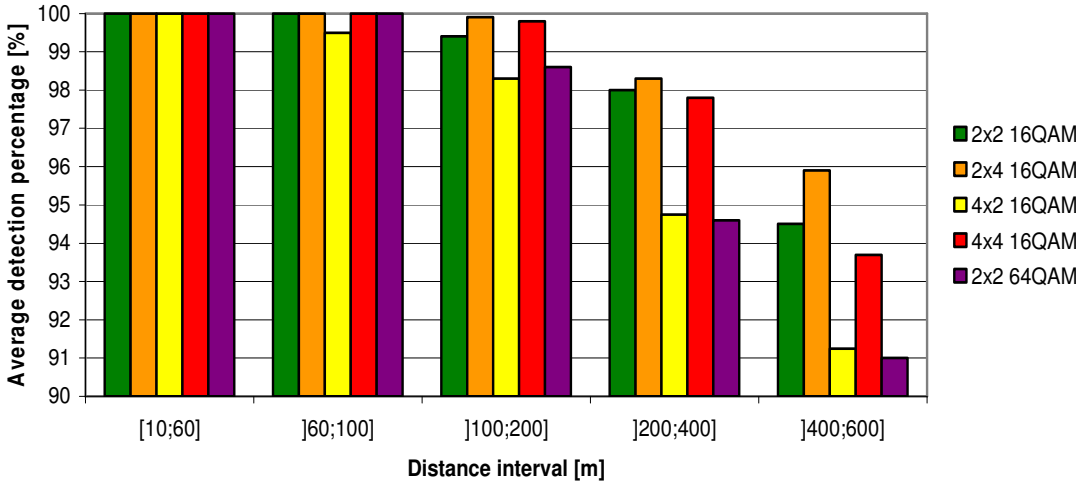

Figure 5.9 Average MIMO detection percentage for different antenna configurations.

From Figure 5.9, it can be noticed that within the pico-cell, there are no connection flaws, hence, the final throughput for this cell type is the same as presented in Figure 5.8. For the micro-cell scenario, the final throughput is presented in Figure 5.10, and it is possible to observe that for all the different antenna configurations, there are throughput decreases related to the ones presented in Figure J.2.

As expected, from Figure 5.9, the highest decrease is for the 2×2 HSPA+ 64QAM system, presenting

at the end of the cell less 1.7 Mbps. On the contrary, the lower decrease is for the 2×4 HSPA+ 16QAM system, which at the end of the cell has about less 0.4 Mbps. In what concerns to the 2×2 and 4×2 configurations for HSPA+ 16QAM, the decreases at the end of the cell, compared with the simulated throughput presented in Figure J.2, are of about 0.8 and 1.3 Mbps, respectively. Note that these results are coherent with the detectors performance.

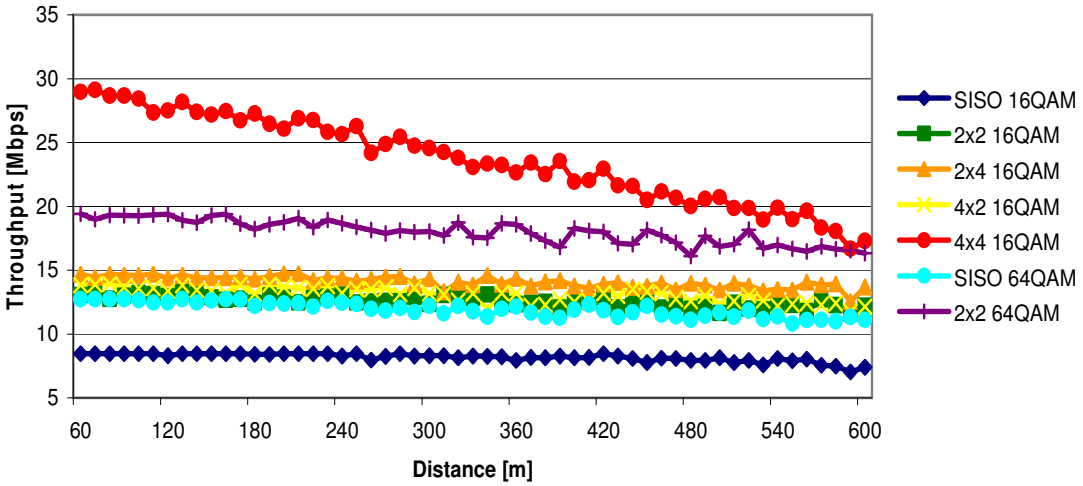

Figure 5.10 Final DL throughput in a micro-cell scenario for different antenna configurations.

5.2.4 Different Antenna Spacing Effect

The use of MIMO brings additional space issues, since more than one antenna is necessary at each side of the connection, thus, it is desirable that antennas are closely spaced, in order to reduce this further amount of space, with this being especially relevant at the MT side, due to space limitations. In this subsection, one presents the effect of varying the antenna spacing at both sides of the connection in DL, Figure 5.11. Note that these results are for a 4×4 MIMO configuration, which regarding the type of MT it is more likely to be applied in a laptop.

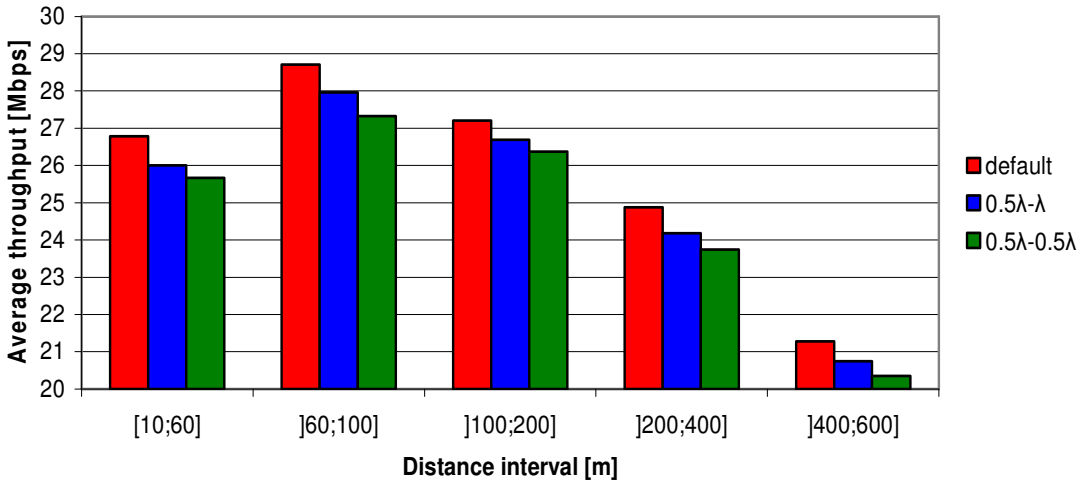

Figure 5.11 DL average throughput vs. distance for different antenna spacing.

As described in Subsection 3.3.3, the antenna spacing is only considered relevant for the 0.5λ-λ and 0.5λ-0.5λ (BS-MT) situations, since for the remaining available combinations the relative mean error presented is below 6%. For a better understanding of the impact of varying the space between the antennas, the average throughput results presented in Figure 5.11 are divided in distance intervals.

As expected, it is possible to observe that by decreasing the spacing between the antennas, even only at the BS side (0.5λ-λ) the average throughput is lower for all the considered distance intervals, with the 0.5λ-0.5λ situation presenting the worst results. For the 0.5λ-λ scenario, the throughput decrease relatively to the default scenario varies for each distance interval, this decrease being, on average, of 2.5 %, which is coherent with the correction value of 0.975 for this antenna spacing. In what concerns the 0.5λ-0.5λ case, similar to the previous situation, different throughput decreases can be observed within the different distance intervals regarding the default scenario, however, this decrease is, on average, also coherent with the correction value of 0.955 for this antenna spacing, thus, being of about 4.5%.

5.2.5 Different Detector Influence

In this subsection, the impact of using a different detector is studied. The simulations were performed by varying the type of detector for the 4×4 configuration, since for 16QAM the MMSE and ZF detectors are only defined for this configuration. Furthermore, simulations for the HSPA+ 64QAM were not performed, due to the lack of results for this modulation regarding the ZF and MMSE detectors. The simulation results are presented in Figure J.3, and it can be noticed that the throughput variation is coherent with the detector complexity; hence, ML presents the highest throughput and the ZF the lowest.

One can further observe that the throughput decrease is not linear, i.e., with the increase of the distance the magnitude of the decrease presents variations. This is due to the fact that the functions that describe the detectors are exponential, thus, one must expect different amplitudes of variation depending on SNR. For the MMSE detector, the throughput decrease rounds 0.3 Mbps, while for the ZF detector this decrease has a value of about 0.5 Mbps.

It is important to point out that, despite the presented throughput decrease associated to the low complexity detectors being of low magnitude, this is not the only drawback of these detectors. As one can observe from Figure 5.12, the percentage of connections is also lower than for ML, since MMSE and ZF present higher BERs for the same SNR, Figure G.8.

Moreover, one must have this in mind when analysing at the average throughput results, since fewer values are being taken into account for the average calculation, thus, explaining the lower variation for the last interval]400;600] m in Figure J.3.

When considering the average detection percentages, the throughput differences among the different detectors remain approximately the same in terms of magnitude, however, the absolute throughput

values are lower than the ones presented in Figure J.3. These throughput results are presented in Figure 5.13, and were obtained by using the same method as for the system variation and different configuration analysis, i.e., applying (3.12) to the plotted results of Figure J.3 and Figure 5.12.

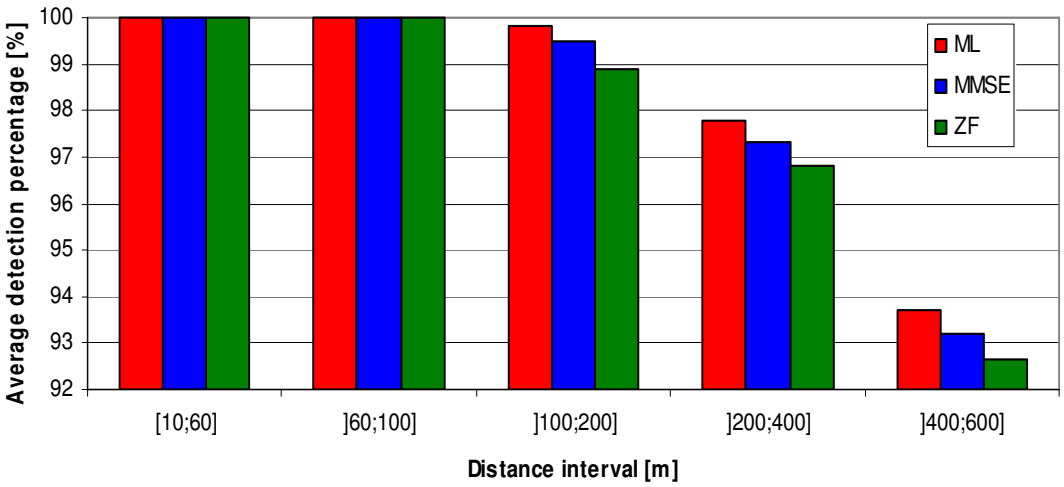

Figure 5.12 DL average detection percentage for different detectors.

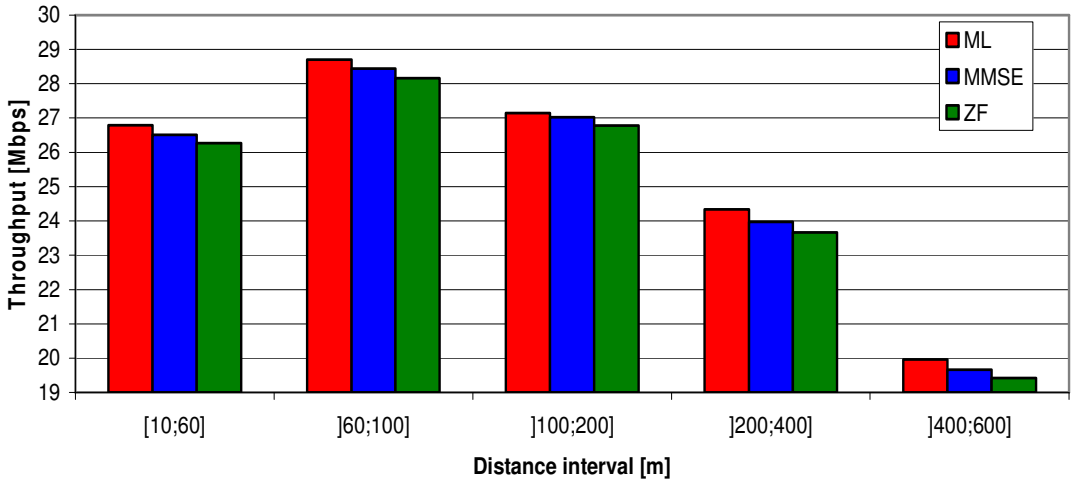

Figure 5.13 Final throughput for different types of MMO detectors.

5.2.6 Split or Dedicated Power Effect

In this subsection, the effect of using split or dedicated antenna power fed is presented. This analysis is quite important, since power consumption is a very important issue for both BS and MT. Regarding the BS, the power amplifier is an expensive feature, thus, the use of dedicated power would bring substantial cost increase to MIMO implementation, not to mention the electricity bill. In the MT side, one must attend for battery limitations, since more power consumption results in less autonomy, which is undesirable.

In Figure J.4, the simulation results for the 2×2 HSPA+ 16QAM and 64QAM are presented, as well as

the results for 4×4 HSPA+ 16QAM, since in the latter power is divided by 4, for the split case. Nevertheless, it was expected that the use of split power among the different antennas would result in significantly lower throughputs, especially for the 4×4 situation, as a consequence of the lower achievable SNR. However, the results presented in Figure J.4, show that this decrease in throughput is not that expressive, being on average less than 0.2 Mbps. Bearing this in mind, similar to the different detector analysis, one performed an analysis regarding the detection percentage for each situation, with the results being plotted in Figure 5.14.

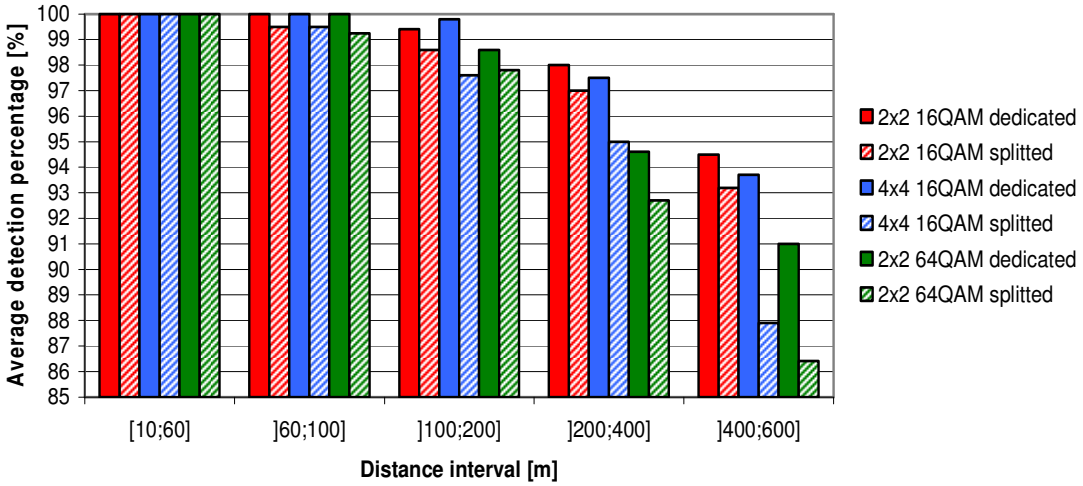

Figure 5.14 DL average detection percentage for different types of antenna power fed.

It is possible to observe that, when using split power, the detection percentage is lower than for the dedicated case, therefore, leading to more unstable and unreliable connections. The values of this detection decrease are more significant for the 4×4 configuration, as expected, since less power is available to meet SNR demands, hence, to establish connection. It can be further noticed that with the increase of distance, the difference of percentage detection between the two situations (dedicated and split) also increases, taking values at the edge of the micro cell]400;600] m of 1.5, 5.5 and 4.5 % for 2×2 HSPA+ 16QAM, 4×4 HSPA+ 16QAM and 2×2 HSPA+ 64QAM, respectively. Within the pico-cell scenario, simulations show that it is indifferent to use one or the other option, with the fact of the low range of distances justifying the accomplishment of the SNR necessary to allow connectivity without problems, even with half or a quarter of the power used for SISO.

Moreover, one can notice that the 2×2 configuration has a lower value of detection percentage than the 4×4 one within the]100;200] m interval, though in]200;400] m the situation inverts. This is due to the fact that, for lower SNR values, the 4×4 detector starts to perform worst than the 2×2 one, thus, for these situations, the BER demands are easier to accomplish by the latter, Figure G.3.

Regarding the previous detection percentages results, and expecting a bigger throughput difference between the two power strategies, similar to what has been done throughout this section, a jointly analysis of the average simulated throughput with the detection percentages was performed, applying (3.12). The result of this analysis is presented in Figure 5.15.

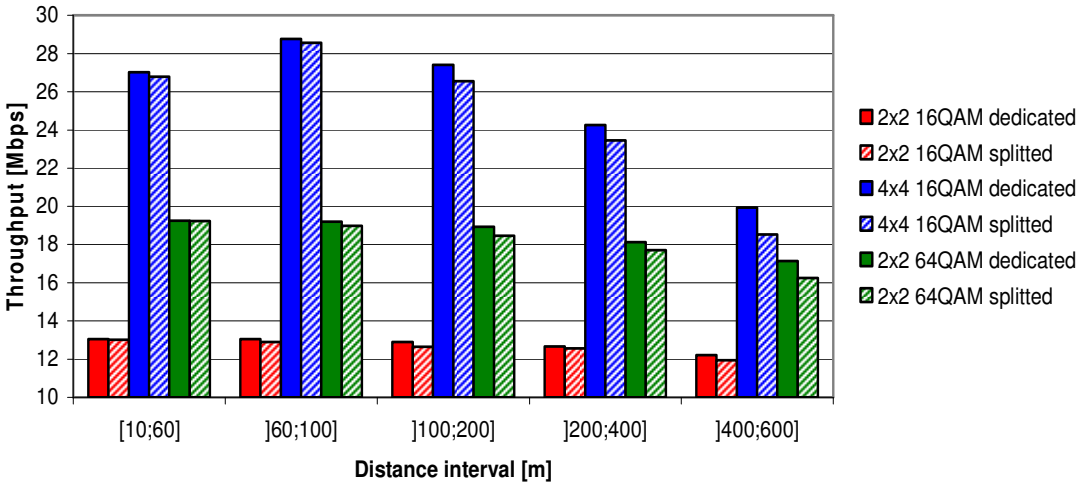

Figure 5.15 Final DL throughput for different types of antenna power fed.

As one can observe, the throughput differences are in fact more expressive if the detection percentages are taken into account, taking values of about 1.5 Mbps at the edge of the micro-cell for the 4×4 configuration. In what concerns the other two systems, these throughput differences are of about 0.3 and 1 Mbps for 2×2 16QAM and 64QAM, respectively.

5.3 UL MIMO Impact Evaluation

In this section, UL simulation results are analysed. First, the results of the default scenario introduced in Section 5.1 are examined. Afterwards, simulation results considering system and MIMO parameters variation, as well as cell type, are studied. Moreover, a comparison between DL and UL is performed within each subsection.

5.3.1 Default Scenario

Like DL, the results are presented separately for pico-cell, Figure K.1, and for the micro-cell scenario, Figure K.2.

From Figure K.1, it can be noticed that the throughput within the pico-cell scenario presents a significant increase from 18 to 26 Mbps in the 10 to 30 m region, after which maintain an approximately constant value of about 26 Mbps. This behaviour is similar to the one presented for DL, with the main difference residing in the lower average throughput values for UL, inherent to the system, and in the lower distance for which the maximum throughput is achieved, which is related to MT power limitations.

In the micro-cell scenario, Figure K.2, as in DL, throughput decreases within the whole cell range, however, one can notice that the MIMO throughput behaviour is less stable than in the DL case.

These wider variations are related to MT power limitations, as a consequence the achievable SNR is lower than for DL, and many times not enough to meet the BER demands that allow detection. However, after this explanation, it might be strange to observe that the SISO throughput presents an approximately constant value within the micro-cell, with only a slightly decrease of about 0.3 Mbps, though as one can observe, for distances higher than about 270 m, the standard deviation, for the MIMO throughput, starts presenting an irregular behaviour, as well as the average throughput, thus, the values for these distances have no significant meaning. For a better understanding of this fact, in Figure 5.16 one presents the average detection percentage within given distance intervals.

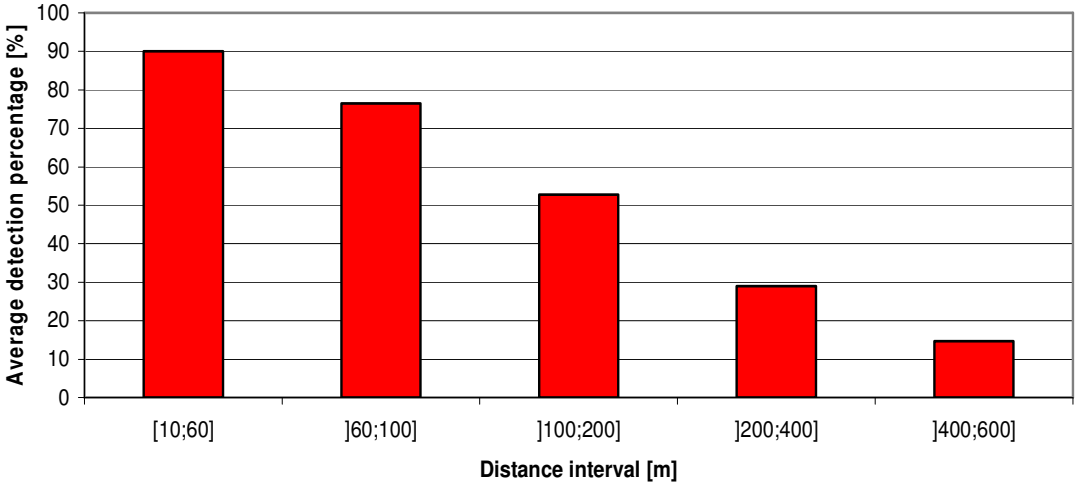

Figure 5.16 Average detection percentage for the default UL scenario.

As one can observe from Figure 5.16, the detection percentage decreases with distance, and for distances higher than 200 m, the detection percentage is, on average, below 30%, which is quite low and explains the irregular behaviour of the throughput as well of the standard deviation. Note that SISO throughput values are only the ones that correspond to a detected MIMO signal, thus, the MIMO throughputs reflect exactly the same variations as the SISO one. Hence, the decrease of the SISO throughput is not wider due to the fact that, on average, only the detected signals are taken into account; when signals are detected for high distances, they are only detected when the channel conditions allow to achieve a sufficiently high SNR, that meet BER demands, hence, these SNR values are very similar, as well as the corresponding throughputs.

One presents in Figure 5.17 and Figure 5.18 the final throughput results, that were obtained by using (3.12), similar to the DL analysis.

It can be observe from Figure 5.17 that, within the pico-cell, when accounting for the detection percentages, throughput is lower than the one presented in Figure K.1. Despite the average detection percentage being of 90 % for this cell type, it is different for each distance, and as expected it decreases with distance. Hence, the throughput reduction that can be seen for the final throughput is not linear, being more expressive with the distance increase, thus, justifying the fact of the throughput increase for the MIMO situation being, at the end of the cell, of about 3 Mbps less than for the average simulated throughput. This behaviour can also be noticed by observing the SISO throughput, which

decreases within the all pico-cell scenario from 7.6 to 6.4 Mbps, being coherent with the previously expected SISO decrease, instead of a constant value.

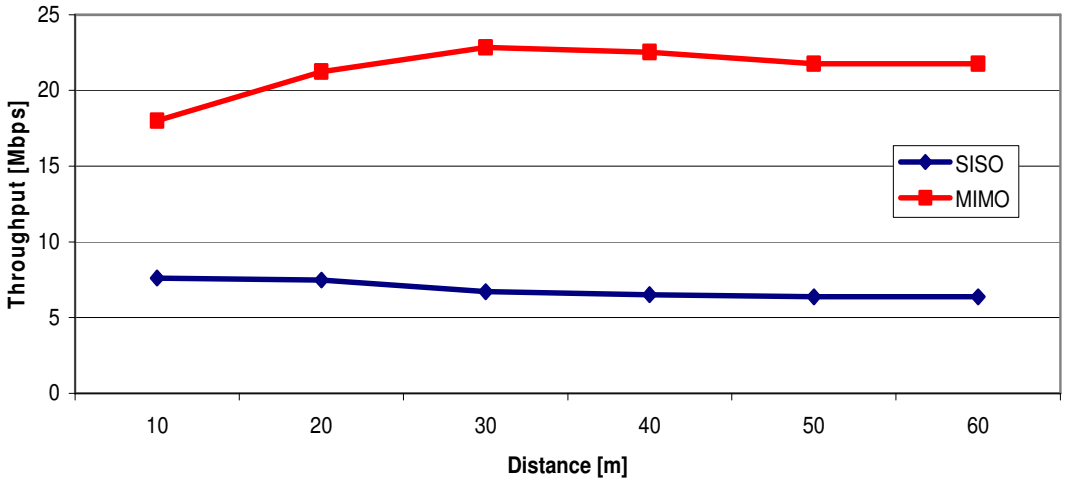

Figure 5.17 Final UL default scenario throughput in a pico-cell scenario.

Within the micro-cell scenario, detection percentages are even more notable, since the higher the distance, the lower the average detection percentage, Figure 5.16, hence, the lower the final throughput. From Figure 5.18, it is possible to observe that both the SISO and MIMO throughputs present significant decreases, and that after about 270 m the throughput starts presenting an irregular behaviour, which is coherent with the irregular standard deviation behaviour shown in Figure K.2. Note that after this distance, the DL SISO throughput for the default scenario starts having a better performance than the UL MIMO one. The SISO throughput decreases from 7.6 to about 0.45 Mbps, and the MIMO one decreases from 21.8 to around 1 Mbps. It can be further noticed that these final throughputs are quite different from the ones presented in Figure K.2, however, they are most likely to represent reality than the previous ones.

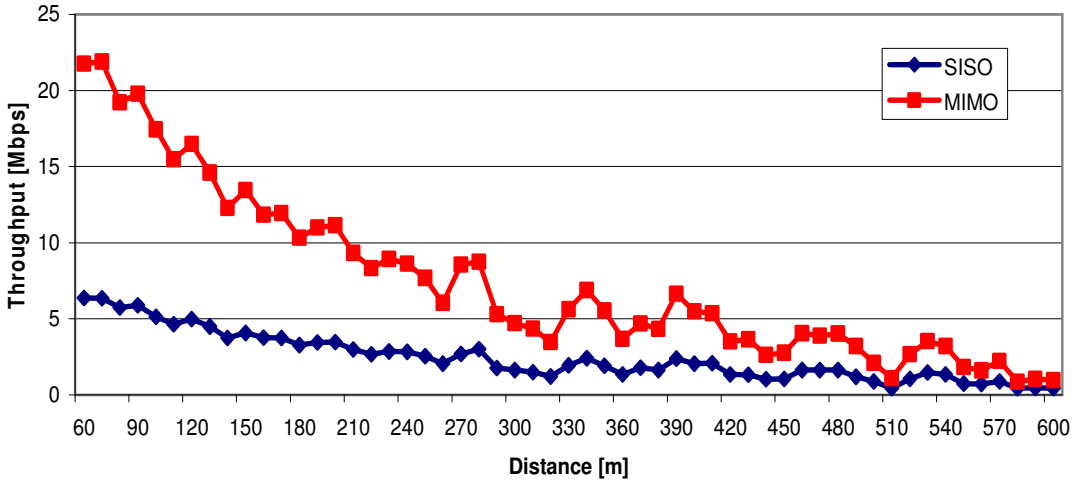

Figure 5.18 Final UL default scenario throughput in a micro-cell scenario.

5.3.2 System Variation

Similar to DL, for a purpose of performance comparison, in the UL analysis, simulations were performed for the other UL systems, namely Release 99 and HSUPA, within the latter concerning both BSPK and QPSK. Note that, with the exception of the default scenario, the SNR target used for the simulations was of 10 dB, which is higher than the one needed to accomplish the maximum throughputs, though it allows a reasonable amount of detected signals. The results are presented in Figure 5.19 and Figure K.3 for pico- and micro-cells, respectively. One can observe that the system with better performance is HSPA+, while the worst one is Release 99. The curves of HSUPA are in between the previous ones, with the one corresponding to QPSK having better performance than the BPSK one.

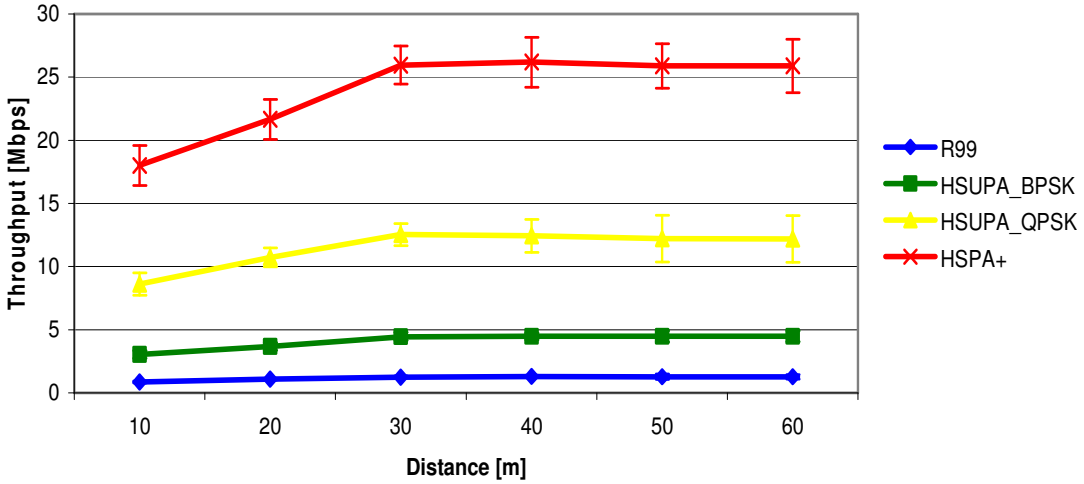

Figure 5.19 UL Throughput vs. distance for various systems and 4×4 MIMO in a pico-cell scenario.

Within the pico-cell, the throughput for Release 99 increases from about 0.9 to 1.3 Mbps from 10 to 40 m, after which the throughput remain approximately constant, while in the micro-cell, the throughput decreases within the whole cell range from 1.3 to 0.7 Mbps. It can be further noticed that the Release 99 throughput variation for UL and DL is the same within the pico-cell scenario. In what concerns the micro-cell scenario, due to MT power limitations, there is a slightly difference between DL and UL, with the former presenting a higher throughput at the end of the cell of 0.1 Mbps. Moreover, one can observe that the use of MIMO on top of Release 99 UL leads to throughputs lower than the ones that can be achieved by HSUPA with BPSK without MIMO, Figure B.3, thus, HSUPA represents a better Release 99 performance improvement than MIMO.

Regarding HSUPA, the throughput behaviour with distance is similar for both modulations, with the main difference being in terms of bit rate magnitude, which is substantially lower for BPSK. In the pico-cell scenario, throughput increases from about 3 to 4.5 Mbps with BPSK and from 8.6 to 12.2 Mbps for QPSK, within 10 to 40 m, becoming approximately constant from 40 to 60 m. However, within the micro-cell scenario, Figure K.3, the throughput decrease experienced for both HSUPA modulations is different, with the underlying reasons of so to happen being the same as for the HSDPA 5 and 10 HS-DPSCH codes, which is the different slope of throughput vs. E_c/N_0 curves.

Therefore, for QPSK the throughput decrease is more intense, being from 12.2 to about 7 Mbps, while for BPSK this decrease is from 4.5 to 2.5 Mbps. Moreover, from these results one can notice that the use of 4×4 MIMO on top of HSUPA with BPSK results in throughputs that can be accomplished by UL HSPA+ SISO.

Despite this average simulated throughput analysis presenting within both cell types better HSPA+ performance, the average detection percentages are not taken into account. Therefore, a further jointly analysis was performed regarding the average detection percentages evolution with distance, Figure 5.20, and the final throughput accounting for it, Figure 5.21. Note that the final throughput is only presented for the micro-cell scenario, since for the pico-cell one it is the same presented in Figure 5.19; the exception is the default scenario that presents a detection percentage lower than 100 %, though regarding this value, the final throughput for the default scenario within a pico-cell has already been depicted and analysed in Figure 5.17.

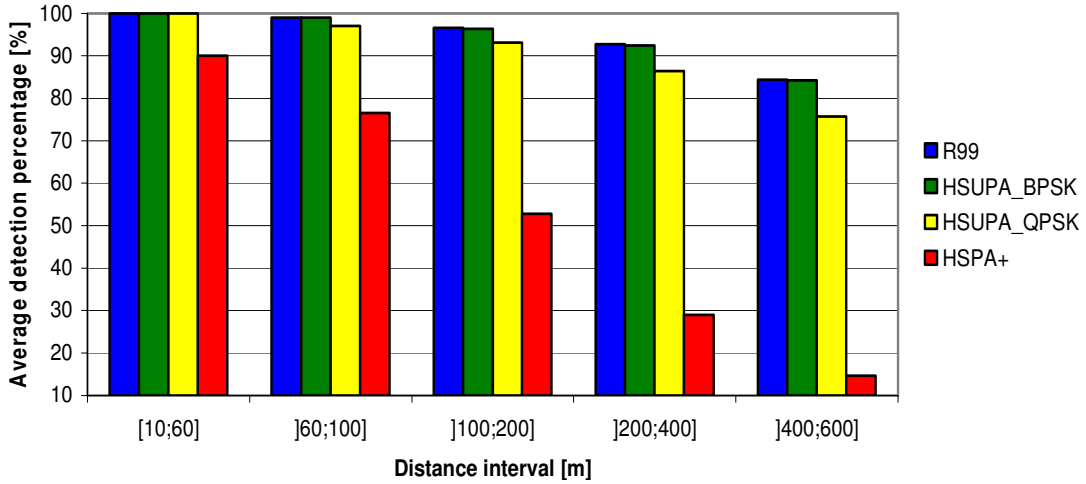

Figure 5.20 Average detection percentage for different UL systems with 4×4 MIMO.

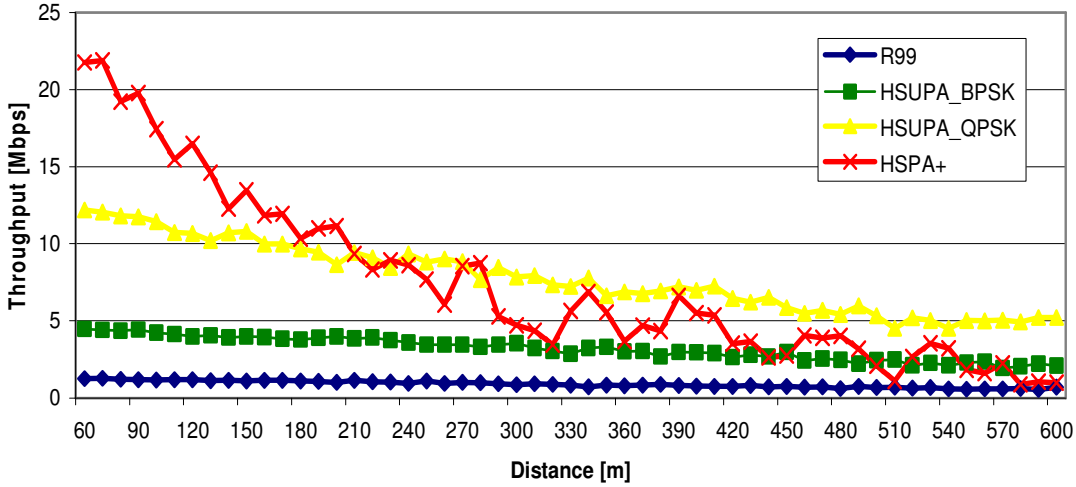

Figure 5.21 Final DL throughput in a micro-cell scenario for different systems.

It is possible to observe from the results in Figure 5.20 that the average detection percentage is much

lower for HSPA+ than for the remaining systems, presenting for the last interval a detection percentage of about 14.7 %, which is less 61 % than the one presented for HSUPA with QPSK, which is the following system with less detection percentage value. For Release 99 and HSUPA with BPSK, the detection percentages are about the same, since the same detector is used for both, due to the use of the same modulation.

Regarding these results, one can notice in Figure 5.21 that the low values of the detection percentages presented for HSPA+ have a major impact in the final throughput, presenting a decrease from 21.8 to about 1 Mbps within the micro-cell scenario. This throughput decrease changes the outcome of the previous observations of the average simulated throughputs, since, when accounting to possible retransmissions, after about 210 m, HSUPA with QPSK modulation and MIMO 4×4 starts having better performance than HSPA+, due to the more robust modulation, which enables a better BER performance, hence, higher connection rate. Despite the irregular behaviour of the default scenario final throughput after 270 m, one can further notice that for distances higher than 500 m, HSUPA with BPSK also starts to presents better results than the default scenario.

Moreover, in what concerns the default scenarios, it is possible to observe that the throughput for UL is lower than for DL for both pico- and micro-cells. However, when comparing with 2×2 HSPA+ DL using 64QAM, the throughput for HSPA+ UL within the pico-cell is lower from 10 to about 15 m, after which it is always higher until the end of the cell. Contrary, on the micro-cell scenario, the throughput is higher for HSPA+ UL until about 100 m, with 2×2 HSPA+ 64QAM performing better above this distance. UL MIMO throughput for the default scenario has worst performance than the SISO DL default system for distances above 300 m.

5.3.3 Different MIMO Configuration Impact

In this subsection, the MIMO configuration is varied regarding the default scenario, with the latter being presented as well, for comparison purposes. The simulation results are plotted in Figure K.4 and Figure K.5 for the pico- and micro-cell scenarios, respectively.

Within the pico-cell scenario, Figure K.4, the throughput achieved by the 2×2 configuration presents a constant behaviour, about 11.7 Mbps, which is lower than the average simulated throughput that can be achieved in DL, using SISO HSPA+ with 64QAM. The same is verified for the 2×4 and 4×2 configurations, with the exception being from 10 to 20 m, since due to MT power limitations, even within the pico-cell scenario there is a slight throughput decrease from around 12.9 to 12.1 Mbps and 12.8 to 12.2 Mbps, respectively. At the end of the pico-cell, the lower throughput for 2×4 related to the 4×2, is due to the detection percentages, which, as one can observe from Figure K.6, is significantly lower for the latter, therefore, leading to higher mean throughputs, since 2×4 allows a wider range of SNR to be detected, hence, a wider range of throughputs is also achieved.

For the micro-cell scenario, Figure K.5, the throughput variation for the different configurations is quite different from the one observed for the pico-cell. In what regards the 2×4 configuration, until about

80 m the throughput is higher than the ones observed for the 2×2 and 4×2 cases, though after this distance the situation inverts drastically, with the throughput for the 2×4 configuration decreasing at a steep slope, from 12.1 to 5.5 Mbps. On the contrary, the 2×2 presents a slightly decrease from 11.8 to 11 Mbps, while the 4×2 configuration maintains an approximately constant value to around 400 m, after which throughput starts to behave irregularly. The reason behind the apparently better performance of 2×2 and 4×2 configurations related to the 2×4 one is the impact of the different detectors for each configuration on the detection percentage, which jointly with MT power limitations results in very low detection percentages and consequently high average throughputs, as previously mentioned. Note that this behaviour had already been noticed for the default scenario, for distances higher than 450 m.

As it can be observed from Figure K.6, for 2×2, 4×2 and 4×4 detection percentages decrease rapidly with distance, with 4×2 having an average percentage detection of about 5.5 %, within the last distance interval. On the contrary, the 2×4 configuration, which has the most robust detector of all configurations, presents for the same interval an average value of 77%. Therefore, for the 2×4 configuration, it has associated a lower average (detected) MIMO throughput, since BER demands are easier to accomplish.

For a better understanding of the detection impact on the throughput of each MIMO configuration, the final throughput, accounting for the detection percentages and the average simulated throughputs, is depicted in Figure 5.22 and Figure 5.23, for the pico- and micro-cell scenarios, respectively.

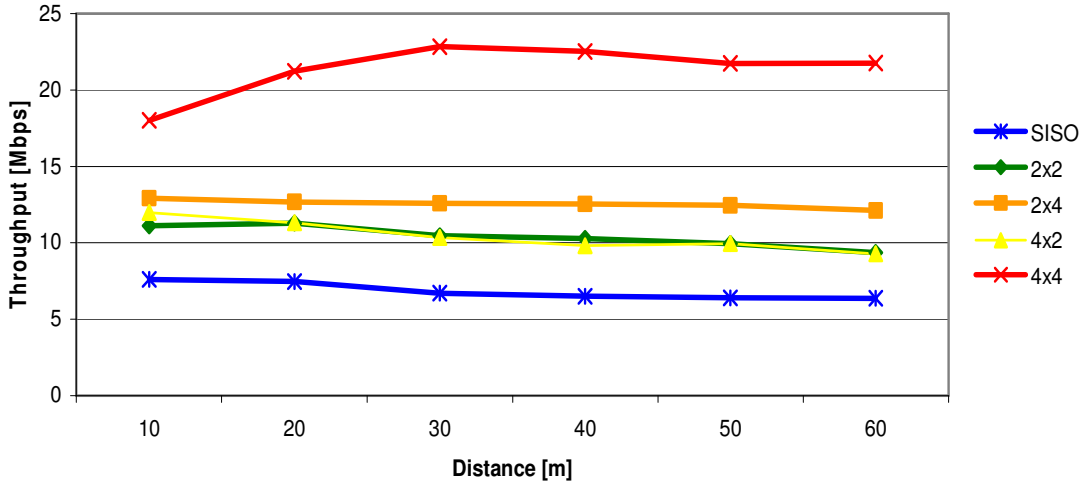

Figure 5.22 Final UL throughput in a pico-cell scenario for different antenna configurations.

Within the pico-cell scenario, the only throughput curve that is the same as the one shown in Figure K.4 is the one corresponding to the 2×4 configuration; all other configurations suffer a throughput decrease, the most notable decrease being for the 4×2 configuration, as expected. Therefore, it can be observed that the final throughputs for the 4×2 and 2×2 configurations, in a pico-cell scenario, decrease from 11.9 to 9.3 Mbps and from 11.1 to 9.4 Mbps, respectively, thus, at the edge of the pico-cell the 2×2 configuration presents slight better performance than the 4×2 one. As one can observe from Figure 5.23, this better performance maintains within the micro-cell, due to the

higher detection percentages that are associated to the 2×2 configuration.

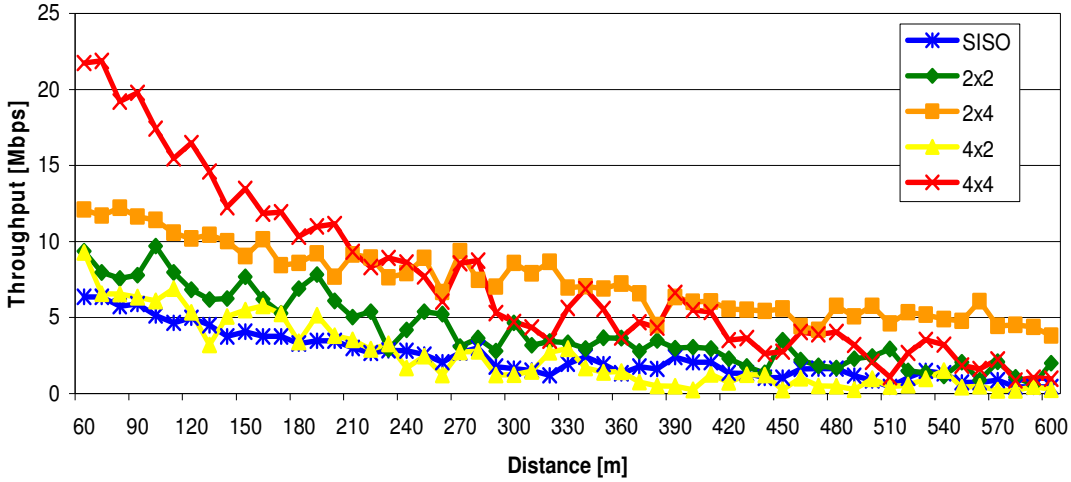

Figure 5.23 Final UL throughput in a micro-cell scenario for different antenna configurations.

For the micro-cell scenario, the throughput associated to the 2×4 configuration, decreases from 12.1 to 3.8 Mbps, therefore, presenting better performance at the end of the cell than the default configuration. However, one can notice that this better performance is achieved at the distance of about 250 m. In what relates to the 2×2 configuration, the throughput decreases from 9.4 to about 1 Mbps, having similar performance related to the default scenario at the edge of the micro-cell. Being the most limitative configuration, the 4×2 configuration presents a throughput decrease from 9.3 to 0.3 Mbps, therefore, having lower throughput values than SISO. Note that this situation is verified not only at the end of the cell, but also for all distances higher than around 350 m.

Moreover, it should be pointed out, that the use of 2×4 in DL corresponds to the use of 4×2 in UL, hence if there are 4 Rx antennas in the DL there will be 4 Tx antennas in the UL, as well. With this in mind, the analysis of performance for each non-symmetric antenna configuration must take which link direction is more limitative into account, despite MT power issues. Hence, despite the worst detection performance of the 4×2 configuration for both links, this configuration is especially attractive when applied to DL, since it corresponds to a 2×4 one in UL, which is the configuration with better detection performance. Therefore, this configuration leads to higher connection radius in the UL, not to mention that it only requires 2 antennas at the MT, similar to the 2×2 configuration, though it allows higher throughputs.

5.3.4 Different Antenna Spacing Effect

The throughput variation regarding the space between the antennas is presented in Figure K.7. With the antenna spacing effect being accounted by the RMG, the space reduction between the antennas for UL results in the same throughput variation as for DL. For the 0.5λ-λ (BS-MT) situation, the throughput decrease is coherent with the correction value presented in Subsection 3.3.3, decreasing on average around 2.5 % within each interval. Likewise, the decrease in the 0.5λ-0.5λ case is also

coherent with the correction value of the RMG to account for the less antenna spacing, being 4.5 % for this situation, which is about the value presented by simulation results. The throughput ratio between the default and the different antenna spacing situations is presented in Table 5.3, for each distance interval, as well as the corresponding mean relation for all the intervals.

Table 5.3 Throughput ratio between the default and the different antenna spacing scenarios.

Ant. Spacing		**Ratio between default and different ant. spacing**					
BS	**MT**	**[10;60]**	**]60;100]**	**]100;200]**	**]200;400]**	**]400;600]**	**Average**
0.5λ	**λ**	0.972	0.978	0.976	0.971	0.977	0.975
0.5λ	**0.5λ**	0.954	0.956	0.955	0.950	0.961	0.955

It should be pointed out that the differences of the throughput ratio value between the default scenario and different antenna spacing situations among the different intervals, are related to the fact that for different SNR values the RMG for the 4×4 configuration takes different values as described in Subsection 3.3.2, thus, for different distances there are different throughput differences.

5.3.5 Different Detector Influence

In this subsection, the analysis of the impact on UL throughput due to a different type of detector is performed, namely for the ML, MMSE and ZF detectors. Simulation results are presented in Figure K.8. Varying the type of detector in UL has the same relative impact as in DL, since the same modulation is considered for the default scenario, over which this analysis is performed, and thus, the ML detector is the one with better performance and ZF the worst. Throughput variation with distance is not constant for the same reasons explained in DL. For the MMSE detector throughput decrease rounds 0.3 Mbps, while for ZF this decrease has a value of about 0.6 Mbps, which is similar to the DL throughput variation. However, it can be noticed that the throughput variation for the higher distances interval regarding the ML ant the MMSE detectors is quite low (0.1 Mbps), since for these distances the achieved SNR values are lower, as a consequence the detectors performance is very similar, Figure G.8 .

Like DL, for UL there are different detection percentages associated to each detector, Figure K.9, and detection percentages are much lower than for DL. For instance, in UL the percentage for the MMSE detector varies from 89.6 to about 13.2 %, while in DL this variation is from 100 to 94.1 %, thus, when considering the presented average throughputs one must bear this in mind, since no telecommunication system can allow to have just a 13% detection percentage. In what concerns the ZF detector, the percentage detections are even lower, varying from 87.6 to 11.3%, which represents for the last interval a decrease of about 81 % in the percentage of established connections for DL and UL.

A further analysis accounting for the detection percentages by using (3.12) has been performed, with

its results being plotted in Figure 5.24. It is possible to observe that the throughput differences increased, while the absolute values have decreased. Therefore, the final impact of using a MMSE or ZF instead of ML results in maximum throughput decreases of 0.8 and 1.5 Mbps, respectively, these values being experienced within the]200;400] m interval.

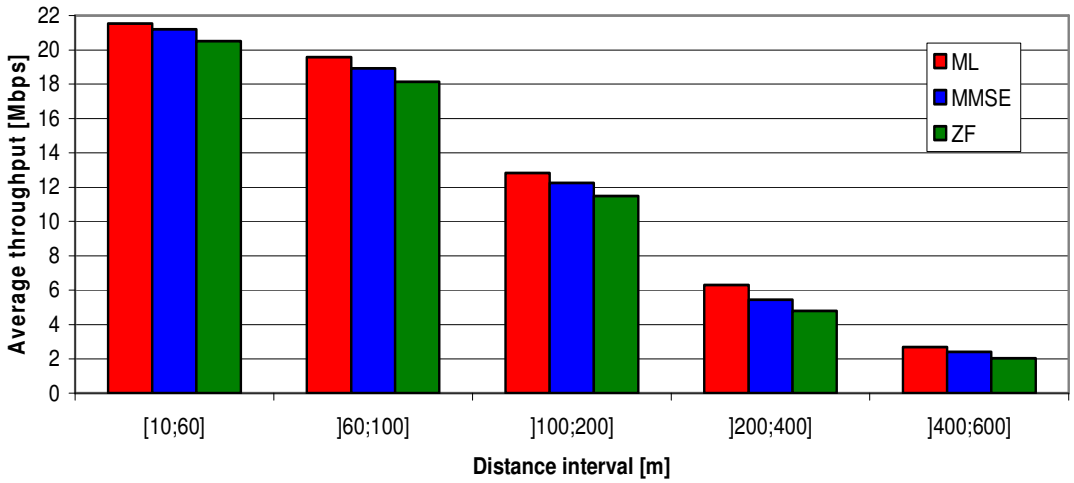

Figure 5.24 Final UL throughput for different types of MMO detectors.

Note that the difference between the detection percentages among the different detectors are wider for]200;400] m. The reason behind this fact is the same as for the throughput variation due to the different detectors, i.e., the different performance inherent to each detector, resulting for high distances in different detection percentages, since lower values of SNR are achieved; sometimes they do not correspond to the minimum needed for a certain detector to accomplish BER demands.

5.3.6 Split or Dedicated Power Effect

The use of split antenna power fed in UL when using MIMO represents a capacity increase relative to SISO with no battery consumption increase, which is desirable. However, from Figure K.10 one can observe that for the 4×4 configuration if split power is used, there is a significant throughput decrease, especially at the end of the micro-cell. In the]400;600] m interval, this throughput decrease if of about 2.7 Mbps, and for the remaining intervals it rounds 0.6 Mbps.

Regarding the 2×2 configuration, the throughput decrease is less notable, though the trend is similar to the 4×4 one, presenting within the last interval a throughput decrease of about 0.5 Mbps. In the remaining intervals, for both presented configurations, the decrease related to the split power use increases with distance due to the increase of detection percentages differences between the dedicated and split situations.

The average detection percentage for both antenna configurations is shown in Figure K.11; as expected, the use of split power fed in UL has significantly more impact in the detection percentage than in DL.

One can further observe that this difference in impact is so huge that, in DL, the 4×4 configuration has a difference in detection percentage of about 6 %, between the split and dedicated cases for]400;600] m, while in UL this difference is felt at much lower distances, i.e., already within the pico-cell scenario. In what relates to the 2×2 configuration, the detection difference within the first interval is of about 1 %, though for the second interval it is 5 %, which is considerably higher than the difference presented for DL in the last interval for this configuration, which is of about 1.5 %. As a consequence, the final throughput, i.e., the throughput that account for the detection percentages, also presents wider variations for UL than for DL, as shown in Figure 5.25.

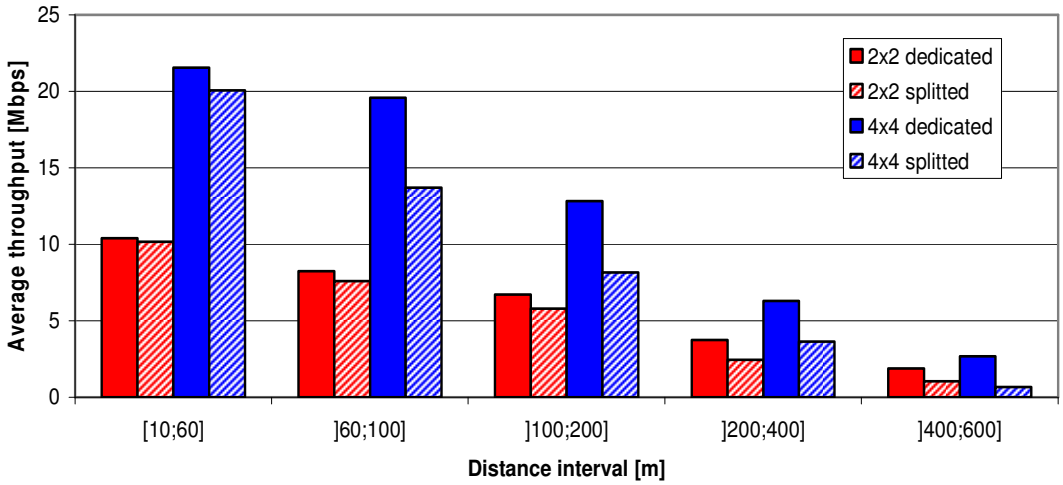

Figure 5.25 Final UL throughput for different types of antenna power fed.

Moreover, for UL the difference in the average detection percentages can reach values of about 11 % for the 2×2 configuration and 22% for the 4×4 one, with these values being reached within the]60;100] m interval instead of the]400;600] m one, since in the former the MT power allows more often to accomplish the BER demands for higher distances.

Despite the overall throughput decrease due to the detection percentages, regarding the results plotted in Figure 5.25, it can be noticed that the wider throughput variations are still for the 4×4 configuration, presenting within the]60;100] m interval, less 5.9 Mbps for the split situation than the dedicated one. However, within the last interval, the final throughput has a throughput difference for both power situations of 2 Mbps, which is less than the one presented in Figure K.10, for the average simulated throughput. This is due to the fact that for these distances the average detection is very low for both power fed options, as well as the difference among them, hence, resulting in lower throughputs for both. In what concerns the 2×2 configuration, the biggest difference is only felt within the]400;600] interval, being of about 1.3 Mbps. Note that this difference, contrary to the 4×4 configuration, is higher than the one presented in Figure K.10, since in this case power is only being divided by 2 when considering the split power fed, thus, allowing detection to higher distances, though at the cost of a lower throughput.

Moreover, these results are once again coherent with the fact that for lower values of SNR (high

distances) the performance of the 4×4 detector is worst than the one of the 2×2 detector, Figure G.3; as a consequence, one can observe that for higher distances the detection percentages of the 4×4 configuration are lower than the ones of 2×2. Therefore, within the]200;400] m interval, the detection differences are higher for the 4×4 situation, since besides the worst detector performance, there is the fact that in this configuration for the split situation the power is divided by 4, hence, half of the power of the 2×2 is available for transmission, therefore, the 2×2 configuration is expected to detect to higher distances for both feeding power situations.

5.3.7 Use of TMA and Reception Diversity

For the UL analysis, it is interesting to consider additional reception gains that can be provided by the use of a TMA and/or reception polarisation diversity. The scheme of the considered polarisation diversity to be used on top of a MIMO system is depicted in Figure K.12. In this subsection the impact of considering such technologies on top of the default scenario is analysed. The analyses are performed by considering the use of each one separately and jointly.

Simulation results for throughput average variation with distance are shown in Figure K.13, in distance intervals for a better perception of the variations. It is possible to observe that the use of TMA leads to a throughput increase, by means of cable losses compensation and 3 dB noise figure reduction; as a consequence higher SNR values are achieved. This throughput increase is of about 0.1 Mbps for the first interval (pico-cell scenario), since for these lower distances the high SNR values needed to achieve the highest throughputs are accomplished with relative easiness, even without TMA. For the following distance interval, the throughput increase experienced by the use of TMA is of about 0.3 Mbps, while for]100;200] m and]200;400] m these differences are of about 0.2 Mbps, which can be justified by the fact that for these distances the detection percentage difference between the default and TMA cases are the highest, Figure K.14. In the last interval the throughput difference is about 0.3 Mbps, since for these distances BER demands are hard to accomplish by both situations, though when detection occurs the value of SNR achieved by the situation that uses TMA is higher, resulting in a higher throughput. Moreover, it should be pointed out that the use of TMA can increase up to 22% the detection percentage of the default scenario, with this maximum being achieved within the]100;200] m interval, Figure K.14.

The use of reception diversity considered in this analysis accounts for a 3 dB polarisation diversity gain; it can be observed from Figure K.13 and Figure K.14 that the relative performance regarding the use of TMA is worst for this case. However, a throughput increase due to the use of reception diversity is also observed, being about 0.2 Mbps maximum, with its trends being similar to the ones presented for TMA, though with lower values. Regarding detection percentages, the use of reception diversity leads to a detection increase up to 9.5%, with this value being experienced in the micro-cell for distances from 100 to 200 m. For distances higher than 200 m, the detection differences are about the same for all intervals (8.4 %), since both situations (with and without reception diversity) are equally unlikely to be detected, though if detected, the use of diversity leads to higher throughputs.

With both, TMA and reception diversity, bringing enhancements in terms of achieved throughput and detection percentage, the use of these technologies jointly was analysed. As expected, the performance for this situation is higher than the ones achieved by the use of the technologies individually. From Figure K.13, it can be observed that the throughput increase is of about 0.1 Mbps for the pico-cell scenario and of about 0.4 Mbps for the micro-cell one. Concerning the detection percentage related to the default scenario, the use of both technologies together brings an increase up to 32%, hence, the highest detection difference related to the default scenario is for the]200;400] m interval instead of being for the]100;200] m as for TMA and reception diversity. Since using these technologies separately brings less performance enhancement than jointly, lower SNR values can be accomplished for the same distances.

Bearing these results in mind, a similar analysis has been performed as for the other parameters variation regarding the final throughput calculation using (3.12), The results of this analysis are depicted in Figure 5.26, and, as expected, it can be noticed that the overall throughput decreases, despite of the considered option. Nevertheless, the benefits of using TMA, reception diversity or both are much more significant in this analysis. The use of TMA can bring a final throughput increase up to 5.3 Mbps, being accomplished for distances from 100 to 200 m, while within the same interval, the use of reception diversity leads to a throughput increase of about 2.4 Mbps. Using both technologies results in the higher throughput increase, being for this interval of about 6.3 Mbps, though the biggest difference is experienced within the]200;400] m interval, leading to a throughput increase of 7.2 Mbps.

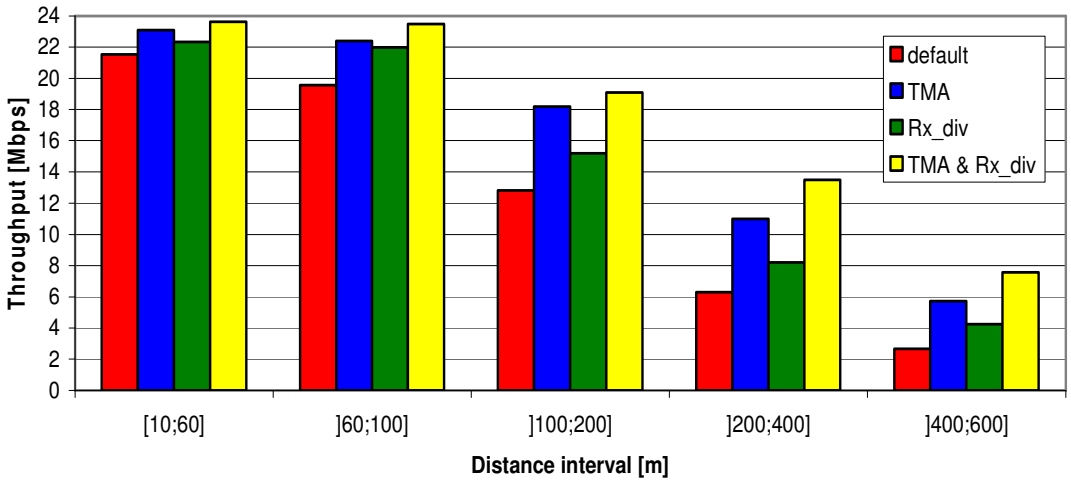

Figure 5.26 Final UL throughput regarding the use TMA and/or reception diversity.

Regardless of the used technology in UL, the throughput experienced in DL for distances up to 400 m is higher than the one that is achieved in UL within a pico-cell. Moreover, for the]400;600] m interval, the DL throughput is higher than the UL one for]100;200] m. However, these enhancements enable a significant UL throughput increase, which is desirable for applications that have (near) symmetric traffic (e.g., video telephony), or that are more demanding in UL transmission (e.g., online gaming and pear-to-pear).

Chapter 6

Conclusions

In this chapter, the main conclusions of this thesis are pointed out, as well as some future work suggestions.

The aim of this work was to analyse the implementation of MIMO in UMTS/HSPA+, in terms of gain dependence on scenarios and other parameters (e.g., MIMO configurations and detectors performance). Bearing this in mind, a great amount of information was gathered in order to develop a model that accounts for as much parameters as possible that can influence MIMO systems performance, with the result being the link model. The link model makes use of some previously developed models and literature results, and it has been implemented in a simulator written in C++. The model enables to calculate SISO and MIMO throughputs for a certain distance, regarding different systems parameters such as, the different layers overheads, modulation, number of codes and throughput functions, as well as regarding MIMO specific parameters, such as the different antenna configurations, different detectors, SNR variation and antenna spacing. All the calculated throughputs are for a single user scenario, which is a substantial constraint of the model. Nevertheless, the link model gives a good estimation of the upper throughput bounders that are related to the use of MIMO. Note that underlying the link model, there is the need to calculate the SNR value for each distance, which strongly depends on the path loss. For the entire path loss calculations the COST 231 Walfisch-Ikegami model was used [DaCo99].

Parallel to the model development and implementation, information was gathered concerning MIMO implementation aspects, i.e., several approaches and literature results were chosen and analysed, with the objective to provide information regarding the changes and/or improvements that have to be performed to BSs and MTs in order to implement MIMO in nowadays systems and respective networks.

To account for the MIMO gain, the link model makes use of the RMG model, developed by [KuCo07], which allows estimating the MIMO gain for a certain distance relatively to SISO. However, inherent to a communication there is a channel over which the communication is established, thus, there is a need to use a channel model to describe it. The GBSB model is the one used by the RMG, with its main advantage being simplicity. This model has been extended by GROW, who suggested grouping scatterers in clusters, which allows to emulate a real behaviour of the radio channel.

The RMG model has several default parameters, though to meet the demands of this work the impact of other parameters on its values, such as the SNR variation and the antenna spacing had to be stressed out. For this purpose, several simulations were performed, with the results for SNR variation being a correction function that was applied to the default RMG value. For the antenna spacing variation, the result was a correction value that was applied to the 0.5λ-λ (BS-MT) and 0.5λ-0.5λ situations, since these were the only situations for which the relative mean error of not considering the different antenna spacing was significant. Note that, for the same reason, the correction function and values were only applied to the 4×4 MIMO configuration, regarding both parameters variation.

The use of MIMO brings additional detection complexity; therefore, an intensive research on this field was performed with the objective to collect coherent information regarding results for BER vs. SNR relation for different antenna configurations, different modulations and different types of detectors, thus, enabling to measure the relative influence on the MIMO throughput of each one. As a result from

this research, 17 detectors performance was gathered, however, this information was not enough and some extrapolations had to be performed in order to account for all the antenna configurations and modulations, so a proper analysis could be performed. Unfortunately for all the considered detectors, the lower value of SNR for which there are values is 5 dB, thus, if a signal has a lower SNR value it is not detected, which is a drawback.

Besides the implementation of HSPA+ on the simulator, Release 99, HSDPA and HSUPA were also implemented, in order to allow the study of the MIMO impact in these systems and perform a comparison with HSPA+. For HSDPA, the analysis can be performed for three different numbers of HS-PDSCH codes, i.e., 5, 10 and 15. Note that for the later number of codes, only 14 were considered, despite one referring to it as 15. In what relates to HSUPA and HSPA+ DL, two different modulations were implemented for each one, i.e., BPSK and QPSK for the former, and 16QAM and 64QAM for the latter.

A first group of simulations was performed for DL and UL, considering HSPA+ with 16QAM and 4×4 MIMO configuration. The use of an ML detector was also contemplated at this point, as well as dedicated power fed, i.e., same power used for MIMO at each antenna, as for SISO. A study regarding both SISO and MIMO throughputs was then performed, for each link, within the pico- and micro-cell scenarios. Note that the macro-cell analysis was not performed, since for this scenario the simulated results do not present statistical relevant results. Within the pico-cell scenario, in DL, throughput increases from 20.5 to 29.5 Mbps, while in UL this increase is from 18 to 23 Mbps. After the distances for which the maximum throughputs are attained, the throughput decreases to the end of the cell down to 1 Mbps for DL and 1.5 Mbps for UL. Concerning the micro-cell scenario, throughput decreases for both links, within the whole cell range. For DL, this decrease is from 29.5 to 17.5 Mbps, which is significantly smoother than the one presented for UL, being from 21.8 to 1 Mbps. The reason for these differences is related to the different detection percentages associated to each link, with DL presenting much higher detection percentages than UL, due to MT power limitations.

Varying the system for DL, within the pico-cell scenario, the higher throughputs are achieved by HSPA+ with 64QAM, and the lower ones by Release 99, as expected. In what concerns HSDPA, the higher the number of codes the higher the throughputs are, for this cell scenario being even higher than the ones presented for HSPA+ with 16QAM. Underlying this fact is the need of a higher SNR value to accomplish the maximum throughput for HSDPA with 15 codes rather than the one needed for HSPA+ with 16QAM, hence, for lower distances this higher SNR target can be achieved most of the times, which results in lower BER and consequently higher throughputs. However, the situation inverts within the micro-cell scenario at about 200 m, since for the same reason, for higher distances lower SNRs are associated, hence, resulting in lower throughputs for HSDPA. From this analysis, one can conclude that the system with better performance is HSPA+ with 64QAM enabling a maximum throughput within the pico-cell scenario of 43.8 Mbps, and having a throughput at the end of the micro-cell of 26.6 Mbps. It should be reinforced that these results are for a 4×4 configuration, however, these throughputs are for most of the distances below the theoretical 42 Mbps presented in the

literature for the 2×2 configuration.

For UL in a pico-cell scenario, the system that presents better performance is HSPA+, and similar to DL the one that has the lower bit rates is Release 99. As a consequence HSUPA performance fits in between the previous ones, with the use of QPSK presenting, as expected, higher throughputs than the use of BPSK. Concerning the micro-cell scenario and accounting for the different detection percentages associated to each system/modulation, the throughput decrease experienced by HSPA+ is much higher than the one presented by the other analysed systems, since 16QAM is a more demanding modulation regarding the symbol decision boundaries. Hence, for distances higher than about 210 m, HSUPA with QPSK starts performing better than HSPA+, presenting at the edge of the cell a bit rate of about 5 Mbps, which is 4 Mbps higher than the one achieved by HSPA+. A better performance related with HSPA+ was also observed for HSUPA with BPSK, though for distances higher than 500 m.

The study of different antenna configurations, namely 2×2, 2×4, 4×2 and 4×4, reveals that for DL within the pico-cell scenario the 4×4 configuration, applied to HSPA+ with 16QAM, is the one capable of accomplishing higher throughputs, 2×2 being the one that accomplishes the lower ones (not to mention SISO). The use of 2×4 configuration leads to throughputs higher than the use of the 4×2 one, despite the RMG value being the same for both configurations; the reason behind this fact is that associated to the latter there is a worst BER vs. SNR performance, since 4 antennas are transmitting and only 2 receiving. The use of 2×2 on top of HSPA+ with 64QAM was also studied, leading to an approximately constant bit rate within the pico-cell scenario of about 19.4 Mbps. Regarding the pico-cell for UL, the throughput relations among the different configurations is similar for the 4×4 and 2×4 ones, however, in what concerns the 2×2 and 4×2 configurations, the situation is slightly different, with the detection percentage effect, leading to a performance decrease of the latter related to the former, after about 20 m. It should be pointed out that, contrary to DL, in the UL pico-cell scenario throughputs do not present a constant value for the 2×2, 2×4 and 4×2 configurations, hence, a decrease is observed.

Moreover, for DL, within the micro-cell scenario, the detection percentages associated to the different MIMO configurations and to the 2×2 one for HSPA+ with 64QAM, have a major impact on the overall results. The use of 64QAM jointly with 2×2 MIMO is the more affected system, since this is the situation that presents the lower detection percentages, hence, the throughput decreases within the whole cell from 19.4 to 17.7 Mbps. Concerning the 2×2 and 4×2 configurations for HSPA+ 16QAM, the throughput also decreases, though with a lower magnitude. The configuration that experiences the lower decrease is the 2×4 one, since it is the one that has the best BER vs. SNR performance and as a consequence the higher detection percentages. Despite the throughput decrease for 4×4, this is the configuration for which the higher throughputs can be achieved in DL, even higher than the ones achieved for the 2×2 one for HSPA+ with 64QAM. However, in UL the situation is quite different from the DL one, since for this link MT power limitations lead to much lower detection percentages. As a consequence of this fact, the configuration for which the higher throughputs are achieved for most of

the micro-cell distances is the 2×4 one, since for the same reason as for DL this is the one that presents the higher detection rates. Although, this configuration does not have a better performance for all distances, the 4×4 configuration is the one that enables higher bit rates for distances up to 250 m. The throughput that can be achieved for the micro-cell scenario by the use of MIMO 2×4 ranges from 12.1 to 3.8 Mbps, these values corresponding to cell edges. Therefore, one can conclude that the use of 2×4 in UL leads to a 2.8 Mbps throughput increase related to the use of 4×4. In what concerns the 2×2 configuration, the throughput decreases from 9.4 to 1 Mbps, having a similar performance than the 4×4 one at the end of the cell. The 4×2 configuration being the most limitative one in terms of detection performance for the previously mentioned reasons, within the micro-cell scenario it experiences a throughput decrease of 9.3 to 0.3 Mbps, which for distances higher than 350 m represents a throughput lower than the one that can be achieved by SISO. It should be further pointed out, that the use of 4×2 in DL corresponds to the use of 2×4 in UL, therefore, despite the worst detection performance of the 4×2 configuration in both links, the use of this configuration for DL is quite attractive for applications that require high UL bit rates, since it enables good UL performance, at the cost of only 2 antennas in the MT, though 4 at the BS.

To evaluate, the impact of different antenna spacing four situations were studied, which resulted from the combination of different antenna spacing options at the BS and MT, the λ and the 0.5λ options being available. The λ-λ (BS-MT) and λ-0.5λ situations had no additional effect on the RMG values and consequently on the throughput value. The throughput for both DL and UL due to the 0.5λ-λ and 0.5λ-0.5λ situations is on average 2.5 and 4.5 % below the default one.

Since detector complexity is a major implementation constraint, the study of different type of detector impact on the throughput was also performed, though only for the 4×4 configuration and HSPA+ with 16QAM. For both links, the use of MMSE leads to a maximum throughput reduction of 0.3 Mbps. Regarding the average detection performances in DL, MMSE has a lower average detection of about 4 % for distances higher than 100 m, presenting the same detection percentage for lower distances as ML. In UL, the differences in detection percentages start being noticed even within the pico-cell scenario, though they are only 1 % lower than ML ones. On the remaining distances these differences can go up to 5 %. The use of ZF has, as expected, the worst performance, thus, the lower throughputs; however, these difference are not very significant, presenting for DL a lower throughput on maximum of 0.5 Mbps related to the ML detector, and for UL of 1.5 Mbps. Associated to ZF, are lower detection percentages of about 1 and 7 % for DL and UL, respectively. Therefore, one can conclude that the use of a different type of detector has a lower impact on the overall throughput.

The power amplifier being an expensive feature of the BS and MT battery autonomy one of the major concerns of the end users, the use of different antenna power fed solutions was also analysed. The two considered options were the ‘dedicated’ power fed and the ‘split’ one. Regarding DL, the analyses were performed for the 2×2 and 4×4 configurations for HSPA+ with 16QAM and for the 2×2 for HSPA+ with 64QAM, with the use of split power fed, as expected, resulting in lower throughputs, these differences being, on average, of about 0.3, 1.5 and 1 Mbps, respectively, for distances from 400 to

600 m. In UL, the situation is quite different, once again due to MT limitations, which for the 4×4 configuration leads to a maximum throughput difference of 5.9 Mbps within a distance interval of 60 to 100 m. The maximum difference is experienced by 2×2 due to the use of split power fed being of 1.3 Mbps, though this difference is felt at higher distances than for the 4×4 case, since the power is only being divided by two, thus, enabling higher detection percentages up to higher distances. From these results, one can conclude that the use of split power fed in DL does not have a major impact on the accomplished throughput, however, for UL this is not true, the throughput decrease being, related to the use of 4×4 with split power, quite significant, i.e., up to about 22 % lower than the use of dedicated power.

Finally, the use of a TMA and/or reception diversity for UL was studied, being noticed a significant throughput improvement for the three situations. Making use of a TMA leads to a detection percentage increase up to 22 % compared to the situation of not using it. As a consequence, higher throughputs can be achieved by its use, this throughput increase being on average of 5.3 Mbps for distances from 100 to 200 m. If reception diversity is used on top of MIMO, the detection percentages, as well as the throughput increase, are lower than for the TMA case; however, they constitute also an improvement compared to the default case of not using it, resulting in an average throughput increase of about 2.4 Mbps within the same distance interval as for the use of TMA. Combining both technologies results in the highest detection and throughput improvements. The average detection percentages for this combined situation present for distances from 200 to 400 m an increase of 32 %, which corresponds to an average throughput increase within the same interval of about 7.2 Mbps. Despite the fact that these UL enhancements are not enough to enable the same throughput as in DL, they constitute an important improvement for applications that demand high UL bit rates.

Underlying the variety of still possible studies that can be performed for this subject, it can be concluded that this is not a finalised work at all. For future work, it is suggested that a multiple users model is developed and implemented on the simulator, in order to allow a multiple users analysis, regarding for instance service type differentiation. The study of the impact on capacity of a different BER value, as well as different channel conditions could also be relevant, and perhaps might enable the macro-cell analysis. The RMG model being based on the GBSB one, which only accounts for one bounce, it should be also interesting to upgrade the RMG model by using a multi bounce channel model, since multiple bounces might have significant influence on the results, as well as the upgrade to a 3D channel model. Moreover, analysis regarding different receiver filter time resolutions would be interesting, since this is one of the most limitative features of MIMO. Finally, one could also suggest the introduction of new systems, such as UMTS/LTE and WiMAX, and the simulator upgrade to account for AMC.

Annex A - UMTS/HSPA Services and Applications

UMTS networks were designed from the beginning for flexible delivery of any type of service. Prioritisation becomes mandatory when the system load gets higher, and services must be differentiated according to their requirements, i.e., QoS differentiation should be applied. 3GPP defined different QoS classes, being, Conversational, Streaming, Interactive and Background.

These four traffic classes are distinguished mainly on the basis of delay sensitivity. This differentiation is shown in Table A.1, where the different characteristics of each class are brought up, allowing a better comprehension of the whole concept.

The Conversational class is the most delay-sensitive one, since it is intended for real-time communication, where traffic is nearly symmetric between UL and DL, and end-to-end delay has to be less than 400ms, this being the maximum acceptable delay for human perception of video and audio conversation. Video telephony has Bit Error Rate (BER) requirements even tighter than voice, due to video compression, and it can be transmitted in CS or PS.

The speech codec used in UMTS employs the Adaptative Multirate (AMR) technique with eight source rates, namely 12.2 kbps. Discontinuous Transmission (DTX) is used in the AMR codec, in order to reduce the average required bit rate, leading to a lower interference level, hence, increased capacity. Another application that fits the Conversational class is Voice over IP (VoIP), which requires QoS differentiation and IP header compression.

Table A.1 UMTS traffic class parameters (extracted from [3GPP01] and [3GPP02d]).

Service Class	**Conversational**	**Streaming**	**Interactive**	**Background**
Real time	Yes	Yes	No	No
Symmetric	Yes	No	No	No
Switching	CS	CS	PS	PS
Guaranteed rate	Yes	Yes	No	No
Delay	Minimum Fixed	Minimum Variable	Moderate Variable	High Variable
Buffer	No	Yes	Yes	Yes
Bursty	No	No	Yes	Yes
Example	Voice	Video-clip	WWW	email

Streaming class services are based on the multimedia streaming technique, which enables the end

user to access data before the transfer is complete. This is achieved through a continuous stream transmission and the use of buffers in the final applications. In this case, traffic is not symmetric; hence, DL traffic is the most significant one.

Web browsing and online multiplayer games are examples of applications from the Interactive class, as well as push-to-talk and location-based services. This class is based on PS connections with a very asymmetric traffic, being tolerant to delay. Web browsing may support large delays, but still, in order to accomplish a good communication, the delay should be lower than 4 to 7 s. For multiplayer games, the Round Trip Time (RTT) is a very important parameter, especially in real time action games, where the end-to-end delay should be below 100 ms.

The main distinguishable characteristic between the Interactive class and the Background one is that in the former the end user is waiting for a response within a certain time, while in the latter he/she is not. Resource transmissions are only used in Background when none of the other classes are active, making this the most delay-insensitive one. This class, like the Interactive one, is intolerant to transmission errors. Some of the applications in this class are the Short Message Service (SMS), Multimedia Message Service (MMS), and e-mail delivery.

Annex B - UMTS/HSPA Capacity and Interference

When dimensioning a UMTS network, there are three main limiting capacity factors that have to be estimated, i.e., the number of channelisation codes, the BS transmitting power, and the traffic load.

The main different characteristic of capacity between GSM and UMTS is that it is user dependent in the latter. In this way, the number of available channelisation codes can limit the system, since they depend directly on the SFs, which are related to channel bit rates, i.e., high bit rate services with low SFs, such as streaming multimedia, will leave fewer resources to others, contrary to services like speech telephony that will let more MTs access the system.

WCDMA has a frequency reuse of one, making UMTS capacity particularly sensitive to the amount of interference. The load factors are given by (B.1) for the UL and (B.2) for the DL.

$$\eta_{UL} = (1+i)\cdot\sum_{j=1}^{N_u}\frac{1}{1+\frac{G_{Pj}}{(E_b/N_0)_j\cdot v_j}} \tag{B.1}$$

$$\eta_{DL} = \sum_{j=1}^{N_u} v_j \cdot \frac{(E_b/N_0)_j}{G_{Pj}}\cdot\left[\left(1-\alpha_j\right)+i_j\right] \tag{B.2}$$

where:

- v_j : activity factor of user *j* (typically 0.67 for speech and 1.0 for data);
- E_b : signal energy per bit;
- G_{Pj} : processing gain of user *j*, defined as:

$$G_{Pj} = R_c/R_{bj} \tag{B.3}$$

- R_{bj} : bit rate of user *j*;
- R_c : WCDMA chip rate (R_c is always 3.84 Mcps);
- *i*: ratio of inter- to intra-cell interferences;
- N_0 : noise spectral density;
- N_u: number of users per cell;
- α_j : DL channel orthogonality of user *j* (typically between 0.4 and 0.9);
- i_j : ratio of inter- to intra-cell interferences for user *j*.

Load equations (B.1) and (B.2) are used to estimate the noise rise and cell capacity, the former being

associated to the interference margin used in the link budget:

$$M_I^{UL/DL}{}_{[\mathrm{dB}]} = -10\log(1-\eta_{UL/DL}) \tag{B.4}$$

The BS transmitting power is shared among all users, being upper bounded, hence, it is a very limiting factor in cell capacity. The total transmission power of the BS can be expressed as:

$$P_{Tx[\mathrm{W}]} = \frac{N_0 \cdot R_c \cdot \sum_{j=1}^{N_u} v_j \frac{(E_b/N_0)_j}{G_{P_j}} \cdot L_{p_j}}{1-\overline{\eta_{DL}}} \tag{B.5}$$

where:

- $\overline{\eta_{DL}}$: average DL load factor value across the cell;
- L_{p_j} : path loss between BS and user *j*;

Concerning HSDPA performance, it depends mostly on network algorithms, deployment scenarios, traffic generated, QoS and MT receiver performance and capability. Despite the HSDPA SF of 16, only 15 codes can be allocated for data transmission, since one is needed for the HS-SCCH transmission. From the BS point of view, all the 15 codes can be allocated, this is not true for The MT which can only allocate 5, 10 or 15 codes. In HSDPA there are 12 MT categories with different DL bit rates, going from 0.9 to 14.4 Mbps [HoTo06].

The performance evaluation in HSDPA is different from the one used by Release 99, which uses E_b/N_0 to denote the signal energy per bit over noise spectral density. However, this is not an adequate measure for HSDPA, since the bit rate varies every TTI on the HS-DSCH, due to the HSDPA fundamental features for link adaptation, such as Adaptive Modulation and Coding (AMC), multicode transmission (multiple HS-PDSCHs), and fast L1 HARQ. Thus, the method used to evaluate performance in HSDPA is the average HS-DSCH Signal to Interference Plus Noise Ratio (SINR), after de-spreading the HS-PDSCH, given by (B.6) for a single-antenna Rake receiver. This metric is an essential measure for HSDPA link budget planning and network dimensioning, since it is independent of the number of HS-PDSCH codes used, the modulation scheme, and the effective code rate.

$$\rho_I = SF_{16} \frac{P_{\text{HS-DSCH}}}{(1-\alpha)\cdot P_{\text{intra}} + P_{\text{inter}} + N} \tag{B.6}$$

where:

- SF_{16}: SF of 16;
- $P_{\text{HS-DSCH}}$: received power of the HS-DSCH summing over all active HS-PDSCH codes;
- P_{intra}: received intra-cell interference;
- P_{inter}: received inter-cell interference;
- N: total noise power;
- α : DL orthogonality factor;

Other metric used, regarding performance, is the instantaneous required HS-DSCH SINR, measuring

the SINR required per-TTI on the HS-DSCH in order to accomplish a certain Block Error Rate (BLER) for a given HS-PDSCH number of codes, type of modulation and coding scheme. One can see the relationship between the average HS-DSCH throughput and the average HS-DSCH SINR for 5, 10 and 15 HS-PDSCH number of codes, in Figure B.1.

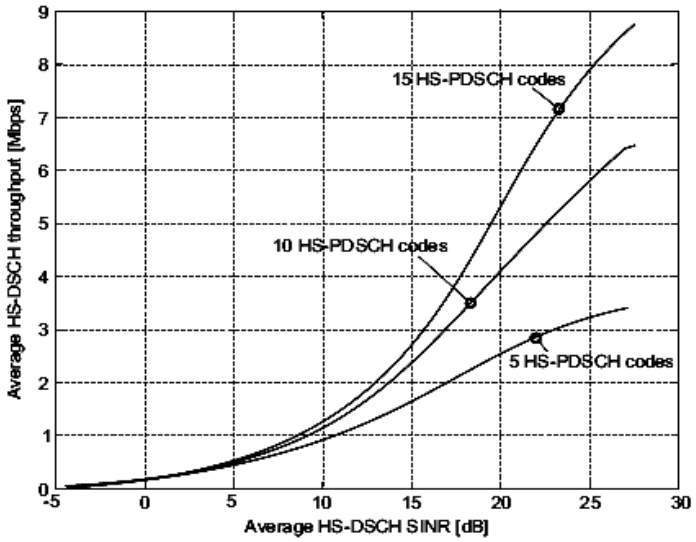

Figure B.1 Average HS-DSCH throughput versus the average HS-DSCH SINR for 5, 10 and 15 HS-PDSCH codes (extracted from [Pede05]).

In order to estimate the achievable HSDPA single-user throughput, aiming at network dimensioning, it is possible to use the wideband average Primary-Common Pilot Channel (P-CPICH) E_c/N_0 pilot. The average HS-DSCH SINR can be expressed as a function of the average P-CPICH,

$$\rho_I = SF_{16} \frac{P_{\text{HSDPA}}}{\frac{P_{pilot}}{\rho_{pilot}} - \alpha P_{Tx}} \tag{B.7}$$

where:

- P_{HSDPA}: HSDPA transmit power;
- P_{Tx}: total Node B transmit power;
- P_{pilot}: P-CPICH transmit power;
- ρ_{pilot}: P-CPICH E_c/N_0 when HSDPA is active.

For single-user performance, the choice of modulation and coding scheme, for link adaptation, is done concerning the instantaneous SINR in order to optimise throughput and delay. For lower SINR, QPSK is used, whereas 16QAM is employed for a high SINR, since it is necessary to provide higher data rates. The effect of different modulations on the performance of a single-user, supporting 5 HS-PDSCH codes, using QPSK/16QAM or only QPSK is shown in Figure B.2 as a function of the HS-DSCH SINR. For lower values of SINR (less than 10 dB), the throughout is similar for both modulations, while for higher values the differences can go to, approximately 2 Mbps.

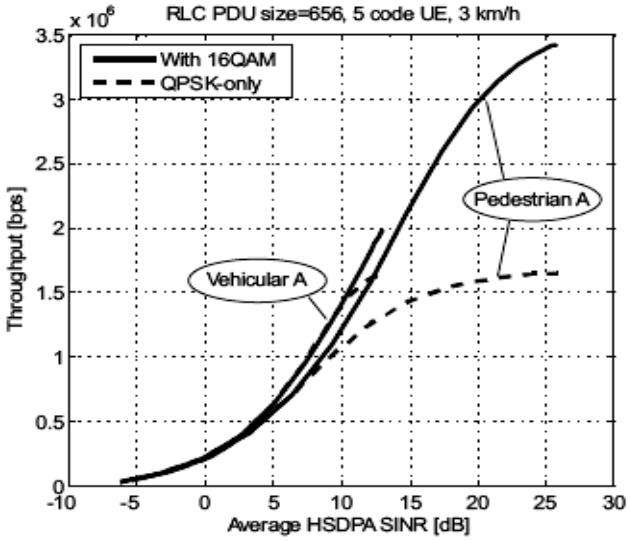

Figure B.2 Single user five code performance with 16QAM or QPSK only (extracted from [HoTo06]).

Similar to HSDPA, performance in HSUPA depends on network algorithms, deployment scenario, type of traffic, BS receiver performance and capability, and MT transmitter capability. In HSUPA, there are 6 MT classes, accommodating theoretically bit rates between 69 kbps and 4.059 Mbps. For performance testing purposes, a set of E-DCH channel configurations are defined, the Fixed Reference Channels (FRCs).

The performance metric used by HSUPA is the energy per chip to noise spectral density ratio E_c/N_0, similar to Release 99 due to the absence of AMC. A high E_c/N_0 at the BS is necessary in order to achieve higher data rates, which leads to an increase of the UL noise, thus, decreasing the cell coverage area. Concerning this, a maximum level for UL noise may be defined for macro-cells, though it limits high data throughputs.

The expected throughput for medium speed MTs as a function of the available E-DCH E_c/N_0, without power control, is plotted in Figure B.3, for FRC2, FRC5 and FRC6, where FRC5 represents a first-phase HSUPA MT, while FRC2 and FRC6 represent future release MTs with advanced capabilities, such as support for a 2ms TTI and higher coding rates. As expected, FRC2 achieves a higher throughput, although the maximum shown can only be accomplished for high E_c/N_0 values, which in real networks may be difficult to achieve. In what concerns the use of QPSK, in Figure E.3, the expected throughput is depicted as function of the available E-DCH E_c/N_0.

The capacity increase from HSUPA is mainly due to the use of L1 HARQ and BS based scheduling. The use of L1 HARQ has two main advantages being: Faster Retransmissions at L1 than in L2 RLC-based, and the use of soft combining of retransmissions. Faster Retransmissions lead to a decrease of E_b/N_0 which increases spectral efficiency, while the combining techniques, can improve BS performance. UL spectral efficiency can be improved by increasing the Block Error Probability (BLEP) at first transmission, which leads to a lower E_b/N_0 requirement. Assuming realistic traffic, the cell throughput gain due to the use of L1 HARQ is approximately 15 to 20 %.

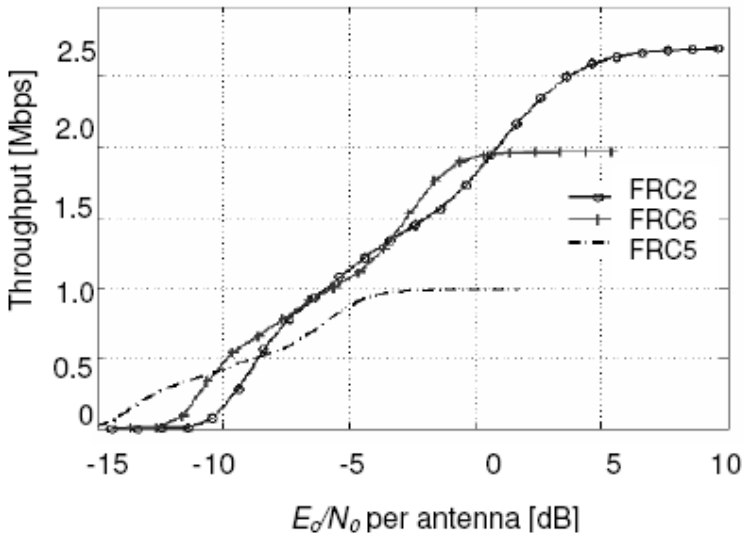

Figure B.3 HSUPA throughput in Vehicular A at 30 km/k, without power control (extracted from [HoTo06]).

Regarding BS based scheduling, it can provide tighter control of total received UL power, as well as faster reallocation of radio resources among users, with the former allowing faster adaptation to interference variations, and the latter dynamically take resources from users with low usage of allocated radio resources, and redistribute them among users with high usage. BS based scheduling provides a cell throughput increase of approximately 15 to 20% on top of the gain from L1 HARQ.

Annex C - RMG Complement

In this annex, one presents complementary information regarding the RMG model. In Table C.1 the simulation parameters of the default RMG model are presented. In Figure C.1, the results from the RMG model are plotted, for a 4×4 MIMO system and at distances of 100, 200 and 300 m. The variance is presented in Table C.2 and the mean results of the RMG model are presented in Table C.3 and Table C.4. Additional results regarding the simulations performed to stress out the SNR variation effect on the default RMG model for the 2×2 and 2×4 (4×2) are presented in Figure C.2 and Figure C.3, respectively.

Table C.1 Simulation parameters (extracted from [KuCo07]).

Carrier frequency [GHz]	2		
Bandwidth [MHz]	5		
Time resolution (receiver filter) [ns]	200		
Antenna spacing	λ		
Noise floor [dBm]	-150		
SNR [dB]	10		
Cluster density [10^{-4} m^2]	**pico**	**Micro**	**macro**
	8.9	2.2	2.2
Avg. number of scatterers per cluster	10		
N_T	[2 - 16]		
N_R	[2 - 16]		
Number of runs	100		
Distance [m]	**pico**	**Micro**	**macro**
	[10 – 60]	[100 – 600]	[1200 – 2400]

Table C.2 Variance for different number of Tx and Rx antennas (adapted from [KuCo07]).

$\sigma^2_{RMG}(10^{-3})$		Pico				micro				macro			
N_R		**2**	**4**	**8**	**16**	**2**	**4**	**8**	**16**	**2**	**4**	**8**	**16**
N_T	**2**	18.5	10.4	4.9	7.3	24.0	15.9	8.7	30.9	1.9	1.8	1.6	0.0
	4	11.8	45.4	29.4	36.7	15.9	71.4	66.1	70.7	0.8	1.1	0.5	0.0
	8	6.2	40.1	112.6	101.7	8.7	66.1	137.4	138.7	0.3	0.3	0.0	0.0
	16	12.3	51.3	118.2	228.6	30.9	70.7	138.7	208.2	0.0	0.0	0.0	0.0

Table C.3 μ_{RMG} for systems with $N_{T/R}$ = 2 for different distances (extracted from [KuCo07]).

$N_{R/T}$	μ_{RMG}
2	1.54
4	1.70
8	1.84
16	1.77

Table C.4 μ_{RMG} for systems with $N_{T/R}$ > 2 for different distances (extracted from [KuCo07]).

$N_T \times N_R$	Range [m]	μ_{RMG}
4×4	10-31	$50.32d_{[km]} + 1.77$
	31-57	3.36
8×4	10-31	$52.56d_{[km]} + 1.84$
	31-57	3.50
8×8	10-29	$117.59d_{[km]} + 2.11$
	29-59	3.36
16×4	10-28	$76.80d_{[km]} + 1.28$
	28-58	3.50
16×8	10-28	$138.23d_{[km]} + 1.51$
	28-58	5.43
16×16	10-27	$225.37d_{[km]} + 1.71$
	27-42	7.86

(a) Pico-cell environment

$N_T \times N_R$	Range [m]	μ_{RMG}
4×4	57-686	$-2.00d_{[km]} + 3.47$
8×4	57-680	$-2.08d_{[km]} + 3.62$
8×8	59-703	$-4.88d_{[km]} + 5.86$
16×4	58-692	$-2.74d_{[km]} + 3.66$
16×8	58-675	$-5.42d_{[km]} + 5.75$
16×16	42-654	$-8.61d_{[km]} + 8.23$

(b) Micro-cell environment

$N_T \times N_R$	Range [m]	μ_{RMG}
4×4	686-2400	2.10
8×4	680-2400	2.21
8×8	703-2400	2.42
16×4	692-2400	1.76
16×8	675-2400	2.09
16×16	654-2400	2.59

(c) Macro-cell environment

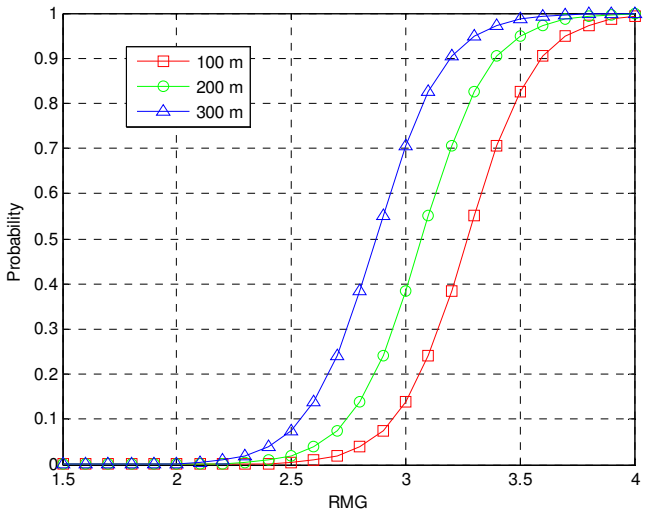

Figure C.1 Modelled distribution of the RMG (adapted from [KuCo07]).

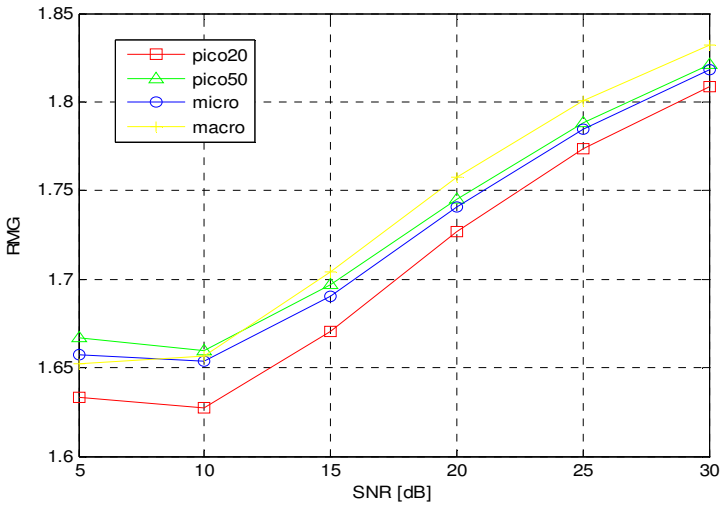

Figure C.2 RMG variation with the SNR for a 2x2 MIMO system.

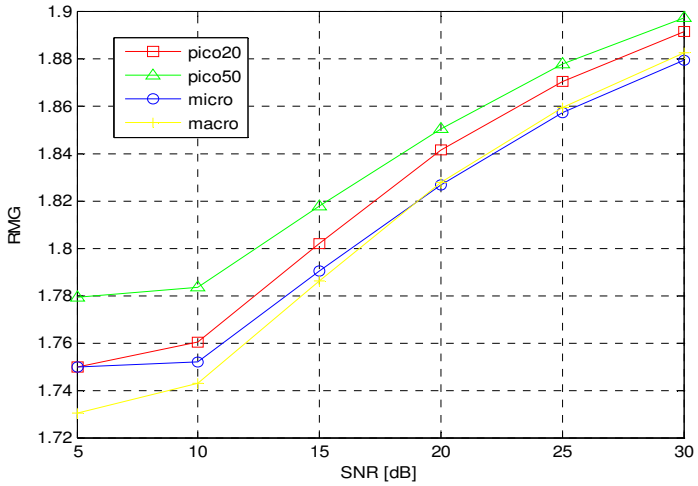

Figure C.3 RMG variation with the SNR for a 2x4 and 4x2 MIMO system.

Annex D - Link Budget

Throughout this thesis the link budget used is based on the Release 99 one, which is described in detail in [CoLa06] and [Sant04], and it has been adapted to HSDPA and HSUPA by [Lope08], which fits better the demands of this work. The link budget considered for HSPA+ is the same considered for HSDPA and HSUPA for DL and UL, respectively.

The path loss can be generally defined for each link as [Corr08]:

$$L_{p[\mathrm{dB}]} = P_{t[\mathrm{dBm}]} + G_{t[\mathrm{dBi}]} - P_{r[\mathrm{dBm}]} + G_{r[\mathrm{dBi}]} = EIRP_{[\mathrm{dBm}]} - P_{r[\mathrm{dBm}]} + G_{r[\mathrm{dBi}]} \quad \text{(D.1)}$$

where:

- L_p: path loss;
- P_t: transmitting power at antenna port;
- G_t: transmitting antenna gain;
- P_r: available receiving power at antenna port;
- G_r: receiving antenna gain.

If diversity is used, G_r must account for the extra gain that is introduced, being substituted in (D.1) by (D.2), where G_{div} is the achieved diversity gain, with a typical value of 3 dB for 2 antennas. When used, it is only considered in UL, since the space in the MT for spatial diversity is limited, and polarisation diversity requires doubling the transmit equipment at the BS. Typical urban sites use, receive, polarisation diversity (cross-polarised antennas), requiring only one antenna per sector, minimising network cost and visual impact [Sant04].

$$G_{rdiv[\mathrm{dB}]} = G_{r[\mathrm{dB}]} + G_{div[\mathrm{dB}]} \quad \text{(D.2)}$$

The Equivalent Isotropic Radiated Power (EIRP) can be calculated using (D.3) or (D.4) if DL or UL is considered, respectively:

$$EIRP_{[\mathrm{dBm}]} = P_{Tx[\mathrm{dBm}]} + G_{t[\mathrm{dBi}]} - L_{c[\mathrm{dB}]} - P_{Sig[\mathrm{dBm}]} \quad \text{(D.3)}$$

$$EIRP_{[\mathrm{dBm}]} = P_{Tx[\mathrm{dBm}]} + G_{t[\mathrm{dBi}]} - L_{u[\mathrm{dB}]} - P_{Sig[\mathrm{dBm}]} \quad \text{(D.4)}$$

where:

- L_c: cable losses between transceiver and the antenna;
- P_{Sig}: signalling power;
- L_u: body losses.

The received power can be calculated by (D.5) for DL and (D.6) for UL:

$$P_{Rx[\mathrm{dBm}]} = P_{r[\mathrm{dBm}]} - L_{u[\mathrm{dB}]} \quad \text{(D.5)}$$

$$P_{Rx[\text{dBm}]} = P_{r[\text{dBm}]} - L_{c[\text{dB}]} \quad \text{(D.6)}$$

where:

- P_{Rx}: received power at receiver input.

The receiver sensitivity can be approximated by:

$$P_{Rx\ \min[\text{dBm}]} = N_{[\text{dBm}]} - G_{P[\text{dB}]} + \rho_{[\text{dB}]} \quad \text{(D.7)}$$

where:

- N: total noise power given by (D.8);
- G_P: processing gain, Table D.1;

Table D.1 Processing gain and SNR definition for the various systems (adapted from [Lope08]).

System	Processing Gain	SNR
R99 DL/UL	R_c/R_b	E_b/N_0
HSDPA	Fixed and equal to 16	SINR
HSUPA	R_c/R_b	E_b/N_0
HSPA+ DL	Fixed and equal to 16	SINR
HSPA+ UL	R_c/R_b	E_b/N_0

The total noise power is:

$$N_{[\text{dBm}]} = -174 + 10 \cdot \log(\Delta f_{[\text{Hz}]}) + F_{[\text{dB}]} + M_{I[\text{dB}]}^{UL/DL} \quad \text{(D.8)}$$

where:

- Δf: signal bandwidth, being equal to R_c in UMTS;
- F: receiver's noise figure;
- $M_{I[\text{dB}]}^{UL/DL}$: interference margin given by (B.4) for DL and UL.

However, the interference margin is not taken into account in the link model, since the model is related to single user situation, which leads to load factors of 0%.

In order to calculate the total path loss, some additional margins must be taken into account to adjust additional losses due to radio propagation:

$$M_{[\text{dB}]} = M_{SF[\text{dB}]} + M_{FF[\text{dB}]} + L_{ind[\text{dB}]} - G_{SHO[\text{dB}]} \quad \text{(D.9)}$$

where:

- M_{SF}: slow fading margin;
- M_{FF}: fast fading margin;
- L_{ind}: indoor penetration losses;
- G_{SHO}: soft handover gain, not considered for HSDPA and HSPA+ DL.

The fast and slow fading are described by Rayleigh and Gaussian distributions, respectively, and are introduced in order to guarantee more realistic results. Expression (D.10) stands for the CDF of the

Rayleigh distribution, while the Gaussian distribution CDF is given by (D.12).

$$P(x) = 1 - e^{-x^2/\overline{x^2}} \tag{D.10}$$

where:

- $\overline{x^2}$: mean square error, defined by:

$$\overline{x^2} = \frac{4\sigma}{4-\pi} \tag{D.11}$$

- σ: standard deviation;

$$P(x) = \frac{1 + \text{erf}\left(\frac{x-\overline{x}}{\sqrt{2}\sigma}\right)}{2} \tag{D.12}$$

where:

- $\overline{x}$: mean;
- erf(): error function, given by:

$$erf(v) \cong 1 - \sqrt{\pi}\frac{e^{-v^2}}{(\pi-1)v + \sqrt{v^2+\pi}}, \quad v > 0 \tag{D.13}$$

The total path loss can then be calculated by:

$$L_{p\ total[\text{dB}]} = L_{p[\text{dB}]} - M_{[\text{dB}]} \tag{D.14}$$

The total pathloss is used to calculate the receiver sensitivity, which allows calculating SNR, in order for it to be mapped onto throughput. The pathloss is calculated using the propagation model COST 231 Walfisch-Ikegami, presented in Annex B. After some basic manipulation of (D.1) and substituting L_p by $L_{p\ total}$, and P_r by $P_{Rx\ min}$, the receiver sensitivity, is given by (D.15), for DL, and by (D.16) for UL.

$$P_{Rx/\text{DL}[\text{dBm}]} = EIRP_{[\text{dBm}]} - L_{p\ total[\text{dB}]} + G_{r[\text{dBi}]} - L_{u[\text{dB}]} \tag{D.15}$$

$$P_{Rx/UL[\text{dBm}]} = EIRP_{[\text{dBm}]} - L_{p\ total[\text{dB}]} + G_{r[\text{dBi}]} - L_{c[\text{dB}]} \tag{D.16}$$

Rearranging (D.7), the SINR for HSDPA and HSPA+ DL, associated to a certain user distance, is calculated by (D.17), while the E_b/N_0, for the UL and Release 99, takes the form of (D.18).

$$\rho_{I[\text{dB}]} = P_{Rx/DL[\text{dBm}]} - N_{[\text{dBm}]} + G_{P[\text{dB}]} \tag{D.17}$$

$$E_b/N_{0\,[\text{dB}]} = E_c/N_{0[\text{dB}]} + G_{P[\text{dB}]} \tag{D.18}$$

Annex E - Systems Throughput

For HSDPA, the values of throughput in function of SINR for 5, 10 and 15 HS-PDSCH codes, are calculated, considering the functions obtained by polynomial interpolation of Figure B.1. These functions are based on the results of [Lope08], plotted in Figure E.1. It is considered that the user is using a category 10 MT, being able to receive all the 15 codes. Despite the fact that the results presented in Figure E.1 are for 15 HS-PDSCH codes, these values where approximated for 14 HS-PDSCH codes, as referred in Section 3.4., since there where no available simulations regarding the latter number of codes.

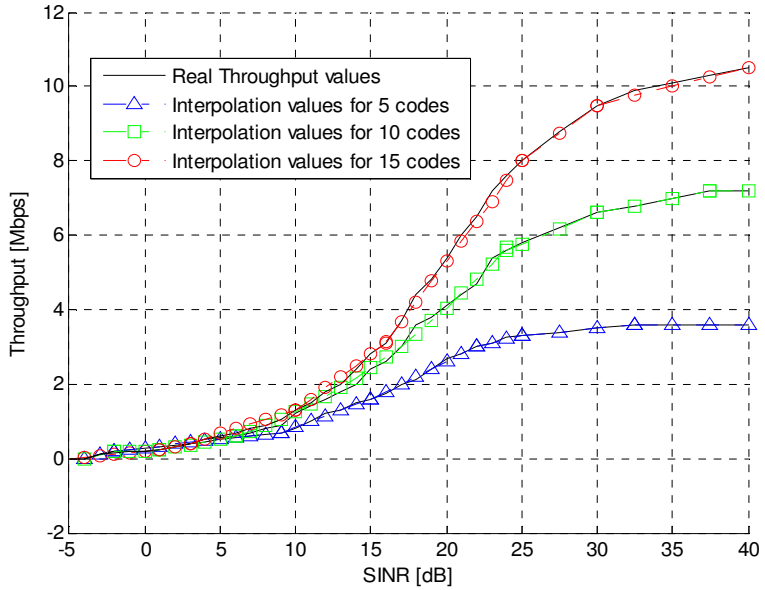

Figure E.1 HSDPA throughput as function of the SINR.

The throughput value in function of the SINR is given by (E.1), (E.2) and (E.3) for 5, 10 and 15 HS-PDSCH codes, respectively.

$$TP_{P[\text{Mbps}]} = \begin{cases} 0.0464 \times \rho_{[\text{dB}]} + 0.2828, & 5 \le \rho_{[\text{dB}]} \le 9 \\ 0.15 \times \rho_{[\text{dB}]} - 0.65, & 9 < \rho_{[\text{dB}]} \le 15 \\ 0.2 \times \rho_{[\text{dB}]} - 1.4, & 15 < \rho_{[\text{dB}]} \le 22 \\ 0.1 \times \rho_{[\text{dB}]} + 0.8, & 22 < \rho_{[\text{dB}]} \le 25 \\ 0.04 \times \rho_{[\text{dB}]} + 2.3, & 25 < \rho_{[\text{dB}]} \le 32.5 \\ 3.6, & \rho_{[\text{dB}]} > 32.5 \end{cases} \quad \text{(E.1)}$$

$$TP_{P[\text{Mbps}]} = \begin{cases} 0.076 \times \rho_{[\text{dB}]} + 0.144, & 5 \le \rho_{[\text{dB}]} \le 6 \\ 0.0085 \times \rho_{[\text{dB}]}^2 + 0.0271 \times \rho_{[\text{dB}]} + 0.1141, & 6 < \rho_{[\text{dB}]} \le 24 \\ 0.1667 \times \rho_{[\text{dB}]} + 1.599, & 24 < \rho_{[\text{dB}]} \le 30 \\ 0.08 \times \rho_{[\text{dB}]} + 4.2, & 30 < \rho_{[\text{dB}]} \le 37.5 \\ 7.2, & \rho_{[\text{dB}]} > 37.5 \end{cases} \quad \text{(E.2)}$$

$$TP_{P[\text{Mbps}]} = \begin{cases} 0.1296 \times \rho_{[\text{dB}]} + 0.014, & 5 \le \rho_{[\text{dB}]} \le 10 \\ 0.3 \times \rho_{[\text{dB}]} - 1.7, & 10 < \rho_{[\text{dB}]} \le 16 \\ 0.54 \times \rho_{[\text{dB}]} - 5.5, & 16 < \rho_{[\text{dB}]} \le 25 \\ 0.3 \times \rho_{[\text{dB}]} + 0.5, & 25 < \rho_{[\text{dB}]} \le 30 \\ 0.1 \times \rho_{[\text{dB}]} + 6.5, & 30 < \rho_{[\text{dB}]} \le 35.8 \\ 10.08, & \rho_{[\text{dB}]} > 35.8 \end{cases} \quad \text{(E.3)}$$

For HSUPA, the SNR used is the required E_b/N_0, as presented in Table D.1. Similar to HSDPA, the E-DPDCH throughput is a continuous function of the SNR at the Node B, however the results present throughput in function of the E_c/N_0, from which the E_b/N_0 can be easily obtained regarding (E.18). The curve and interpolation functions for the throughput calculation in function of the E_c/N_0 for HSUPA with BPSK modulation, were adapted from [Lope08], being given by equation (E.4) and is depicted in Figure E.2.

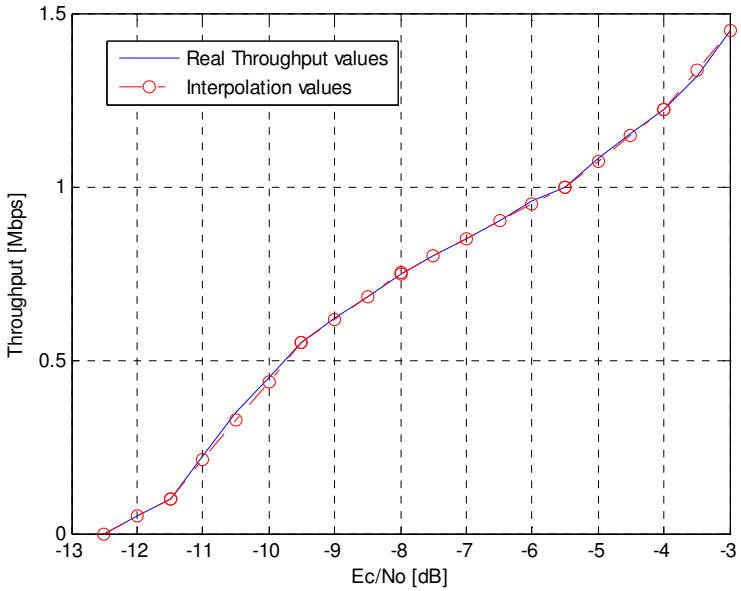

Figure E.2 HSUPA throughput as function of the E_c/N_0, for BPSK modulation (adapted from [Lope08]).

Note that, for the interpolation, [Lope08] has used the FRC6 curve, which results consider a Vehicular A channel [HoTo06], although the same values are used, due to the lack of information regarding other channel types. The minimum considered value of E_c/N_0 is -11.86 dB, since for the first step of the function it is the value that results in a throughput of 64 kbps, the minimum throughput value considered for transmitting, in this thesis.

$$TP_{P[\text{Mbps}]} = \begin{cases} 0.1 \times E_c/N_{0[\text{dB}]} + 1.25, & -11.86 \le E_c/N_{0[\text{dB}]} \le -11.5 \\ 0.225 \times E_c/N_{0[\text{dB}]} + 2.6875, & -11.5 < E_c/N_{0[\text{dB}]} \le -9.5 \\ 0.1333 \times E_c/N_{0[\text{dB}]} + 1.8167, & -9.5 < E_c/N_{0[\text{dB}]} \le -8 \\ 0.1 \times E_c/N_{0[\text{dB}]} + 1.55, & -8 < E_c/N_{0[\text{dB}]} \le -5.5 \\ 0.1467 \times E_c/N_{0[\text{dB}]} + 1.8067, & -5.5 < E_c/N_{0[\text{dB}]} \le -4 \\ 0.23 \times E_c/N_{0[\text{dB}]} + 2.14, & -4 < E_c/N_{0[\text{dB}]} \le -3 \\ 1.45, & E_c/N_{0[\text{dB}]} > -3 \end{cases} \quad \text{(E.4)}$$

Considering the QPSK modulation for HSUPA, the values of the throughput as function of the E_c/N_0, were calculated by interpolating the curve presented in Figure 2.3, which do not contemplate any coding rate, hence, a 75% coding rate, similar to HSUPA for BPSK, is applied to the values given by the interpolation function (E.5). The reference curve, as well as, the interpolated one, is depicted in Figure E.3.

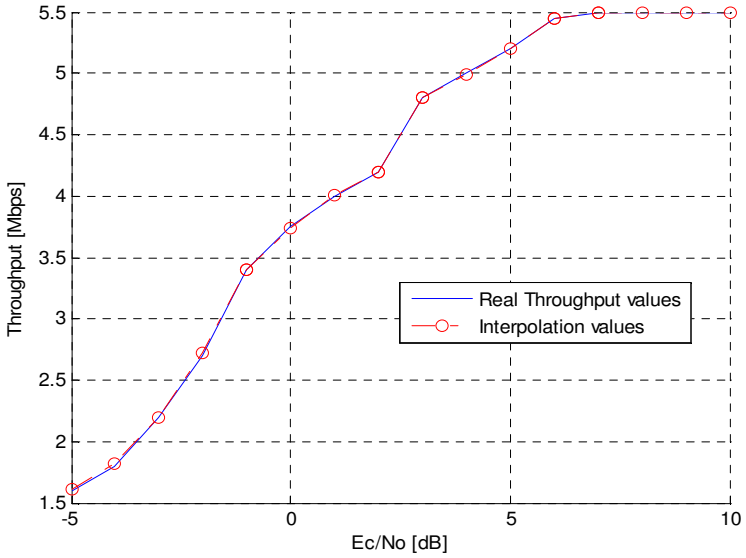

Figure E.3 HSUPA throughput as function of the E_c/N_0, for QPSK modulation.

$$TP_{P[\text{Mbps}]} = \begin{cases} 0.0786 \times E_c/N_{0[\text{dB}]}^2 + 0.9214 \times E_c/N_{0[\text{dB}]} + 4.2478, & -5 \le E_c/N_{0[\text{dB}]} < -1 \\ -0.0375 \times E_c/N_{0[\text{dB}]}^2 + 0.3025 \times E_c/N_{0[\text{dB}]} + 3.7450, & -1 \le E_c/N_{0[\text{dB}]} < 2 \\ 0.6 \times E_c/N_{0[\text{dB}]} + 3.0, & 2 \le E_c/N_{0[\text{dB}]} < 3 \\ 0.0125 \times E_c/N_{0[\text{dB}]}^2 + 0.1025 \times E_c/N_{0[\text{dB}]} + 4.38, & 3 \le E_c/N_{0[\text{dB}]} < 6 \\ 0.055 \times E_c/N_{0[\text{dB}]} + 5.115, & 6 \le E_c/N_{0[\text{dB}]} \le 7 \\ 5.5, & E_c/N_{0[\text{dB}]} > 7 \end{cases} \quad \text{(E.5)}$$

Following the same procedure as for HSDPA, the throughputs for HSPA+ DL with 16QAM and 64QAM modulation, are calculated using functions obtained by interpolating the simulated results presented in Figure 2.2, hence, the throughput associated to each modulation is given by (E.6) and (E.7), respectively. The results are plotted in Figure E.4

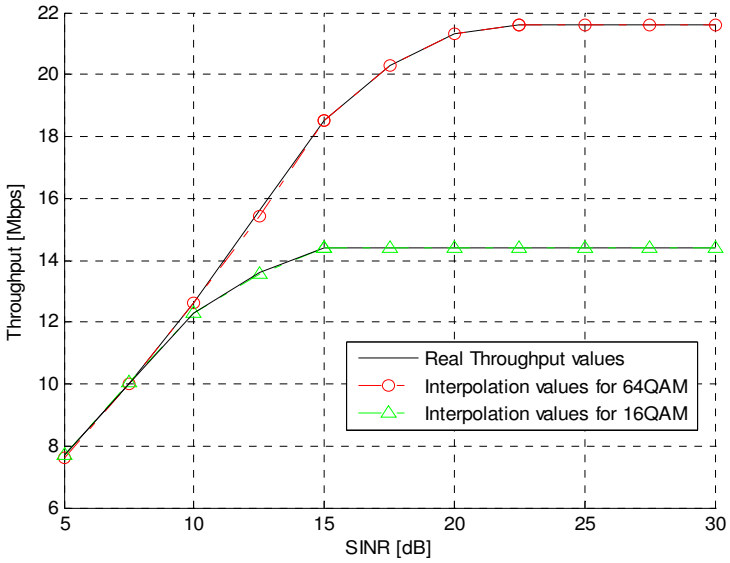

Figure E.4 HSPA+ throughput as function of the SINR for DL.

$$TP_{P[\text{Mbps}]} = \begin{cases} 0.0015\times\rho_{[\text{dB}]}^4 - 0.0619\times\rho_{[\text{dB}]}^3 + 0.8699\times\rho_{[\text{dB}]}^2 - 4.11\times\rho_{[\text{dB}]} + 13.2975, & 5 \le \rho_{[\text{dB}]} \le 15 \\ 14.4, & \rho_{[\text{dB}]} > 15 \end{cases} \quad \text{(E.6)}$$

$$TP_{P[\text{Mbps}]} = \begin{cases} 0.0183\times\rho_{[\text{dB}]}^2 + 0.7223\times\rho_{[\text{dB}]} + 3.558, & 5 \le \rho_{[\text{dB}]} \le 15 \\ -0.06\times\rho_{[\text{dB}]}^2 + 2.662\times\rho_{[\text{dB}]} - 7.92, & 15 < \rho_{[\text{dB}]} \le 22.5 \\ 21.6, & \rho_{[\text{dB}]} > 22.5 \end{cases} \quad \text{(E.7)}$$

Note that the results are for 15 HS-PDSCH codes, however an approximation is made and the same results are used for 14 HS-PDSCH codes, with the maximum considered throughput value being 13.44 for 16QAM and 20.16 Mbps for 64QAM, as described in Section 3.4. The functions that describe these approximations are given by (E.8) and (E.9), and are very similar to (E.6) and (E.7) respectively, with the main differences being the fact that in the latter ones, the maximum throughput value is for 14 HS-PDSCH codes, and one can note that these values are achieved with the need of a lower SNR value. In what concerns the coding rate it is not taken into account in the simulation results from [BEGG08], hence, it as to be applied later on. The value considered for the coding rate is 75%, for a matter of coherence.

$$TP_{P[\text{Mbps}]} = \begin{cases} 0.0015\times\rho_{[\text{dB}]}^4 - 0.0619\times\rho_{[\text{dB}]}^3 + 0.8699\times\rho_{[\text{dB}]}^2 - 4.11\times\rho_{[\text{dB}]} + 13.2975, & 5 \le \rho \le 12.15 \\ 13.44 \quad , & \rho > 12.15 \end{cases} \quad \text{(E.8)}$$

$$TP_{P[\text{Mbps}]} = \begin{cases} 0.0183\times\rho_{[\text{dB}]}^2 + 0.7223\times\rho_{[\text{dB}]} + 3.558, & 5 \le \rho_{[\text{dB}]} \le 15 \\ -0.06\times\rho_{[\text{dB}]}^2 + 2.662\times\rho_{[\text{dB}]} - 7.92 \quad , & 15 < \rho_{[\text{dB}]} \le 17.28 \\ 20.16 \quad , & \rho_{[\text{dB}]} > 17.28 \end{cases} \quad \text{(E.9)}$$

The procedure to calculate the throughput for HSPA+ UL with 16QAM modulation is the same as for

HSUPA, with the only difference being the use of a different reference curve, Figure 2.3. The results of the interpolation are presented in Figure E.5, and (E.10) is the expression that gives the throughput as function of the E_c/N_0. Similar to HSUPA with QPSK modulation and HSPA+ DL, the coding rate is not considered, thus the value of 75% is considered and applied to each value in order to get the throughput at the physical layer, which jointly with the SNR, will be the input of the link model.

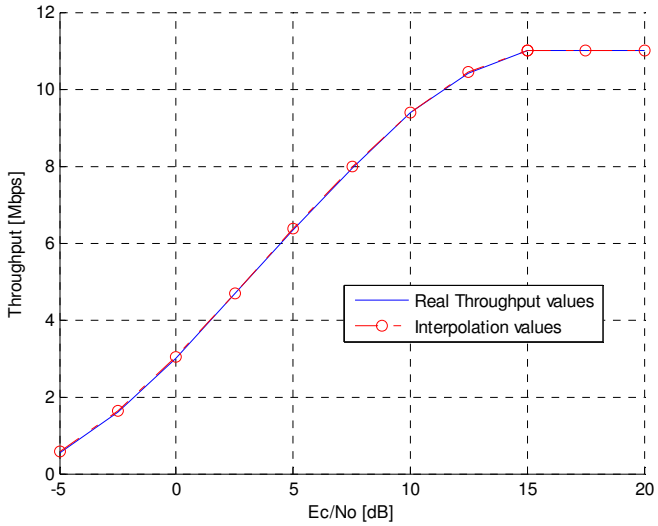

Figure E.5 HSPA+ throughput as function of the E_c/N_0 for UL and 16QAM modulation.

$$TP_{P[\text{Mbps}]} = \begin{cases} -0.0015 \times E_c/N_{0[\text{dB}]}^3 + 0.0166 \times E_c/N_{0[\text{dB}]}^2 + 0.6184 \times E_c/N_{0[\text{dB}]} + 3.0515, & -5 \le E_c/N_{0[\text{dB}]} \le 15 \\ 11.0, & E_c/N_{0[\text{dB}]} > 15 \end{cases} \quad \text{(E.10)}$$

It should be pointed out that the expressions for the throughput were obtained using Matlab, and they are step-wise in order to maintain the validity of the approximations, hence, a relative mean error below 5% seems appropriate. In Table E.1, the relative mean errors are presented for all the interpolated curves. The maximum throughputs for the various systems without considering the BER is are described in Table C.2.

Table E.1 Relative mean error for the throughput interpolated curves (adapted from [Lope08]).

System	Number of HS-PDSCH codes	Relative mean error [%]
HSDPA	5	2.2
	10	3.0
	15	4.9
HSUPA (BPSK)	---	0.7
HSUPA (QPSK)	---	0.2
HSPA+ DL (16QAM)	15	0.8
HSPA+ DL (64QAM)	15	0.2
HSPA+ UL	---	0.7

Table E.2 Maximum throughput values for the considered systems without BER.

System	Number of HS-PDSCH codes	Throughput [Mbps]	Required SNR [dB]	Required E_c/N_0 [dB]
R99 DL/UL	---	0.064	[1.1, 3.8]	---
	---	0.128	[0.9, 3.5]	---
	---	0.384	[0.4, 3.2]	---
HSDPA	5	3.040	32.5	---
	10	6.090	37.5	---
	15	8.520	35.8	---
HSUPA (BPSK)	---	1.350	1.3	-3
HSUPA (QPSK)	---	3.840	5.5	7
HSPA+ DL (16QAM)	15	8.520	12.2	---
HSPA+ DL (64QAM)	15	12.790	17.3	---
HSPA+ UL	---	7.680	10.5	15

Annex F - Propagation Model

In this annex, the COST231 Walfisch-Ikegami (COST231 W-I), [DaCo99], propagation model is presented, being the one used throughout this thesis.

COST231 W-I is a combination of both Ikegami and Walfisch-Bertoni models, with the considered urban structure being the same as for these models. For improved path-loss estimation, the model considers additional parameters to describe the urban environment, namely buildings height, roads width, building separation and road orientation with respect to the direct radio path (φ), as shown in Figure F.1 and Figure F.2. The model assessment is based on measurements in European cities, [Corr08].

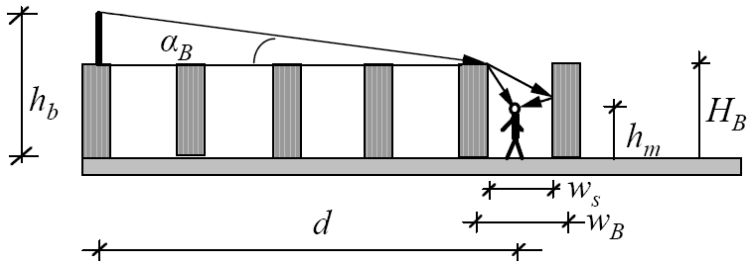

Figure F.1 Definition of the parameters used in the COST231 W-I model in an urban environment (extracted from [Corr08]).

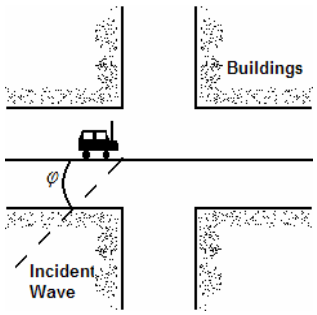

Figure F.2 Definition of the street orientation angle φ (extracted from [DaCo99]).

The existence of LoS or NLoS in the propagation path is taken into account by the model. In the LoS situation ($\varphi = 0$), between base and mobile antennas within a street scenario, a simple propagation loss formula, is applied (F.1), being based on measurements performed in the city of Stockholm, [DaCo99].

$$L_{p[\mathrm{dB}]} = 42.6 + 26\log(d_{[\mathrm{km}]}) + 20\log(f_{[\mathrm{MHz}]}), \quad d > 0.02 \text{ km} \tag{F.1}$$

Note that (F.1) is different from the free space loss equation, which is given by (F.2), and for 20 m takes the value of 42.6, thus explaining this value at (F.1).

$$L_{0[\mathrm{dB}]} = 32.4 + 20\log(d_{[\mathrm{Km}]}) + 20\log(f_{[\mathrm{MHz}]}) \tag{F.2}$$

For NLoS propagation the loss is calculated using (F.3) and it is composed by three terms: free space loss, roof-top-to-street diffraction and scatter loss L_{rm}, and multiple screen diffraction loss L_{rt}.

$$L_{p[\mathrm{dB}]} = \begin{cases} L_{0[\mathrm{dB}]} + L_{rt[dB]} + L_{rm[\mathrm{dB}]}, & L_{rt} + L_{rm} > 0 \\ L_{0[\mathrm{dB}]} \quad , & L_{rt} + L_{rm} \le 0 \end{cases} \tag{F.3}$$

The term L_{rm} basically describes the loss between last roof-top and MT. The street orientation and its width are taken into account for the calculation of this parameter, which is mainly based on Ikegami's model. However, a different street-orientation function is applied by COST 231 W-I, contrary to Ikegami (F.4).

$$L_{rm[\mathrm{dB}]} = -16.9 - 10\log(w_{s[\mathrm{Km}]}) + 10\log(f_{[\mathrm{MHz}]}) + 20\log(H_{B[\mathrm{m}]} - h_{m[\mathrm{m}]}) + L_{ori[\mathrm{dB}]} \tag{F.4}$$

where:

- w_s: street width;
- H_B: buildings height;
- h_m: mobile terminal height;
- L_{ori}: street orientation loss (F.5):

$$L_{ori[\mathrm{dB}]} = \begin{cases} -10.0 + 0.354\varphi_{[^\circ]}, & 0^\circ < \varphi < 35^\circ \\ 2.5 + 0.075(\varphi_{[^\circ]} - 35), & 35^\circ \le \varphi < 55^\circ \\ 4.0 - 0.114(\varphi_{[^\circ]} - 55), & 55^\circ \le \varphi < 90^\circ \end{cases} \tag{F.5}$$

While the Walfisch and Bertoni original model is valid in the case that the base station antenna is located above rooftops, COST 231 extends this model for base station antenna heights below rooftops levels, using an empirical function based on measurements. The heights of the buildings and their spatial separations, along with the direct radio path are modelled by absorbing screens for the determination of L_{rt} (F.6), which basically describes the loss between BS antennas and the last rooftop before the MT.

$$L_{rt[\mathrm{dB}]} = L_{bsh[\mathrm{dB}]} + k_a + k_d\log(d_{[\mathrm{km}]}) + k_f\log(f_{[\mathrm{MHz}]}) - 9\log(w_{B[\mathrm{m}]}) \tag{F.6}$$

where:

- w_B: distance between middle points of adjacent buildings;
- L_{bsh}: losses due to the fact that BS antennas are above or below the roof-top level:

$$L_{bsh[\mathrm{dB}]} = \begin{cases} -18\log(h_{b[\mathrm{m}]} - H_{B[\mathrm{m}]} + 1), & h_b > H_B \\ 0 \quad , & h_b \le H_B \end{cases} \tag{F.7}$$

- h_b: BS height;
- k_a: increase of the path loss for BS antennas below the roof tops of the adjacent buildings:

$$k_a = \begin{cases} 54 & , \ h_b > H_B \\ 54 - 0.8(h_{b[\mathrm{m}]} - H_{B[\mathrm{m}]}) & , \ d \ge 0.5 \text{ km} \\ 54 - 1.6(h_{b[\mathrm{m}]} - H_{B[\mathrm{m}]})d_{[\mathrm{Km}]} & , \ d < 0.5 \text{ km} \end{cases} \Bigg\} h_b \le H_B \tag{F.8}$$

- k_d: control the dependence of the multi-screen diffraction loss vs. distance:

$$k_d = \begin{cases} 18 & , \ h_b > H_B \\ 18 - 15\dfrac{h_{b[\mathrm{m}]} - H_{B[\mathrm{m}]}}{H_{B[\mathrm{m}]}}, & h_b \le H_B \end{cases} \tag{F.9}$$

- k_f: control the dependence of the multi-screen diffraction loss vs. frequency;

$$k_f = \begin{cases} -4 + 0.7\left(\dfrac{f_{[\mathrm{MHz}]}}{925} - 1\right), & \text{urban and suburban} \\ -4 + 1.5\left(\dfrac{f_{[\mathrm{MHz}]}}{925} - 1\right), & \text{dense urban} \end{cases} \tag{F.10}$$

The validity of the model is shown in Table F.1. As can be observed, the UMTS frequencies are not fully covered, as well as the distances considered for simulation in this thesis (10 to 2400 m).

Table F.1 Restrictions of the COST231 W-I (extracted from [DaCo99]).

Parameters	Internal Values
Frequency	[800, 2000] MHz
BS Height	[4, 50] m
MT Height	[1, 3] m
Distance between BS and MT	[0.02, 5] Km

In what concerns the standard deviation, it takes values from 4 to 7 dB, with the prediction error increasing when h_b decreases relative to H_B.

In the absence of specific values for the environment structure definition, the following are recommended [Corr08]:

- $w_B \in [20,50]$ m
- $w_S = w_B/2$
- φ=90°
- $H_{B[\mathrm{m}]} = 3 \times (\#\ \text{floors}) + H_{roof[\mathrm{m}]}$
- $H_{roof[\mathrm{m}]} = \begin{cases} 3, & \text{pitched} \\ 0, & \text{flat} \end{cases}$

Annex G - Detectors

In order to calculate the application throughput, the BER has to be known, therefore, several detectors are considered for simulations, since for each modulation and MIMO scheme, different BERs are associated. In this annex the MIMO detectors used in the simulator are presented.

Three types of detectors have been considered in this thesis, the ML, the ZF and the MMSE. Due to the lack of coherent information, only the ML is defined for all available antenna configurations and systems, with the ZF being defined for 2×2 QPSK, 2×4 QPSK, 4×4 QPSK and 4×4 16QAM, and the MMSE only for 4×4 QPSK and 16QAM. Despite the fact that the ZF and the MMSE are not defined for all situations, it is still interesting to have them defined for some situations, in order to stress out the relative influence of using one in detriment of the other. Note that, for the SISO system, again due to lack of information, only the ML detector with BPSK modulation is defined, hence the BERs used to calculate the SISO throughput in all systems considered in this thesis, are based on it. However the use of this detector for the SISO throughput calculation represents a best case situation, since ML is the detector with better performance, and BPSK the most robust modulation, leading to lower BER values, thus higher throughputs are obtained.

The BER values for almost all MIMO schemes and modulations are obtained by interpolation of plotted simulation results, however for the 2×4 BPSK, 2×4 16QAM and 4×2 16QAM, the curves had to be extrapolated, since no (coherent) results for these systems were found, thus the error relative to these extrapolated curves is unknown. Besides these extrapolations, others minor extrapolations had to performed, in order to have the same range, in terms of SNR, for all the considered detectors. Therefore, the maximum SNR value was chose considering the higher value of SNR value common to the most detectors, which turn out to be 22.5 dB. For the detectors that had more information beyond this value, that data has been ignored, while for the ones of which information did not reach the SNR value of 22.5 dB, extrapolations were performed, namely for the ML 4×4 BPSK, ML 2×4 QPSK, ML 4×4 QPSK, ML 4×4 16QAM, ML 2×2 64QAM and the ZF ML 2×4 QPSK. It is assumed, for all the detectors, that the BER value for SNR values higher than 22.5 dB is constant and equal to the one that corresponds to this SNR value. Moreover, common to all detectors, is the 5 dB minimum SNR value, for which it is assumed in this work that a signal is detected, since for the majority of the detectors, the plotted results are for values of SNR above 5dB. Hence, with previous extrapolations performed to complete the ML combinations of MIMO schemes and modulations and fix the range of detection, performing more extrapolations would result in an even more inaccurate analysis, thus 5 dB is the chosen minimum SNR value for which a signal is detected.

The interpolations for the ML detector for 1×1, 2×2, 4×2 and 4×4 BPSK, and for 2×2 and 4×2 QPSK are based on the results of [NeZA00]. Regarding the ML detector, for the 2×4 QPSK and 2×2 16QAM

systems, the interpolations are based on [ZhMu02], as well as for the ZF detector for the 2×2 and 2×4 QPSK systems. In what concerns the interpolations for the 4×4 systems, for the ML, ZF and MMSE detectors with 16QAM, they are based on [WBKK04], while for QPSK are based on [BWKK03]. Finally, the source for the 2×2 64QAM ML detector is [LoBC04].

The real and interpolated curves, for the ML detector, are plotted in Figure G.1, Figure G.2, Figure G.3 and Figure G.4, for BPSK, QPSK, 16QAM and 64QAM modulation, respectively. Note that the curves are plotted for all, considered, antenna configurations, were 'real' and 'inter' stand for, real values and interpolated ones, respectively.

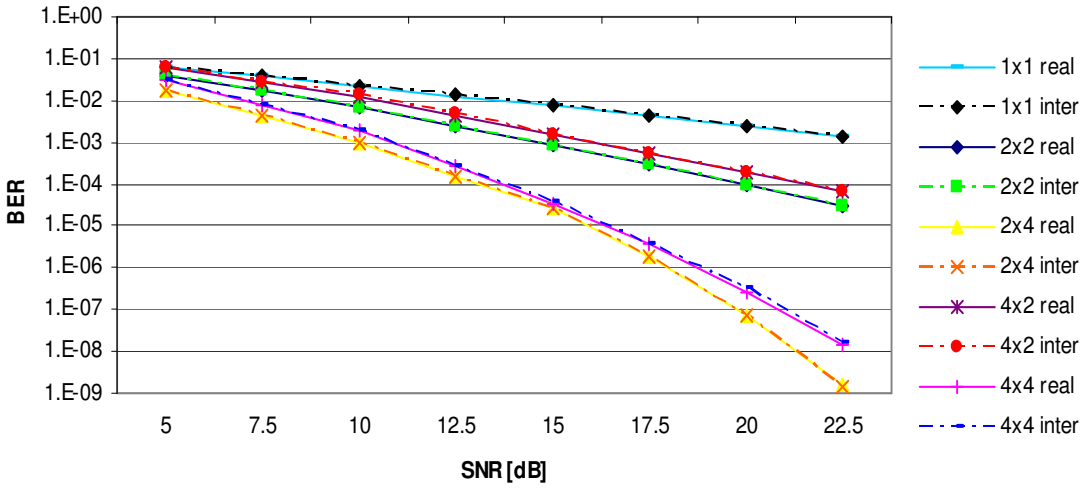

Figure G.1 BER vs. SNR for BPSK modulation using ML detector.

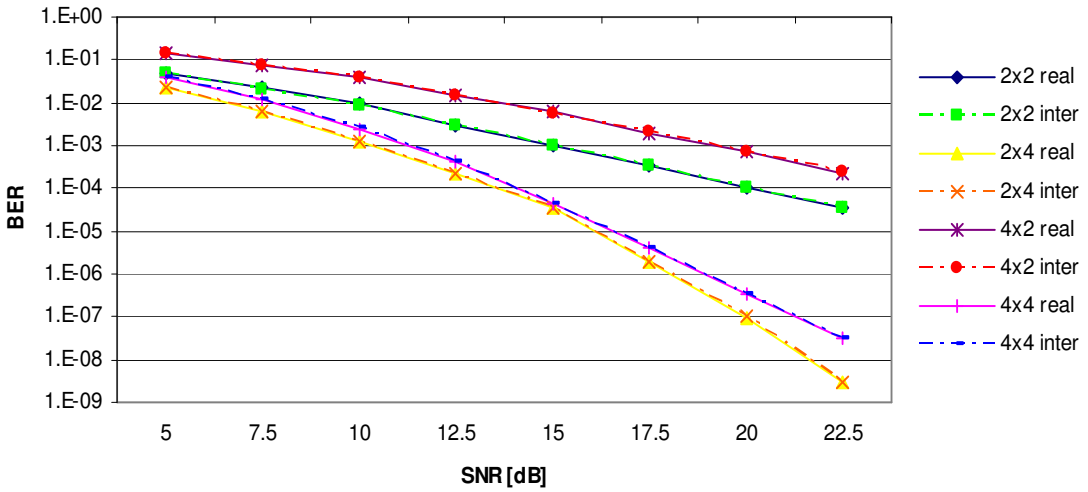

Figure G.2 BER vs. SNR for QPSK modulation using ML detector.

For the ZF and MMSE detectors, the curves are respectively plotted in Figure G.5 and Figure G.6, with the same principles applied as for the ML detector, in what concerns antenna configurations and legend.

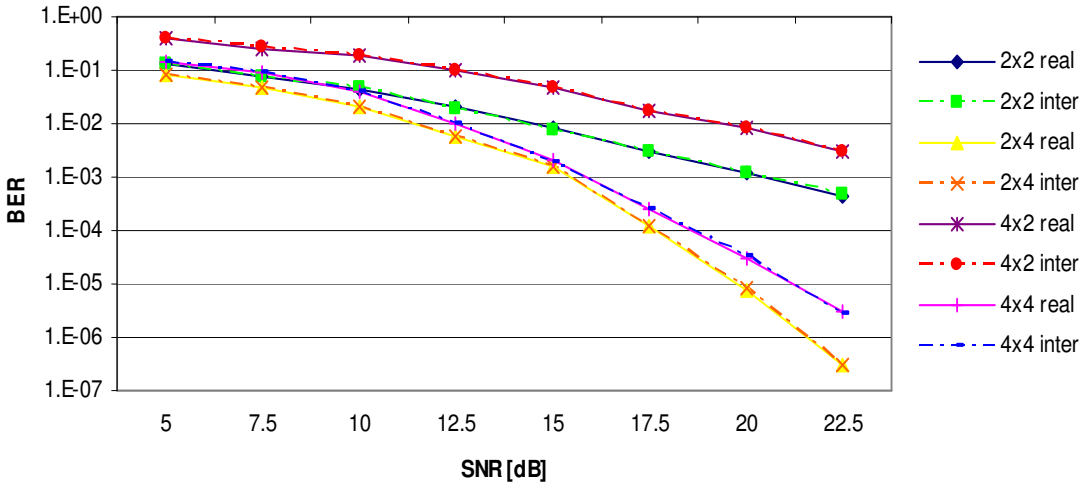

Figure G.3 BER vs. SNR for 16QAM modulation using ML detector.

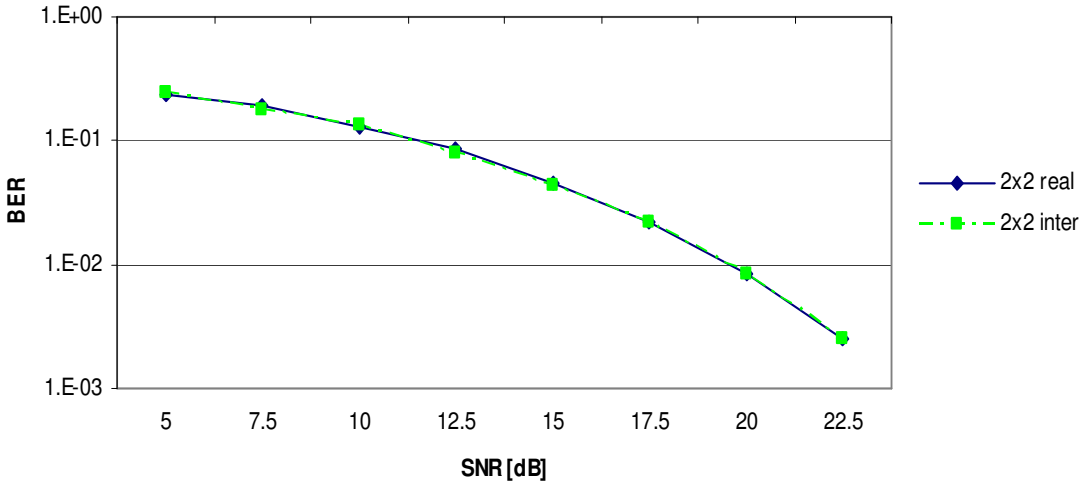

Figure G.4 BER vs. SNR for 64QAM modulation using ML detector.

Regarding coherence, in Figure G.7, are plotted various curves, corresponding to different modulations for the same detector (ML) and antenna configuration (2×2). It can be observed, as expected, that higher order modulations correspond to higher values of BER. A variation in the BER is also observed in Figure G.8, where the modulation and MIMO scheme are the same (16QAM, MIMO 2×2), varying the type of detector. As expected, the best performance is achieved with the ML detector, while the worst is for the ZF detector.

In order to verify the validity of the interpolated functions, the relative mean error has been calculated, and is below 3.5%, for all the interpolated curves.

The ML detector interpolation function for the SISO system with BPSK modulation is given by (G.1), while for the 2×2, 4×2, 4×2 and 4×4 MIMO systems, the interpolation functions for the BPSK modulation, using ML detector are given by the equations from (G.2) to (G.5). Concerning the QPSK and 16QAM modulation, the ML detector interpolation functions are given by the equations from (G.6)

to (G.9), and (G.10) to (G.13) respectively, for the 2×2, 4×2, 4×2 and 4×4 MIMO systems. The 2×2 64QAM ML detector interpolation function is given by (G.14).

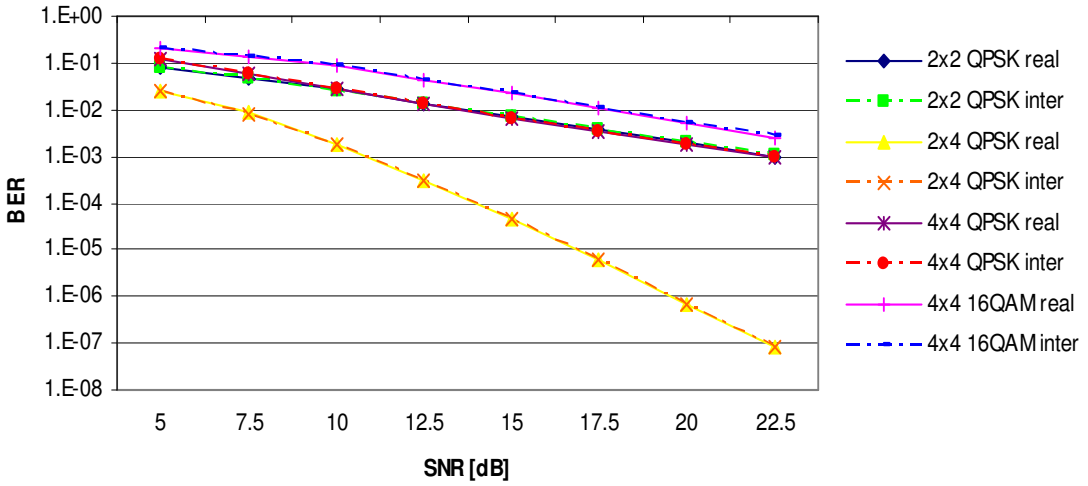

Figure G.5 BER vs. SNR using ZF detector for QPSK and 16QAM.

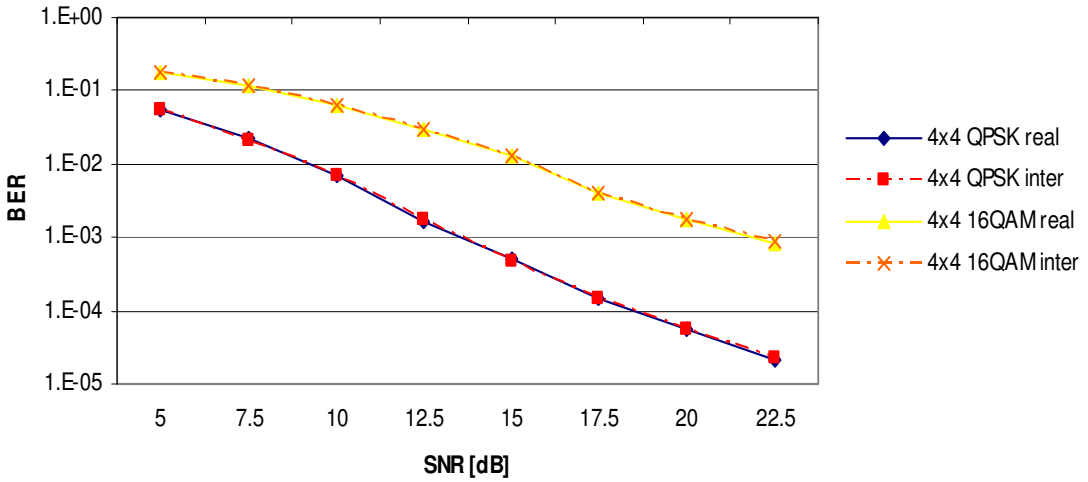

Figure G.6 BER vs. SNR using MMSE detector for QPSK and 16QAM.

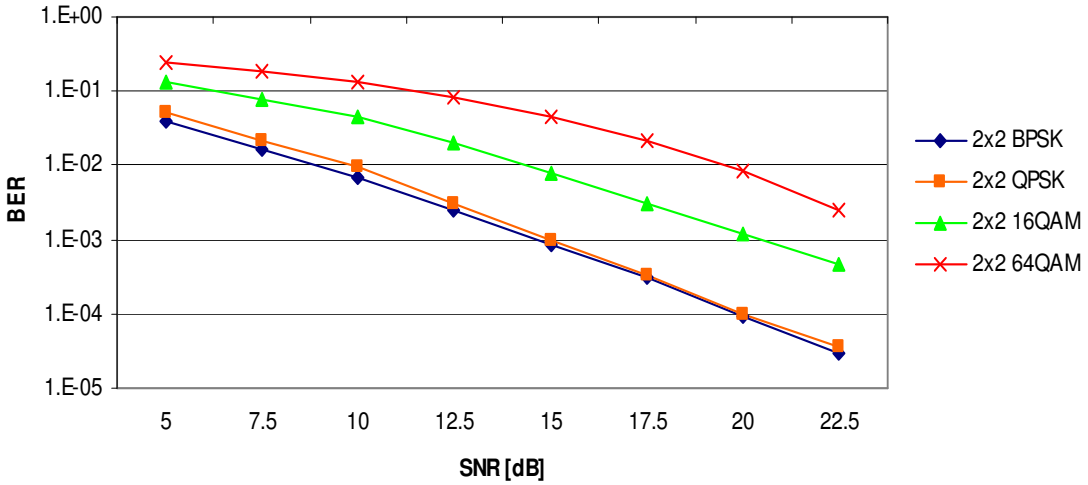

Figure G.7 BER vs. SNR for different modulations and same antenna configuration using ML detector.

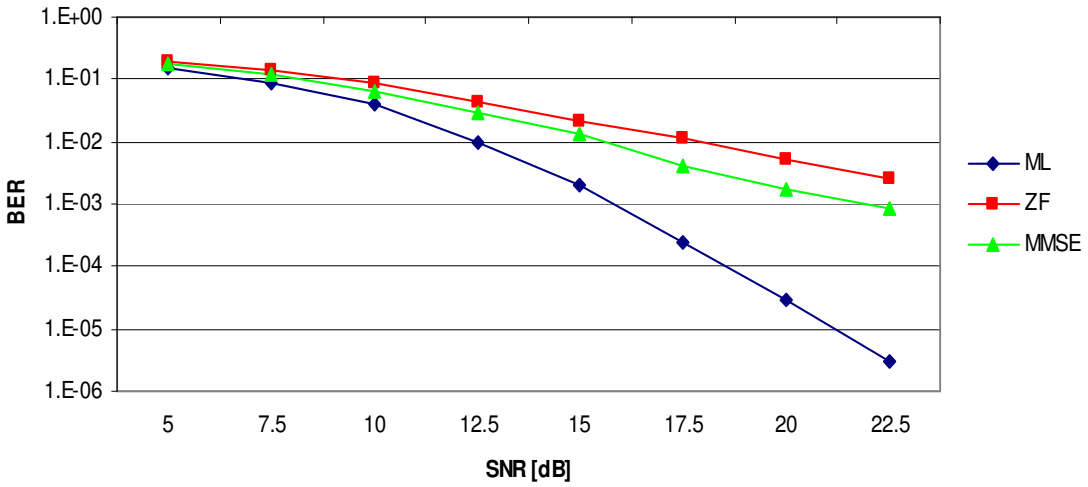

Figure G.8 BER vs. SNR for MIMO 4×4 and 16QAM modulation, using different detectors.

$$\beta_{SISO} = \begin{cases} 0.1585 \times e^{(-0.193 \times \rho_{[dB]})}, & 5 \le \rho_{[dB]} < 10 \\ 0.19 \times e^{(-0.21 \times \rho_{[dB]})} - 0.00038, & \rho_{[dB]} \ge 10 \end{cases} \quad \text{(G.1)}$$

$$\beta_{MIMO} = \begin{cases} 0.22 \times e^{(-0.34 \times \rho_{[dB]})} - 0.00035, & 5 \le \rho_{[dB]} < 10 \\ 0.445 \times e^{(-0.417 \times \rho_{[dB]})} - 0.000008, & \rho_{[dB]} \ge 10 \end{cases} \quad \text{(G.2)}$$

$$\beta_{MIMO} = \begin{cases} 0.3 \times e^{(-0.565 \times \rho_{[dB]})} - 0.00005, & 5 \le \rho_{[dB]} < 10 \\ 2.4 \times e^{(-0.78 \times \rho_{[dB]})} + 0.0000075, & 10 \le \rho_{[dB]} < 15 \\ 259.8 \times e^{(-1.071 \times \rho_{[dB]})}, & 15 \le \rho_{[dB]} \le 17.5 \\ 17000.0 \times e^{(-1.30999 \times \rho_{[dB]})} - 0.0000000012, & \rho_{[dB]} > 17.5 \end{cases} \quad \text{(G.3)}$$

$$\beta_{MIMO} = \begin{cases} 0.28 \times e^{(-0.307 \times \rho_{[dB]})}, & 5 \le \rho_{[dB]} < 10 \\ 0.845 \times e^{(-0.417 \times \rho_{[dB]})} - 0.000005, & \rho_{[dB]} \ge 10 \end{cases} \quad \text{(G.4)}$$

$$\beta_{MIMO} = \begin{cases} 0.53 \times e^{(-0.56 \times \rho_{[dB]})} - 0.00005, & 5 \le \rho_{[dB]} < 10 \\ 4.8 \times e^{(-0.78 \times \rho_{[dB]})} - 0.000002, & 10 \le \rho_{[dB]} < 17.5 \\ 57.0 \times e^{(-0.946 \times \rho_{[dB]})} - 0.000000017, & \rho_{[dB]} \ge 17.5 \end{cases} \quad \text{(G.5)}$$

$$\beta_{MIMO} = \begin{cases} 0.26 \times e^{(-0.327 \times \rho_{[dB]})} - 0.0008, & 5 \le \rho_{[dB]} < 10 \\ 0.73 \times e^{(-0.44 \times \rho_{[dB]})} - 0.000002, & \rho_{[dB]} \ge 10 \end{cases} \quad \text{(G.6)}$$

$$\beta_{MIMO} = \begin{cases} 0.22 \times e^{(-0.45 \times \rho_{[dB]})} - 0.00115, & 5 \le \rho_{[dB]} < 10 \\ 1.3 \times e^{(-0.69 \times \rho_{[dB]})} - 0.0000055, & 10 \le \rho_{[dB]} < 15 \\ 1300.0 \times e^{(-1.16 \times \rho_{[dB]})} - 0.000000003, & \rho_{[dB]} \ge 15 \end{cases} \quad \text{(G.7)}$$

$$\beta_{MIMO} = \begin{cases} 0.56 \times e^{(-0.265 \times \rho_{[dB]})}, & 5 \le \rho_{[dB]} < 10 \\ 2.1 \times e^{(-0.395 \times \rho_{[dB]})} - 0.00005, & \rho_{[dB]} \ge 10 \end{cases} \quad \text{(G.8)}$$

$$\beta_{MIMO} = \begin{cases} 0.38 \times e^{(-0.44 \times \rho_{[dB]})} - 0.0021, & 5 \le \rho_{[dB]} \le 10 \\ 2.5 \times e^{(-0.691 \times \rho_{[dB]})} - 0.000035, & 10 < \rho_{[dB]} \le 15 \\ 100.0 \times e^{(-0.973 \times \rho_{[dB]})} - 0.000000003, & \rho_{[dB]} > 15 \end{cases} \quad \text{(G.9)}$$

$$\beta_{MIMO} = \begin{cases} 0.38 \times e^{(-0.215 \times \rho_{[dB]})}, & 5 \le \rho_{[dB]} < 10 \\ 1.6 \times e^{(-0.355 \times \rho_{[dB]})} - 0.000075, & \rho_{[dB]} \ge 10 \end{cases} \quad \text{(G.10)}$$

$$\beta_{MIMO} = \begin{cases} 0.255 \times e^{(-0.1 \times \rho_{[dB]})} - 0.073, & 5 \le \rho_{[dB]} < 10 \\ 3.1 \times e^{(-0.5 \times \rho_{[dB]})} - 0.00014, & 10 \le \rho_{[dB]} < 15 \\ 11000.0 \times e^{(-1.05 \times \rho_{[dB]})} - 0.0000003, & \rho_{[dB]} \ge 15 \end{cases} \quad \text{(G.11)}$$

$$\beta_{MIMO} = \begin{cases} 0.83 \times e^{(-0.176 \times \rho_{[dB]})} + 0.046, & 5 \le \rho_{[dB]} < 10 \\ 2.36 \times e^{(-0.243 \times \rho_{[dB]})} - 0.015, & 10 \le \rho_{[dB]} < 17.5 \\ 0.8 \times e^{(-0.201 \times \rho_{[dB]})} - 0.0057, & \rho_{[dB]} \ge 17.5 \end{cases} \quad \text{(G.12)}$$

$$\beta_{MIMO} = \begin{cases} 0.45 \times e^{(-0.1 \times \rho_{[dB]})} - 0.125, & 5 \le \rho_{[dB]} < 10 \\ 9.0 \times e^{(-0.54 \times \rho_{[dB]})} - 0.00075, & 10 \le \rho_{[dB]} < 15 \\ 400.0 \times e^{(-0.815 \times \rho_{[dB]})} - 0.0000015, & \rho_{[dB]} \ge 15 \end{cases} \quad \text{(G.13)}$$

$$\beta_{MIMO} = \begin{cases} 0.45 \times e^{(-0.12 \times \rho_{[dB]})} - 0.0055, & 5 \le \rho_{[dB]} < 10 \\ 0.9 \times e^{(-0.18 \times \rho_{[dB]})} - 0.0165, & 10 \le \rho_{[dB]} \le 17.5 \\ 9.3 \times e^{(-0.34 \times \rho_{[dB]})} - 0.0019, & \rho_{[dB]} > 17.5 \end{cases} \quad \text{(G.14)}$$

In what regards the ZF detector, equations from (G.15) to (G.18) define the interpolation functions for the 2×2 QPSK, 2×4 QPSK, 4×4 QPSK, and 4×4 16QAM MIMO systems, respectively.

$$\beta_{MIMO} = \begin{cases} 0.233 \times e^{(-0.19 \times \rho_{[dB]})} - 0.01, & 5 \le \rho_{[dB]} < 10 \\ 0.31 \times e^{(-0.252 \times \rho_{[dB]})} - 0.00003, & \rho_{[dB]} \ge 10 \end{cases} \quad \text{(G.15)}$$

$$\beta_{MIMO} = \begin{cases} 0.215 \times e^{(-0.41 \times \rho_{[dB]})} - 0.00175, & 5 \le \rho_{[dB]} < 10 \\ 2.7 \times e^{(-0.73 \times \rho_{[dB]})} - 0.0000015, & 10 \le \rho_{[dB]} \le 17.5 \\ 22.7 \times e^{(-0.865 \times \rho_{[dB]})}, & \rho_{[dB]} > 17.5 \end{cases} \quad \text{(G.16)}$$

$$\beta_{MIMO} = \begin{cases} 0.47 \times e^{(-0.26 \times \rho_{[dB]})} - 0.0075, & 5 \le \rho_{[dB]} < 10 \\ 0.45 \times e^{(-0.283 \times \rho_{[dB]})} + 0.0002, & 10 \le \rho_{[dB]} \le 22.5 \end{cases} \quad \text{(G.17)}$$

$$\beta_{MIMO} = 0.31 \times e^{(-0.252 \times \rho_{[dB]})} - 0.00003, \ \rho_{[dB]} \geq 5 \quad \text{(G.18)}$$

Finally, the interpolation functions for the MMSE detector regarding the 4×4 QPSK MIMO system is given by (G.19), and for the 4×4 16QAM is given by (G.20).

$$\beta_{MIMO} = \begin{cases} 0.335 \times e^{(-0.348 \times \rho_{[dB]})} - 0.0033, \ 5 \leq \rho_{[dB]} < 10 \\ 1.55 \times e^{(-0.54 \times \rho_{[dB]})} + 0.000025, \ 10 \leq \rho_{[dB]} < 20 \\ 0.087 \times e^{(-0.37 \times \rho_{[dB]})} + 0.0000014, \ \rho_{[dB]} \geq 20 \end{cases} \quad \text{(G.19)}$$

$$\beta_{MIMO} = \begin{cases} 0.53 \times e^{(-0.065 \times \rho_{[dB]})} - 0.21, \ 5 \leq \rho_{[dB]} < 10 \\ 1.035 \times e^{(-0.27 \times \rho_{[dB]})} - 0.0052, \ 10 \leq \rho_{[dB]} \leq 17.5 \\ 0.9 \times e^{(-0.312 \times \rho_{[dB]})} - 0.0019 + 0.000055, \ \rho_{[dB]} > 17.5 \end{cases} \quad \text{(G.20)}$$

Note that, with the exception of the interpolation function for the ZF detector for the 4×4 16QAM system, all the other interpolation functions for all detectors, MIMO systems and modulations are step-wised, in order to fit better the real values, thus minimizing the relative mean error. All the interpolations were performed using Matlab.

Annex H - User's Manual

This annex includes the simulator's user manual. The simulator platform was developed to be the most self explanatory as possible, by means of presenting a user friendly interface.

The first window that appears when running the simulator is the one corresponding to the link module, Figure H.1. In this window, the user is requested to input the data parameters related to the SNR calculation, as well as the simulation interval, step, and number of desired simulations. These input parameters are listed in Subsection 4.2.1, where the link module is described in detail. The simulator has already defined several default values as one can see from Figure H.1, however the user is allowed to modify each of them.

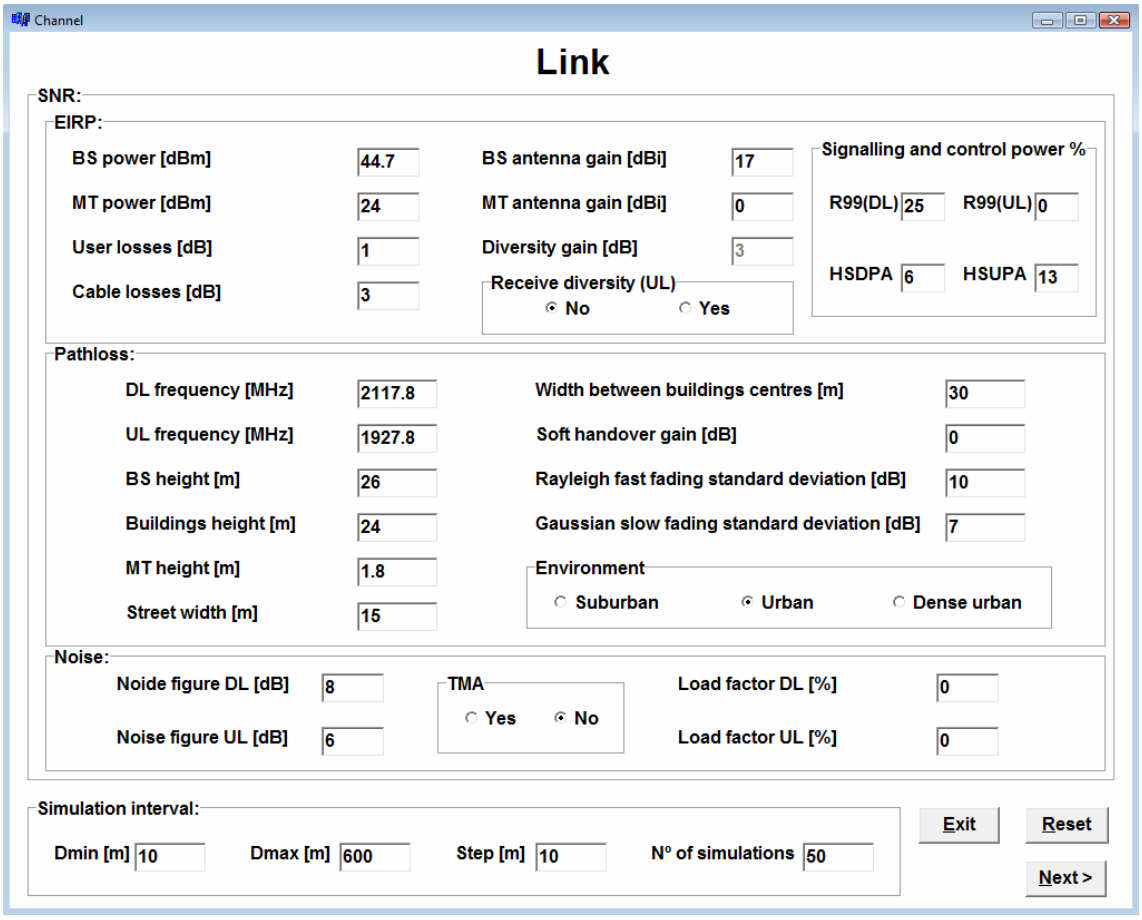

Figure H.1 Link window.

After the input of the requested data, or the accordance to the default one, by pressing the 'Next' button the user proceed to the next step. There is also the option to reset the default values or to exit

the simulator by pressing the ‘Reset’ or ‘Exit’ buttons.

After pressing ‘Next’, at the link module window, the Antennas/Receiver window is displayed, Figure H.2. At this window the user is requested to chose specific MIMO data, being:

- MIMO configuration;
- antenna spacing;
- type of antenna power fed;
- type of detector.

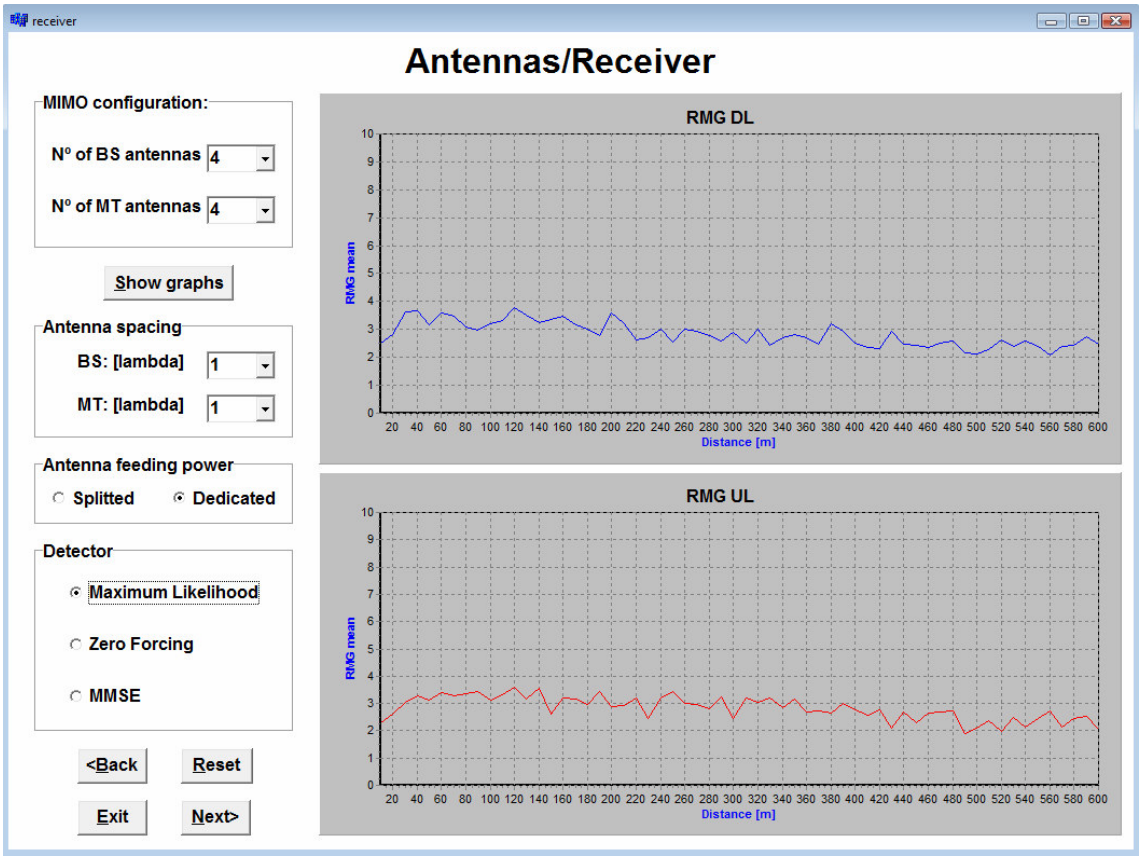

Figure H.2 Antennas and receiver window.

For the MIMO configuration, options up to 16×16 are defined, though only for a RMG value visualisation. The configurations that are implemented for simulation are the 2×2, 2×4, 4×4 and 4×4 ones. Concerning the antenna spacing, the user can chose between 1 or 0.5λ. The remaining options can be observed in Figure H.2.

Moreover, by pressing the ‘Show graphs’ button, the user can visualise, the order of the RMG value for the desired antenna configuration, though this do not represent the exact value for each simulation, since the RMG model has some inherent randomness.

With all the options are taken, the user can now proceed to the next window or go back to the previous one, by pressing ‘Next’ or ‘Back’, respectively. Similar to the link window, the default data can be re-established by pressing ‘Reset’ or the simulator can be exited by pressing ‘Exit’.

The next and last window is the System window, Figure H.3. In this window data referring to the type of system, link direction, and modulation is requested, as well as the BER target, SNR target, and type of power control.

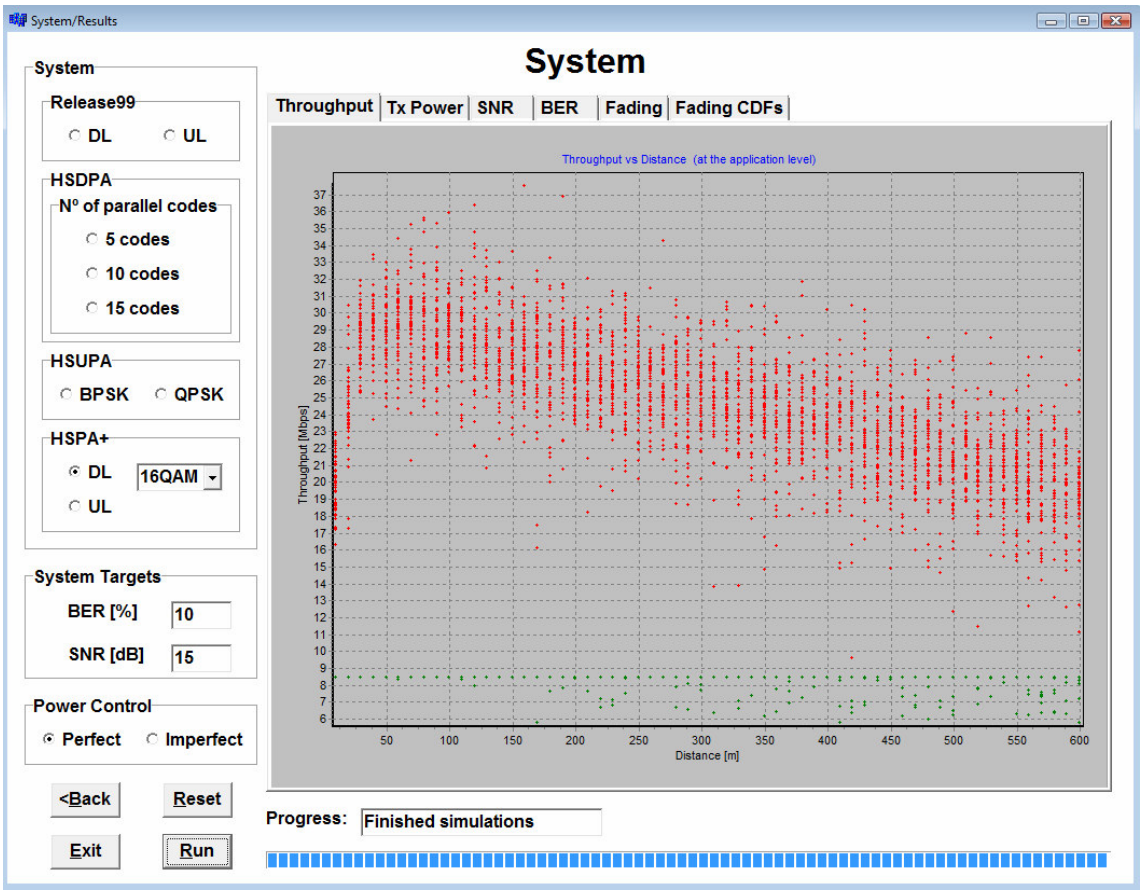

Figure H.3 System window.

For R99, the user have to chose which link direction it wants to simulate, since different modulations are associated to each one. The number of HS-PDSCH codes has to be also defined for HSDPA, being available 5, 10 and 15. In what concerns HSUPA the modulation has to be chose, between BPSK or QPSK. To perform simulations for HSPA+, besides choosing the link direction, in the DL situation the user has to define the modulation for which it which it wants to simulate. Following these decisions, are the BER, and SNR targets request. In order to achieve the maximum throughputs for each system, regarding the SNR target, the user has to know which value corresponds to the minimum SNR required, since if a lower one is given, those values will not be accomplished. Moreover, the detectors performance must also be known, since for instance if the minimum value of SNR is chosen for HSPA+ with 16QAM and a 4×2 configuration was defined, then no signals will be

detected, since the correspondent MIMO detector needs a higher value to be detected.

The last requested option is the type of power control, which can be perfect or imperfect. Within the former the SNR calculation is performed with perfect channel information, while in the latter the fading margins are not known, thus resulting in different throughput values.

With all the options taken and values defined, by pressing the 'Run' button the simulations start. The number of simulation as well as a progress bar is shown with the objective to observer the simulations evolution. After the simulations, the results are shown in several graphs that can be visualised by pressing the correspondent tab, Figure H.3. However the one with the throughput evolution with distance is presented on front, since the other ones are presented mainly for assessment purposes.

Likewise the previous windows in the system one, there is the possibility to navigate back, reset or exit, by pressing the 'Back', 'Reset' or 'Exit' buttons.

It should be pointed out that the file with the output results is only closed when the 'Exit' button is pressed. This file is generated in the root directory 'c:\' and is named results.xls. Note that the generated file is already in an Excel readable format, in order to allow easier results analysis.

In the results.xls file, the first column contains the distances of simulation, while the next columns contain the SISO throughput for each simulation (one by column). With each row of the simulation columns corresponding to a distance of simulation, presented in the first column. The values for the simulated MIMO throughput come below the SISO throughput, being separated by a blank row, and are aligned with the previous. Hence, the same procedure for writing the MIMO throughput values as for the SISO ones is applied. This way, for the same simulation, SISO and MIMO throughput values are presented in the same column.

Annex I – Power Control Algorithm

In this annex, the power control algorithm used in the simulator is shown in Figure I.1.

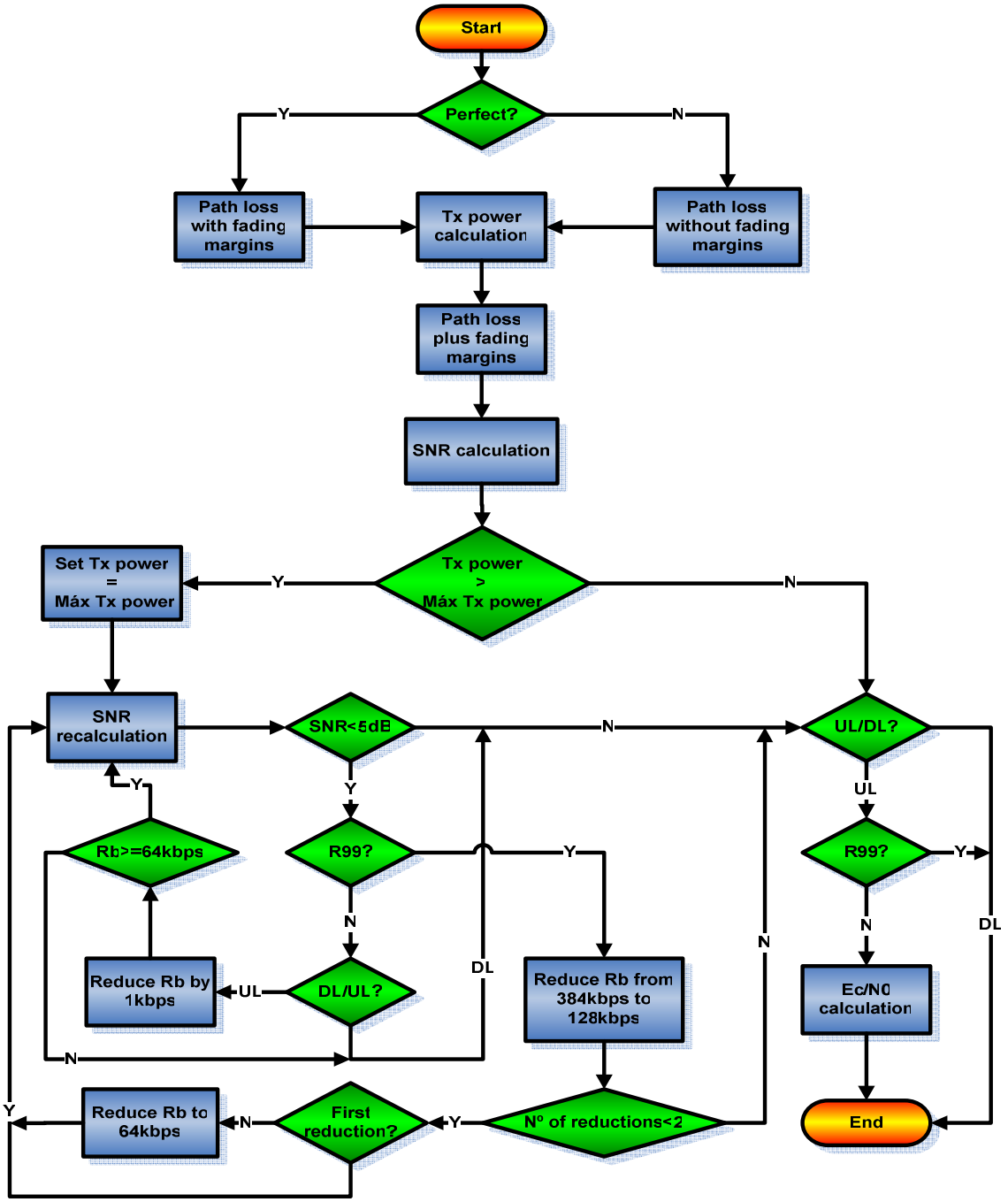

Figure I.1 Power control algorithm.

Annex J – DL Additional Results

In this annex, one presents additional results for the UL, in order to allow a better comprehension of the final results. Concerning the various systems and MIMO configurations considered in this thesis, in Figure J.1and Figure J.2 the average simulated throughput in function of the distance is presented, for a micro-cell scenario.

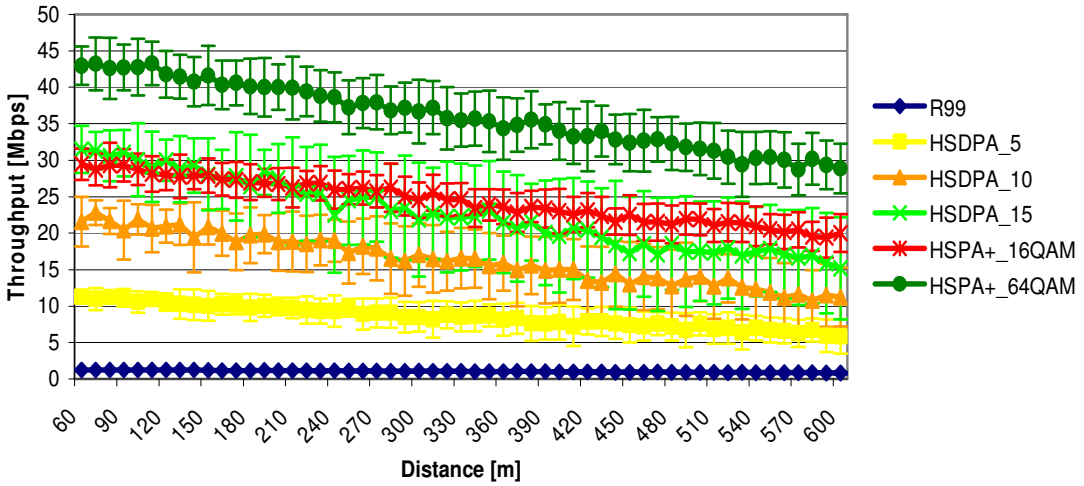

Figure J.1 DL Throughput vs. distance for various systems and 4×4 MIMO in a micro-cell scenario.

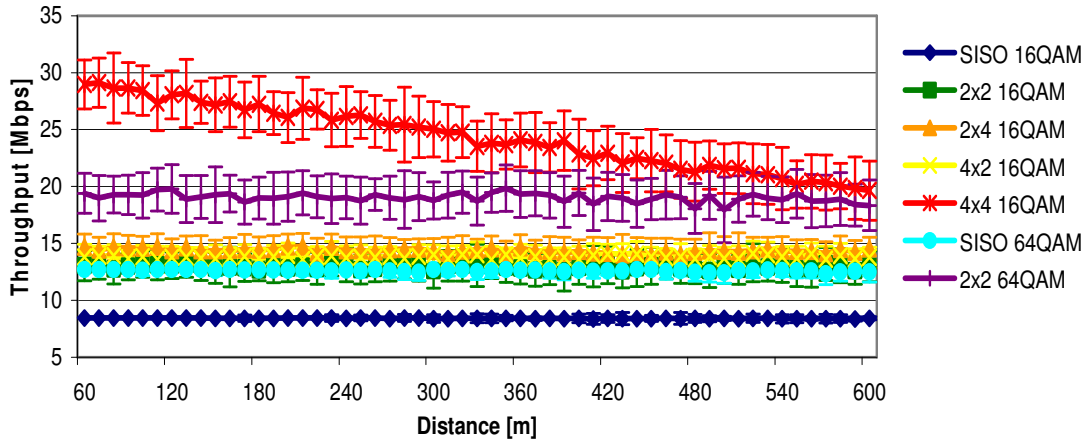

Figure J.2 DL Throughput vs. distance for different MIMO configurations applied to the default system in a micro-cell scenario.

The average simulated throughput regarding different type of detectors and type of antenna power fed is shown in Figure J.3 and Figure J.4, respectively.

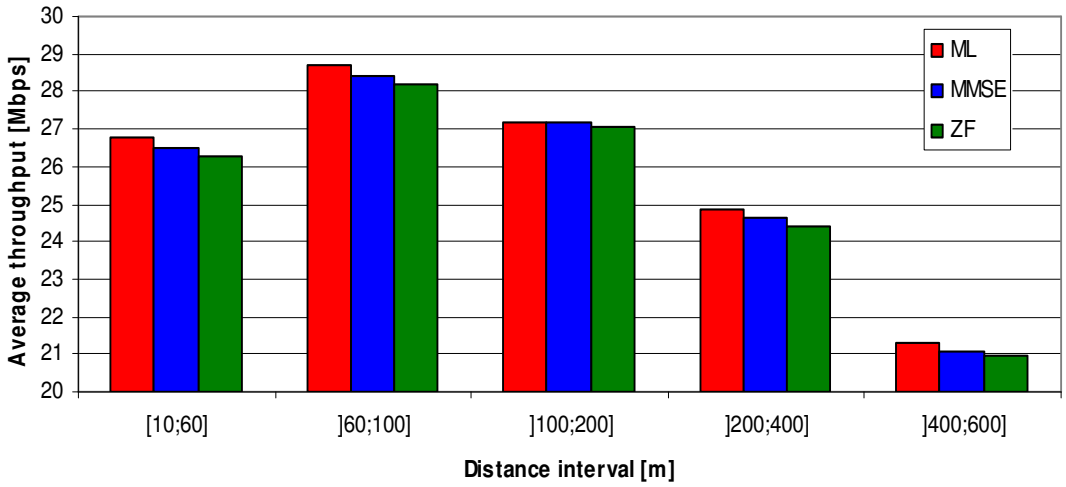

Figure J.3 DL average throughput vs. distance for different detectors.

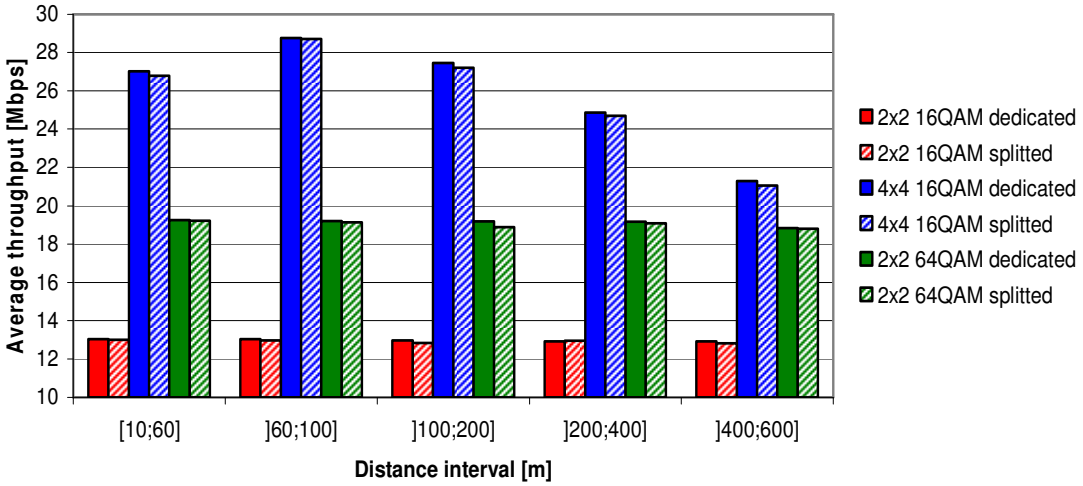

Figure J.4 DL Throughput vs. distance in a pico-cell scenario for split and dedicated power.

Annex K - UL Additional Results

In this annex, one presents additional results for the UL, in order to allow a better comprehension of the final results. In Figure K.1 and Figure K.2, one presents the default average simulated throughput in function of the distance for both pico- and micro-cell scenarios, respectively.

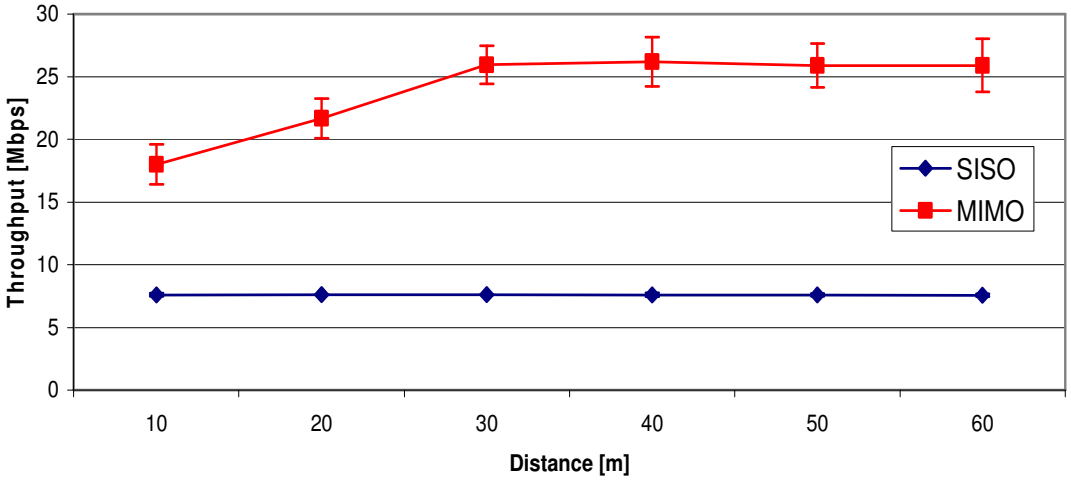

Figure K.1 Default scenario throughput vs. distance for UL in a pico-cell scenario.

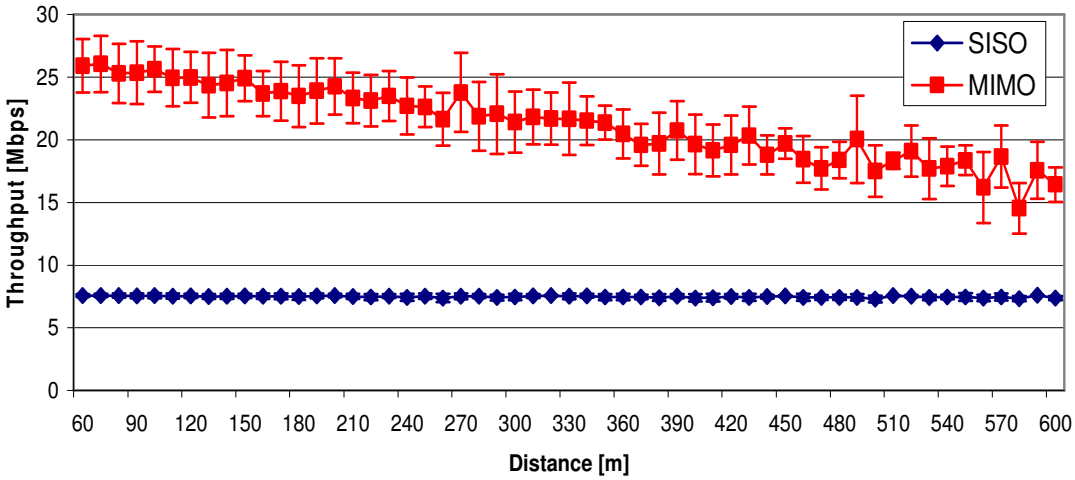

Figure K.2 Default scenario throughput vs. distance for UL in a micro-cell scenario.

For the micro-cell scenario, the average simulated throughput for the different UL systems is presented in Figure K.3. In Figure K.4 and Figure K.5 the average simulated throughput regarding different MIMO configurations is depicted, being the detection percentages associated to each configuration presented in Figure K.6.

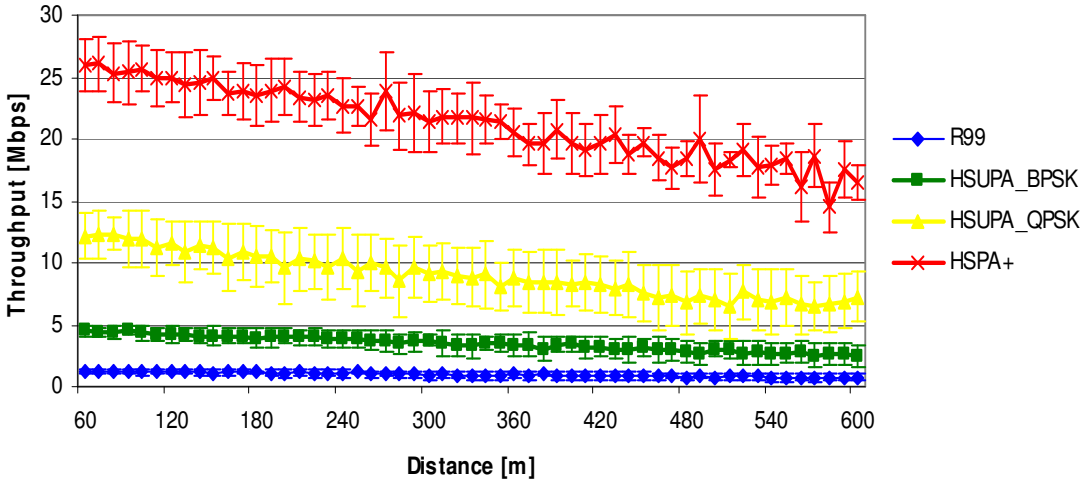

Figure K.3 UL Throughput vs. distance for various systems and 4×4 MIMO in a micro-cell scenario.

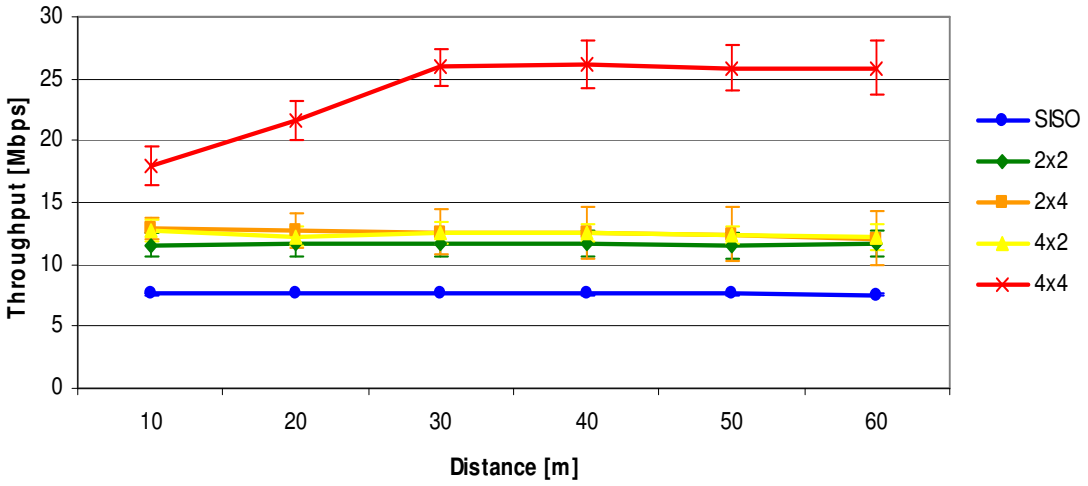

Figure K.4 UL Throughput vs. distance for different MIMO configurations applied to the default system in a pico-cell scenario.

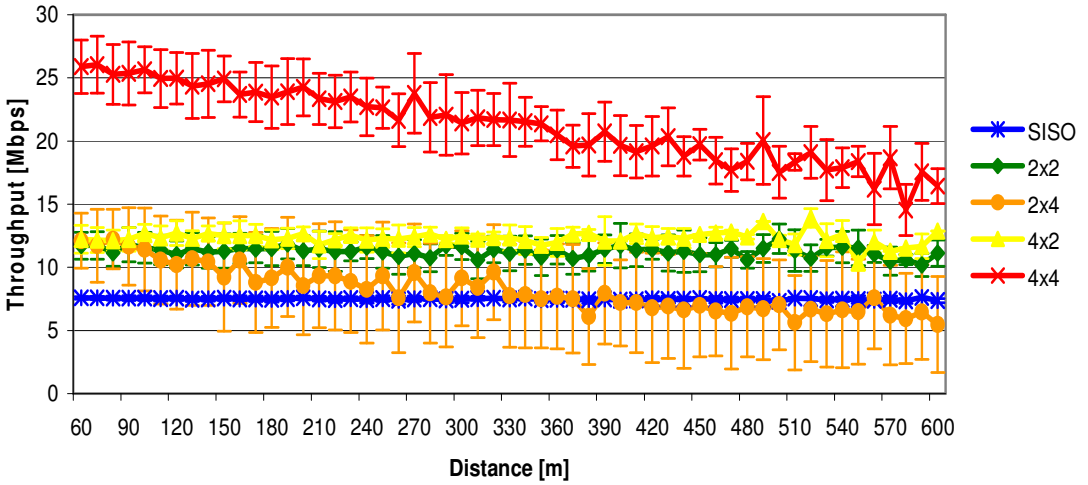

Figure K.5 UL Throughput vs. distance for different MIMO configurations applied to the default system in a micro-cell scenario.

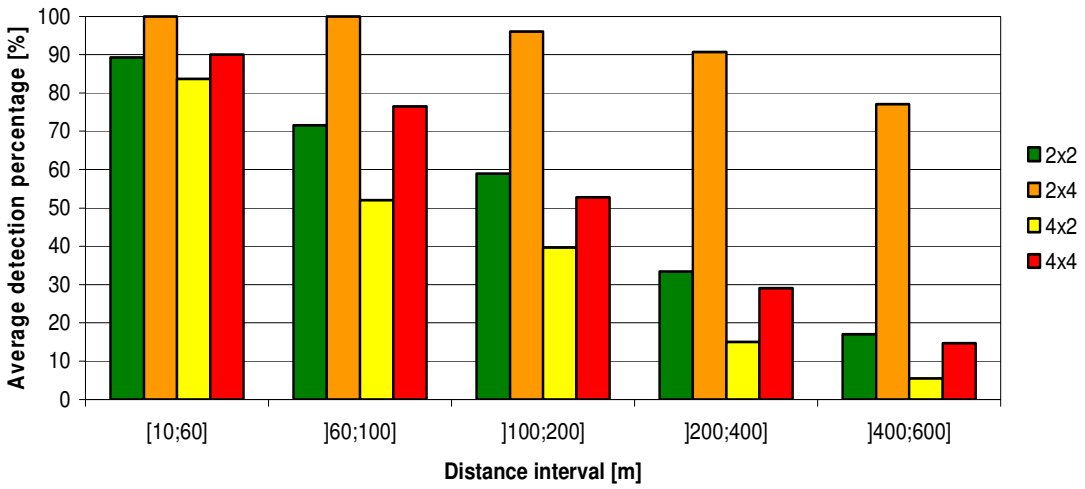

Figure K.6 UL detection percentage vs. distance for different MIMO configurations.

Concerning different antenna spacing, the average throughput is shown in Figure K.7. The different detectors average throughput and average detection percentages in function of distance are presented in Figure K.8 and Figure K.9, respectively.

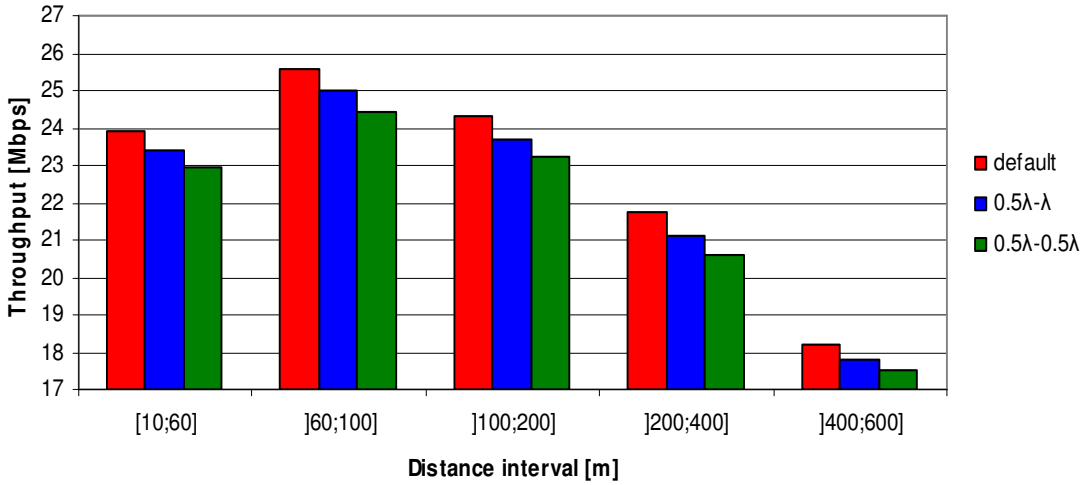

Figure K.7 UL average throughput vs. distance for different antenna spacing.

In Figure K.10 the average simulated throughput is presented while the average detection percentages are presented in Figure K.11.

Regarding the use of a TMA and/or reception diversity, in Figure K.13 and Figure K.14 is shown the average simulated throughput and the average detection percentages, respectively.

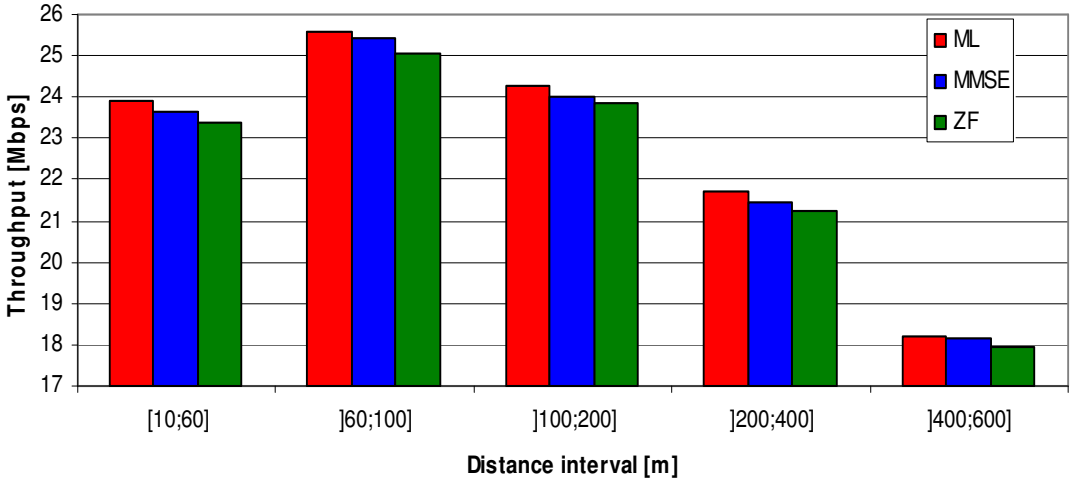

Figure K.8 UL average throughput vs. distance for different detectors.

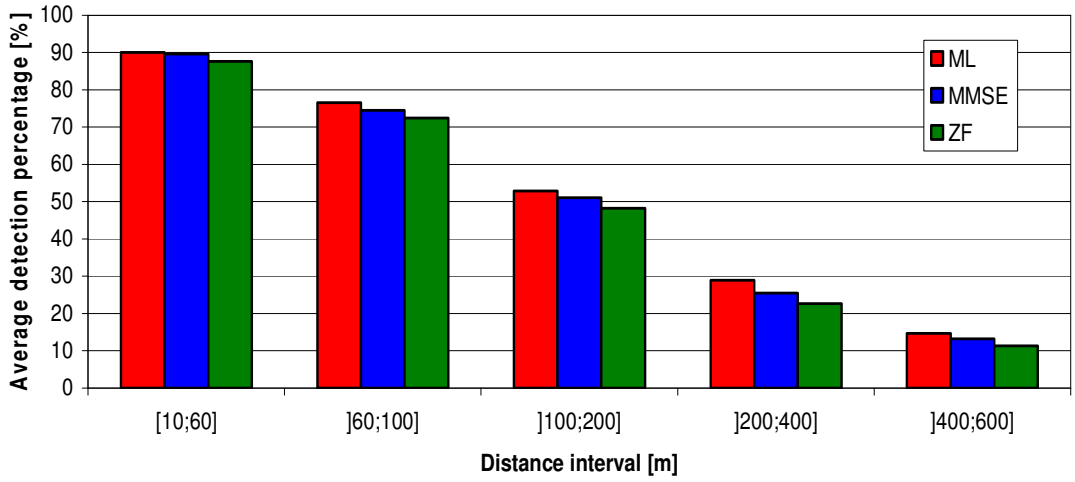

Figure K.9 UL average detection percentage for different detectors.

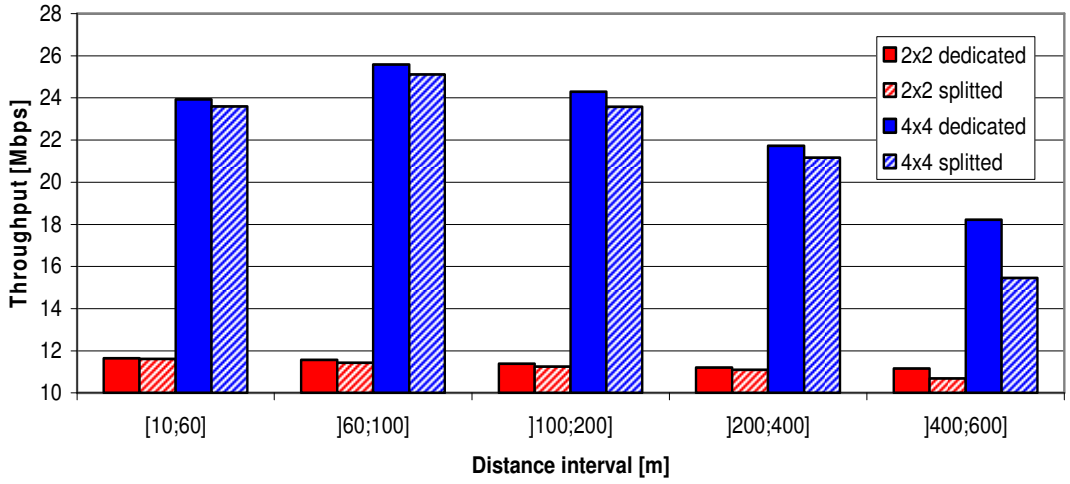

Figure K.10 UL Throughput vs. distance for split and dedicated power.

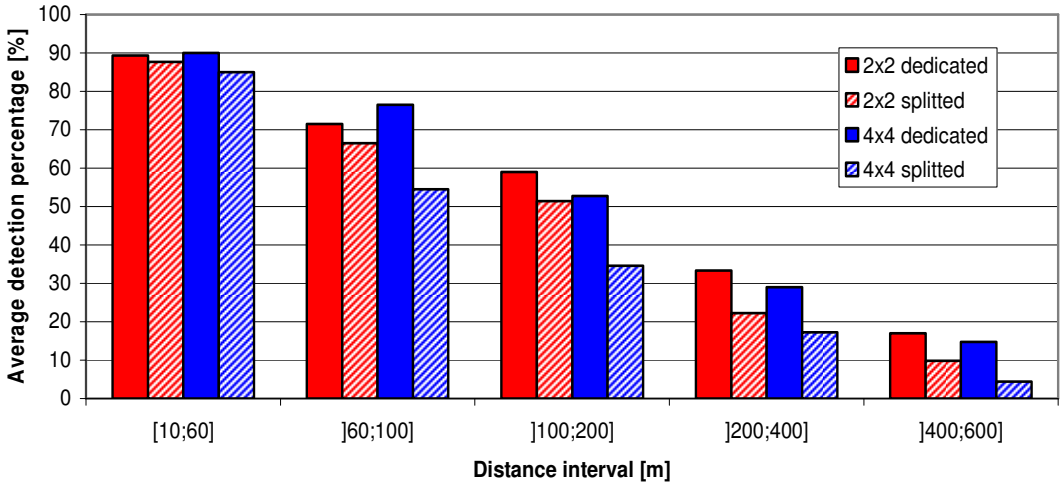

Figure K.11 UL average detection percentage for different types of antenna power fed.

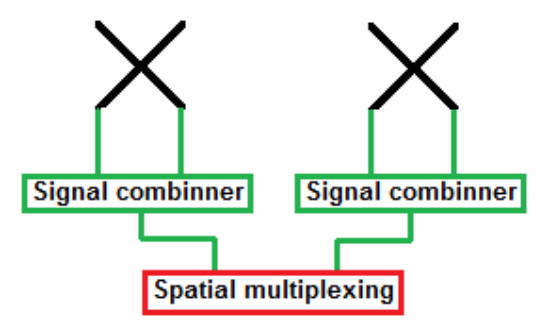

Figure K.12 Polarisation diversity on top of MIMO scheme.

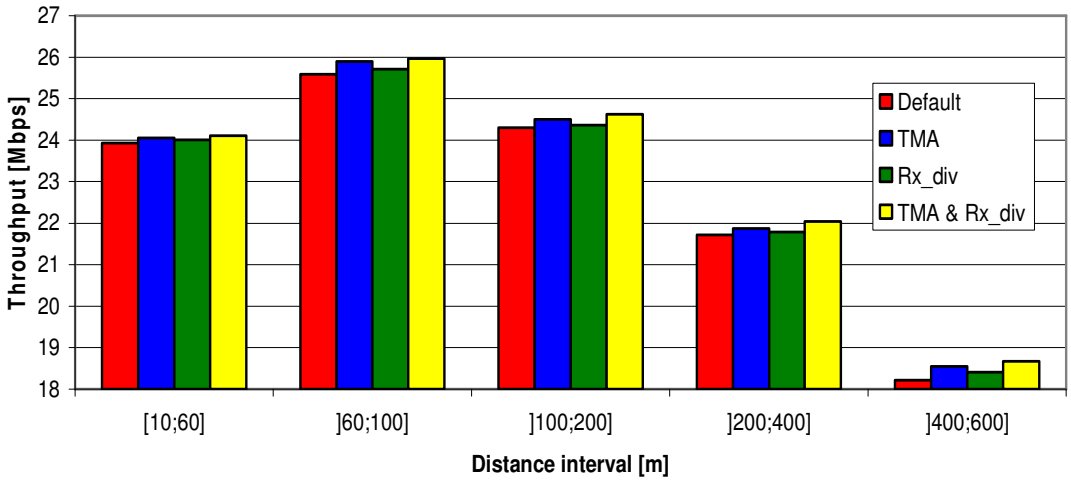

Figure K.13 UL Throughput vs. distance regarding the use TMA and/or reception diversity.

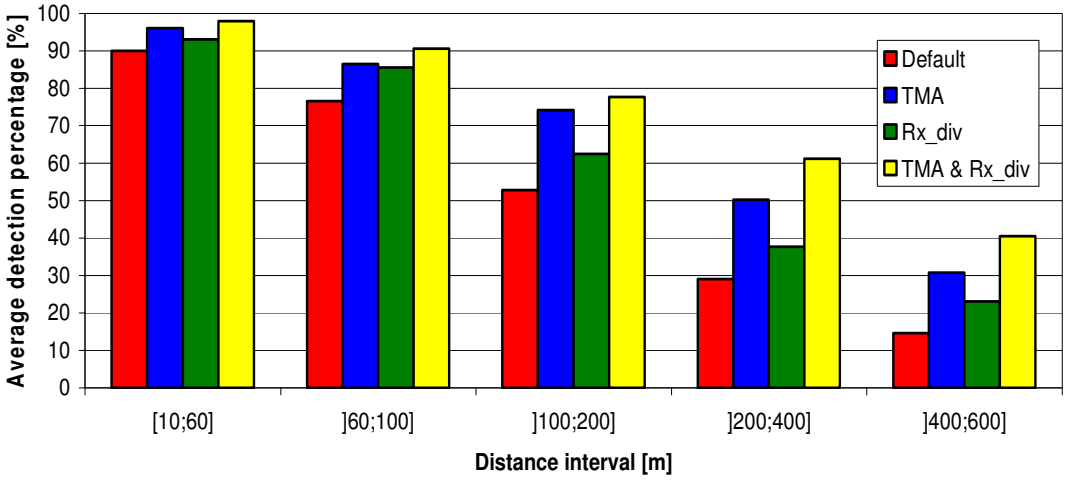

Figure K.14 UL average detection percentage regarding the use TMA and/or reception diversity.

References

[3GPP01] 3GPP, Technical Specification Group Services and System Aspects, *Service aspects; Services and Service Capabilities (Release 99)*, Report TS 22.105, V3.10.0, Oct. 2001 (http://www.3gpp.org/).

[3GPP02d] 3GPP, Technical Specification Group Services and System Aspects, *Quality of Service (QoS) concept and architecture (Release 99)*, Report TS 23.107, V3.9.0, Sep. 2002 (http://www.3gpp.org/).

[AsZe04] Assaad,M. and Zeghlache,D., "MIMO/HSDPA with fast fading and mobility: capacity and coverage study", in *Proc. of PIMRC'04 - 15th IEEE International Symposium on Personal, Indoor and Mobile Radio Communications*, Barcelona, Spain, Sep. 2004.

[ATEM02] Almers,P., Tufvesson,F., Edfors,O. and Molisch,A., "Measured Capacity gain using waterfilling in frequency selective MIMO channels", in *Proc. of PIMRC'02 - 13th IEEE International Symposium on Personal, Indoor and Mobile Radio Communications*, Lisbon, Portugal, Sep. 2002.

[BEGG08] Bergman,J., Ericson,M., Gerstenberger,D., Göransson,B., Peisa,J. and Wager,S., "HSPA Evolution – Boosting the performance of mobile broadband access"*, Ericsson Review,* Nº1, 2008.

[BWKK03] Böhnke,R., Wübben,D., Kühn,V. and Kammeyer,K-D., "Reduced Complexity MMSE Detection for BLAST Arquitectures", in *Proc. of GLOBECOM'03 - IEEE Global Telecommunications Conference,* San Francisco, CA, USA, Dec. 2003.

[BWLY07] Baek,M.-S., Woo,M., Lim,J.H., You,Y.-H. and Song,H.K., "SMLD: Enhanced MIMO-Signal Detection for Wireless MIMO Communications Receivers", *ETRI Journal*, Vol. 29, No. 2, Apr. 2007, pp. 240-242.

[CoLa06] Costa,P. and Ladeira,D., *Planning of UMTS Cellular Networks for Data Services Based on HSDPA* (in Portuguese), Graduation Thesis, IST-UTL, Lisbon, Portugal, 2006.

[Corr08] Correia,L.M., *Mobile Communication Systems,* Course Notes*,* IST-UTL, Lisbon, Portugal, Mar. 2008.

[DaCo99] Damasso,E. and Correia,L.M., *Digital Mobile Radio Towards Future Generation,* COST231 Final Report, 1999 (http:/www.lx.it.pt/cost231/).

[DGWB03] Davis,L.M., Garret,D.C., WoodWard,G.K., Bickerstaff,M.A. and Mullany,F.J., "System Architecture and ASICs for a MIMO 3GPP-HSDPA Receiver", in *Proc. of VTC'03 – 57th IEEE Vehicular Technology Conference*, Jeju, Korea, Apr. 2003.

[DPSB07] Dahlman,E., Parkvall,S., Sköld,J. and Beming,P., *3G Evolution: HSPA and LTE for Mobile Broadband*, Academic Press, Jordan Hill, Oxford, UK, 2007.

[Dziu04] Dziunikowski,W., *Multiple-Input Multiple-Output (MIMO) Antenna Systems*, in Chandran,S. (ed.), *Adaptive Antenna Arrays*, Springer, Berlin, Germany, 2004.

[FoGa98] Foschini,G.J. and Gans,M.J., "On Limits of Wireless Communications in a Fading Environment when Using Multiple Antennas", *Wireless Personal Communication*, Vol. 6, No. 3, Autumn 1998, pp. 311-335.

[GaKg07] Gabriel,R. and Kg K.W., "Virtual Receive Antennas for Spatial Multiplexing System", in *Proc. of CMCS'07 – Workshop on Commercial MIMO Components and Systems,* Duisburg, Germany, 2007.

[GDBH04] Garret,D., Davis,L., Brink,S.t., Hochwald,B. and Knagge,G., "Silicon Complexity for Maximum Likelihood MIMO Detection Using Spherical Decoding", *IEEE Journal of Solid-State Circuits*, Vol. 39, No. 9, Sep. 2004, pp.1544-1552.

[GuMP04] Guterman,J., Moreira,A.A. and Peixeiro,C., "Microstrip Fractal Antennas for Multistandard Terminals", *IEEE Antennas and Wireless Propagation Letters,* Vol.3, 2004, pp. 351-354.

[HenI06] Hen,I., "MIMO Architecture for Wireless Communication", *Intel Technology Journal*, Vol.10, No. 2, May 2006, pp.157-165.

[HoTo04] Holma,H. and Toskala,A., *WCDMA for UMTS* (3rd Edition), John Wiley & Sons, Chichester, UK, 2004.

[HoTo06] Holma,H. and Toskala,A., *HSDPA/HSUPA for UMTS*, John Wiley & Sons, Chichester, UK, 2006.

[HoTo07] Holma,H. and Toskala,A., *WCDMA for UMTS – HSPA Evolution and LTE* (4rd Edition), John Wiley & Sons, Chichester, UK, 2007.

[KiLB07] Kim,R.-W., Lee,D.-J. and Byun,Y.-S, "Near Maximum Likelihood Detection Schemes on RD Algorithm for MIMO Systems", in *Proc. of SPAWC'07 - IEEE 8th Workshop on Signal Processing Advances in Wireless Communications,* Incheon, Korea, June 2007.

[Koko05] Kokoszkiewicz,H., *MIMO Geometrically Based Channel Model*, M.Sc. Thesis, IST-UTL, Lisbon, Portugal, 2005.

[KuCo07] Kuipers,M., Correia, L.M., "Modelling the Relative MIMO Gain", in *Proc. of PIMRC'08 - IEEE Personal, Indoor and Mobile Radio Communications*, Cannes, France, Sep. 2008 (accepted for publication).

[LaWN06] Laiho,J., Wacker,J. and Novosad,T., *Radio Network Planning and Optimisation for UMTS*, John Wiley & Sons, Chichester, UK, 2006.

[LePB06] Lee,D.-J., Park,M.-H. and Byun,Y.-S., "Near-Maximum Likelihood Detection of MIMO Systems Using Error Detection Scheme Based Lattice Reduction", in *Proc. of APCC'06 - Asia-Pacific Conference on Communications,* Incheon, Korea, Aug. 2006.

[LiRa99] Liberti,J. and Rappaport,T., *Smart Antennas for Wireless Communication: IS-95 and Third Generation CDMA Applications*, Prentice Hall, Upper Saddle River, NJ, USA, 1999.

[LoBC04] Lo,J., Brito,A. and Correia,A., "Wireless Techniques for Capacity Enhancements of Broadcast and Multicast for UMTS networks", in *Proc. of VTC'04 - 60th IEEE Vehicular Technology Conference*, Los Angeles, CA, USA, Sep. 2004.

[Lope08] Lopes,J., *Performance of UMTS/HSDPA/HSUPA at the Cellular Level,* M.Sc. Thesis, IST-UTL, Lisbon, Portugal, 2008.

[Maćk07] Maćkowiak,M., *Geometrically Based Multibounce MIMO Channel Models*, M.Sc. Thesis, IST-UTL, Lisbon, Portugal, 2007.

[MaCo04] Marques,M.G. and Correia,L.M., *A Wideband Directional Channel Model for Mobile Communication Systems*, in Chandran, S. (ed.), *Adaptive Antenna Arrays*, Springer, Berlin, Germany, 2004.

[MaGH05] Marinis,E., Gasparini,O. and Hart,M.J. "Advanced spectral processing based MIMO receiver algorithms not requiring a cyclic prefix", in *Proc. of VTC'05 - 61st IEEE Vehicular Technology Conference*, Stockholm, Sweden, June 2005.

[MCRS05] Mehlführer,C., Caban,S., Rupp,M. and Scholtz,A.L., "Effect of Transmit and Receive Antenna Configuration on the Throughput of MIMO UMTS Downlink", in *Proc. of DSPCS'05 – 8th International Symposium on Digital Signal Processing and Communication Systems*, Noosa Heads, Australia, Dec. 2005.

[MeML05] Mehlführer,C., Mayer,L., Langwieser,R., Scholtz,A.L. and Rupp,M., "Free Space Experiments with MIMO UMTS High Speed Downlink Packet Access", in *Proc. of the 2nd IEEE/EURASIP Conference on DSP Enabled Radio*, Southampton, UK, Sep. 2005.

[MeRu04] Mecklenbrüker,C.F. and Rupp,M., "Generalized Alamouti Codes for Trading Quality of Service against Data Rate in MIMO UMTS", *EURASIP Journal on Applied Signal Processing*, Vol. 2004, No. 5, May 2004, pp. 662-675.

[NeZA00] Nee,R.v., Zelst,A.v. and Awater,G., "Maximum Likelihood Decoding in a Space Division Multiplexing System", in *Proc. of VTC'00-Spring - 51st IEEE Vehicular Technology Conference Proceedings,* Tokyo, Japan, May 2000.

[NSZL06] Ni,W., Shen,G., Zou,W. and Luoning,G., "Multi-User MIMO Detection for Enhanced High Speed Uplink Packet Access (HSUPA)", in *Proc. of PIMRC'06 - 17th IEEE International Symposium on Personal, Indoor and Mobile Radio Communications*, Helsinki, Finland, Sep. 2006.

[Pede05] Pedersen,K.I., "Quality Based HSDPA Access Algorithms", in *Proc. of VTC'05 – 62nd IEEE Vehicular Technology Conference*, Dallas, Texas, EUA, Sep. 2005.

[Pras98] Prasad,R., *Universal Wireless Personal Communications*, Artech House, London, UK, 1998.

[Proa01] Proakis,J.,G., *Digital Communications*, MacGraw Hill, New York, USA, 2001.

[PWST07] Peisa,J., Wager,S., Sågfors,M., Torsner,J., Göransson,B., Fulghum,T., Cozzo,C. and Grant,S., "High Speed Packet Access Evolution – Concept and Technologies", in *Proc. of VTC'07 – 65th IEEE Vehicular Technology Conference,* Dublin, Ireland, Apr. 2007.

[RuGW04] Rupp,M., Gritsch,G., and Weinrichter,H., "Approximate ML Detection for MIMO Systems With Very Low Complexity", in *Proc. of ICASSP'04 – IEEE/International Conference on Acoustics, Speech, and Signal Processing,* Montreal, Quebec, Canada, May 2004.

[Sant04] Santo,L., *UMTS Performance in Multi-Service Non-Uniform Traffic Networks,* M.Sc. Thesis, IST-UTL, Lisbon, Portugal, 2004.

[Segg03] Seggern,D.von, *CRC Standard Curves and Surfaces*, CRC Press, Boca Raton, FL, USA, 1993.

[So07] So,D., "Virtual Receive Antennas for Spatial Multiplexing System", in *Proc. of CMCS'07 – Workshop on Commercial MIMO Components and Systems,* Duisburg, Germany, 2007.

[SoSS07] Soares,A., Silva,J.C., Souto,N., Leitão,F. and Correia,A., "MIMO Based Radio Resource Management for UMTS Multicast Broadcast Multimedia Services", *Wireless Personal Communications*, Vol.42, No 2, July 2007, pp. 225-246.

[TrLF05] Tran,X.N., Le, A.T. and Fujino,T., "Combined MMSE-ML Detection for wireless MIMO-SDM Communication", in *Proc. of ISAP'05 – International Symposium on Antennas and Propagation,* Seoul, Korea, Aug. 2005.

[UMFO08] http://www.umts-forum.org/index2.php?option=com_content&do_pdf=1&id=2315, June, 2008.

[ViQR05] Vieira,P., Queluz,M.P. and Rodrigues,A., “HSDPA capacity enhancement using MIMO in a pico-cell environment”, in *Proc. of WCACEM’05 - IEEE/ACES International Conference on Wireless Communications and Applied Computacional Electromagnetics*, Honolulu, HI, USA, Apr. 2005.

[ViRo04] Vieira,P. and Rodrigues,A., “Multi user MIMO performance applied to UMTS HSDPA”, in *Proc. of VTC’04 - 59th IEEE Vehicular Technology Conference,* Milan, Italy, May 2004.

[WBKK04] Wübben,D., Böhnke,R., Kühn andV., Kammeyer,K-D., “MMSE-Based Lattice-Reduction for Near-ML Detection of MIMO Systems”, in *Proc. of ITG Workshop on Smart Antennas,* Bremen, Germany, Mar. 2004.

[WFGV98] Wolniansky,P.W., Foschini,G.J., Golden,G.D. and Valenzuela,R.A., “V-BLAST: An Architecture for Realizing Very High Data Rates Over the Rich-Scattering Wireless Channel”, in *Proc. of ISSSE - 1998 URSI International Symposium on Signals, Systems and Electronics,* Pisa, Italy, Sep. 1998.

[ZhMu02] Zhu,X. and Murch,R.D., “Performance Analysis of Maximum Likelihood detection in a MIMO antenna System”, *IEEE Transactions on Communication,* Vol. 50, No 2, Feb. 2002, pp. 187-191.